# On the environment-induced decoherence in quantum devices

Håkon Brox


Thesis submitted for the degree of Philosophiae Doctor
Department of Physics
University of Oslo
October 15, 2012

*Series of dissertations submitted to the*
*Faculty of Mathematics and Natural Sciences, University of Oslo*
*No. 1272*

ISSN 1501-7710



Cover: Inger Sandved Anfinsen.
Printed in Norway: AIT Oslo AS.

Produced in co-operation with Akademika publishing.
The thesis is produced by Akademika publishing merely in connection with the thesis defence. Kindly direct all inquiries regarding the thesis to the copyright holder or the unit which grants the doctorate.

## Acknowledgements

I would like to thank the following people for their contributions to the completion of this thesis.

I would like to thank Joakim Bergli for close collaboration and deep discussions covering all areas of physics. The discussions with Joakim has been invaluable to me in the sense that it has broadened and matured my grasp of physics.

My main supervisor professor Yuri M. Galperin for close collaboration and guidance. His physical insight and practical approach has pointed me in the right direction several times.

I would also like to thank all the members and former members at the AMCS group for discussions, friendship and making the workplace a thriving place to be. Especially I would like to thank my current and former office mates Jørn I. Vestgården and Martin Kirkengen, it has been a pleasure sharing office with you. Henry J. Wold for beeing a close collaborator in one of my papers and Ken Tore Tallakstad for friendship in general.

During my stay at UiO I am also thankful for the opportunity to take part in discussions in the group of Arnt I. Vistnes on experimental quantum optics. These discussions has been an excellent opportunity for me to increase my knowledge of this very interesting subject.

Finally, I would like to thank my friends and family, especially my significant other Julie M. Haabeth for her support and bearing over with my many late days and of course my parents for raising me and supporting my curiousity in general.

## Structure of the thesis

This thesis is organized in two parts. The first part is an introductory part, which can be seen as background material for the second part containing the papers with the main results of this thesis. The first part is structured as follows. First we give a motivation for the study of noise in qubits and a brief introduction to quantum physics and quantum computing. Later we move on to more specific background material such as theories of noise in qubits, the microscopic origin of the noise and further material that is directly related to the papers.

The second part consists of the published papers, which independently form a self contained presentation of the main results obtained in this thesis. I also give a summary of the papers where I discuss the motivation behind each paper and some prospects for further research.

# List of papers

- **Paper 1: Effects of external driving on the coherence time of a Josephson junction qubit in a bath of two level fluctuators.**
  **Håkon Brox, Joakim Bergli and Yuri M. Galperin**
  **Phys. Rev. B 84, 245416 (2011)**

- **Paper 2: The importance of level statistics for the decoherence of a central spin due to a spin environment.**
  **Håkon Brox, Joakim Bergli and Yuri M. Galperin**
  **Phys. Rev. A. 85. 052117 (2012)**

- **Paper 3: Bloch-sphere approach to correlated noise in coupled qubits.**
  **Håkon Brox, Joakim Bergli and Yuri M. Galperin**
  **Submitted to Journal of Physics A: Mathematical and Theoretical**

- **Paper 4: Decoherence of a qubit due to a quantum fluctuator or to a classical telegraph noise.**
  **Henry J. Wold, Håkon Brox, Yuri M. Galperin and Joakim Bergli**
  **Submitted to Phys. Rev. B**

# Contents

# Part I

# Introduction

# Chapter 1

# Background

In this section I will briefly give some background information for the work done in this thesis. First we give a motivation for the work and a brief outline of quantum mechanics, the fundamental theory used throughout this thesis. Secondly we move into the subject of quantum computing and the physics of quantum bits.

In this section I have attempted to write in a way so that those without much previous knowledge of physics should be able to learn at least something from it. Still parts of this chapter contains material which is hardly readable without a background on the level of a university degree in physics, this is of course a major problem encountered in the presentation of modern physics.

I will not give a formal introduction to the theory of quantum mechanics, for that I refer the reader to standard textbooks. Rather, I will in this section attempt to illustrate the basic features of quantum mechanics that are relevant to this thesis: the superposition principle, entanglement and decoherence, by use of the double slit experiment with single particles. This particular experiment is chosen both because of its beauty, its thought provoking character and its ability to illustrate the essence of quantum mechanics.

Here we will not go into any detailed description of quantum computing. What is relevant to this thesis is the physics of the basic building block, the qubit. In order to illustrate the basic mechanisms behind a qubit I here choose a flux qubit. In principle we could choose any qubit design, but since parts of the papers are focused on superconducting qubits this is a natural choice. I choose to use the flux qubit rather than the charge or the phase qubit as an example since the concept of a superposition of current

states through a loop is to me more intriguing than the superposition of an extra Cooper pair on a superconducting grain.

## 1.1 Motivation

In this thesis we study the subject of noise and decoherence in quantum devices, in particular in quantum bits or qubits. There are two main motivations behind why research in this field is interesting in itself and might potentially be beneficial for society.

Firstly, it is crucial in the quest for the ambitious goal of constructing a quantum computer, a computer who could solve certain tasks dramatically faster than ordinary classical computers. The fundamental unit in any quantum computer is the qubit, the quantum analogue of the classical bit. Many research groups and companies all over the world are at present time working with almost equally many different physical designs for qubits and ways to make them operate together, with the goal of finally realizing a design which can be scaled up to make a real quantum computer.

By far the largest and most fundamental problem encountered in the design of qubits and other quantum devices is decoherence, the inevitable loss of quantum properties in the device due to interaction with its environment. When the quantum behavior of a qubit is lost, it can not be used for quantum computing. Understanding decoherence in qubits is therefore extremely important in order to improve the design of qubits and other quantum devices. This can be achieved by improving the protection and shielding of the qubit from its noisy environment, and by development of other countermeasures which can potentially reduce the rate and the impact of decoherence in qubits.

Secondly, the study of qubits and other mesoscopic quantum devices might shed light on maybe the greatest fundamental problem in modern physics, the border between the quantum and the classical realm. For soon a full century our theoretical description of nature has been divided in two parts, with a fuzzy boundary. On one hand we have classical physics, which includes mechanics, electromagnetism and the general theory of relativity. These theories describe the familiar macroscopic realm, from the motion of planets, stars and galaxies to the working of the familiar objects and machines we surround ourself with in our everyday life. On the other hand quantum mechanics, and its generalization quantum field theory, describes the microscopic properties of atoms, electrons and even more exotic particles, the emission and absorptions of light and is also required to understand a long list of macroscopic properties of solids such as the behavior of semiconductors and superconductors.

Both theories, the quantum and the classical, describes the properties of the physical world with astounding precision within their area of validity. Unfortunately the two theories are incompatible. The linear dynamics of quantum mechanics cannot be used to derive the classical world, while classical mechanics fails in describing experiments such as the double slit experiment with single particles, and the violation of Bell's inequalities [1, 2]. In quantum mechanics one circumvents this problem by postulating the nonlinear collapse of the quantum wavefunction in the moment of measurement of the quantum state. The collapse takes place when a quantum state is measured by a classical apparatus [3, 4], an object outside of the theory of quantum mechanics. But why is the measurement apparatus, which is itself built up of atoms, not described by the same quantum theory as describes it constituents to such a high degree of precision? Quantum theory itself has no clear answer. We cannot predict from the theory what makes an object classical. The border between the two theories is therefore not well defined and quantum mechanics is not a self-contained theory since it depends on notions outside the theory itself.

Mesoscopic quantum devices, such as e.g. superconducting qubits, are devices whose size and nature lies very close to the fuzzy border between the quantum and the classical. Therefore, in addition to tremendous technological prospects, research on qubits and other mesoscopic quantum devices might lead to increased understanding, through empirical input, of the borderline between the two realms. It is tempting to believe that the search for coherent manipulation and measurement of mesoscopic, and may be even larger quantum devices, might eventually lead to a greater understanding of quantum theory and perhaps lead to hints useful for the development of corrections to quantum theory. The ultimate, but may be unachievable goal, would be to create a unified theory which contains both classical and quantum physics as limiting cases. Attempts to develop such theories has already been made, see e.g. Ref. [5] for a review, however the testing of these theories require control of coherent superpositions of quantum object of mass or size much larger than what is currently achieved. The main issue in designing such experiments is again the decoherence of the quantum states due to environments.

## 1.2 A brief introduction to quantum mechanics

In this section I will attempt to illustrate the basic notions of quantum mechanics that are essential to this thesis. We start with the double slit

experiment, which in my opinion covers the most fundamental features of the theory. Then we will briefly describe the basic formalism used to describe decoherence.

### 1.2.1 The double slit experiment

The double slit experiment with single particles is said to capture the essence of quantum mechanics. In a classical double slit experiment, a

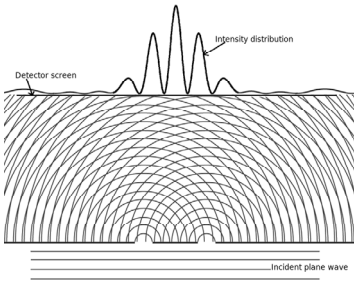


Figure 1.1: A double slit experiment. Plane waves are incident from below on a wall with two small slits. The diffracted waves originating from each of the two slits interfere. The resulting measured intensity, at the detector screen (e.g. a photographic plate), shows a typical interference pattern. The amplitude at each point on the detector is determined by the relative difference in the distance traveled from the two slits to the particular point of interest on the detector.

plane wave is incident on a impenetrable wall, with two small slits, see Fig. 1.1. The diffracted waves from each slit interfere with each other, just like classical waves on water. Theoretically, we describe the propagating wave pattern after the slits, the distribution of wave amplitudes in space and time, by adding together (or superposing) the diffraction pattern originating from each of the slits in isolation. More formally, we denote the amplitude of the wave originating from slit 1 and 2 at time $t$ and position $\mathbf{r}$ by $\psi_1(\mathbf{r}, t)$ and $\psi_2(\mathbf{r}, t)$, respectively. Such that $\psi_1(\mathbf{r}, t)$ describes the wave pattern on the water if we close slit 2. Then the total wave amplitude is simply the sum of the waves from each source $\psi_{tot}(\mathbf{r}, t) = \psi_1(\mathbf{r}, t) + \psi_2(\mathbf{r}, t)$. This is the superposition principle, the response at a single point due to two different sources is the sum of the responses which would have been caused by each source individually.

The beautiful nature and richness of the classic double slit experiment is indeed fascinating, but should not be a mystery. We encounter similar phenomena in our everyday life, water waves, sound waves and light all behave according to the superposition principle. The real mystery is encountered if we use a single particle source, a source where the intensity of photons, electrons, neutrons or even large molecules [6] can be tuned sufficiently low such that only a few particles each second is measured at the detector screen, and the probability to measure two particles at the same time is negligibly small. The particles arrive one by one at the detector screen, but their density sums up to an interference pattern identical to that formed by classical waves, see Fig. 1.2. It seems like each particle moves through both slits at the same time, as a wave interfering with itself, before ending up as a single point particle on the detector screen. Quoting Richard Feynman: *[on the double slit experiment] A phenomenon which is impossible, absolutely impossible, to explain in any classical way, and which has in it the heart of quantum mechanics. In reality, it contains the only mystery [of quantum mechanics] [7].*

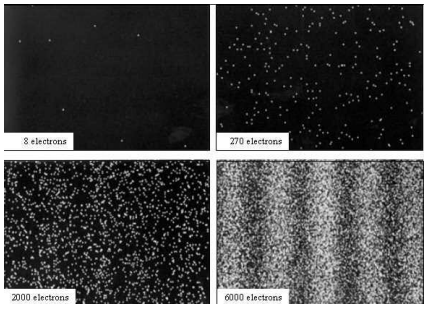


Figure 1.2: The build-up of the interference pattern in a single particle double slit experiment with electrons. A. Tanamura et al., Am. J. Phys. 57 117 (1989)

Quantum mechanics explains the double slit experiment in the following way: In order to obtain the interference pattern, we need a source emitting particles in such a way that it is impossible, even in principle, to tell the exact direction of the emitted particle. Such a source is not that hard to obtain, a photon emitted by an atom will e.g. according to quantum mechanics in general be emitted continuously as a spherical wave, and if we neglect the intensity of the wave in all directions except those two corre-

sponding to the two slits of the double-slit experiment we are required to describe the state of the particle incident on the slits as a superposition of a particle incident on the right and the left slit, respectively. We might write this state formally as

$$|\psi\rangle = \frac{1}{\sqrt{2}} \left( |\psi_L\rangle + |\psi_R\rangle \right), \tag{1.1}$$

where $|\psi_L\rangle$ is the state of a single particle incident on the left slit and $|\psi_R\rangle$ denotes the particle state incident on the right slit. The situation is illustrated in Fig. 1.3 a).

The states $|\psi_R\rangle$ and $|\psi_L\rangle$ is here written in the so called bra-ket notation. This is a general notation we use to describe quantum states, without the need to refer to a specific basis. If we want we can re express the state in a specific basis. As an example we can re express the general state $|\psi_R\rangle$ in the position basis, which means that we specify the amplitude of the wavefunction at each point in space and time

$$|\psi_R\rangle \rightarrow \psi(\mathbf{r}, t).$$

The state can be expressed in any basis, which is the quantum mechanical equivalent to expressing classical mechanics in an arbitrary set of coordinates. For particles the most commonly used bases are the position basis and the momentum basis. In the following we will express the state of the system passing the left and the right slit, respectively by the amplitude of the wavefunction as a function of the position on the detector screen which can be related to the angle of diffraction at the slits $\theta$, see Fig. 1.3.

To describe the interference pattern theoretically, we need to compute the intensity $I(\theta)$ at each point on the detector. A position $\mathbf{r}$ on the detector screen can be related to an angle $\theta$ in spherical coordinates, see Fig. 1.3 a) for a illustration. The intensity distribution is computed by adding together the amplitudes of the wavefunctions for particles traveling through either the left or the right slit independently, according to the superposition principle. Assuming that the distance from the slits to the detector is much larger than the distance between the slits, we can write

$$\begin{aligned} I(\theta) \propto |\psi_L(\theta) + \psi_R(\theta)|^2 &= |\psi_L(\theta)|^2 + |\psi_R(\theta)|^2 + \psi_L^*(\theta)\psi_R(\theta) + \psi_R^*(\theta)\psi_L(\theta) \\ &= A(\theta) \cos^2 \left( \frac{\pi \delta \sin\theta}{\lambda} \right), \end{aligned} \tag{1.2}$$

where $\psi_L(\theta)$ and $\psi_R(\theta)$ is the particle wavefunction at the detector due to particles going through the left and the right slit, respectively, $A(\theta)$ is a modulating function determined by the degree of diffraction at each slit, $\delta$

is the distance between the two slits and $\lambda$ is the de Broglie wavelength of the particle.

The interference pattern is due to the coherence term $\psi_L^*(\theta)\psi_R(\theta) + \psi_R^*(\theta)\psi_L(\theta)$. The size of this term at a given angle $\theta$ depends on the phase difference between the waves originating from each slit. In analogy with classical waves, the phase of the wavefunction $\psi_{R/L}(\mathbf{r}, t)$ oscillates in space and time and the relative phase difference between the waves from the left and the right slit depends on the difference in distance traveled from the slit. At some points the two wavefunctions will interfere destructively resulting in zero particle density, while at other points they interfere constructively giving a higher measured particle density than expected by simple addition of the individual densities originating from each of the slits.

The visibility of the interference pattern in the double slit experiment is due to the quantum coherence of the particles emergent from the source, this means that the phase information of each particle needs to be conserved and unperturbed while it travels from the source to the detector. Let us now assume that there exists other particles between the source and the double slit, we might call them electrons, which might potentially interact with the particle emitted from the source (we might call those neutrons).

This situation is illustrated in Fig. 1.3 b), where an electron is moving in proximity to the left slit. We might assume that if the trajectory of the electron is in sufficiently close proximity to that of the neutron emitted from the source, the two will interact and the electron is scattered due to the interaction. In quantum mechanical notation we might denote the outgoing state of the unperturbed electron by $|e_0\rangle$ and the state of the scattered particle by $|e_1\rangle$. We might denote the overlap between these two states by $\alpha = |\langle e_1|e_0\rangle| \leq 1$. We have that $\alpha = 1$ if the two states are identical, i.e. if the interaction does not disturb the trajectory of the electron at all. If the two states are orthogonal (in Hilbert space, a mathematical construction which allows us to treat quantum states as points in a special vector space and make use of the familiar geometrical concepts of vector algebra) we have that $\alpha = 0$, note that the scattered trajectories are not required to be orthogonal in real space in order to make the states $|e_1\rangle$ and $|e_0\rangle$ orthogonal. In fact only a small deviation in the trajectory is sufficient to make the two states orthogonal if the momentum of the incoming electron was sharply defined.

Since the two particles interact, we can no longer write down the state of the neutron impending on the double slit as a single isolated object, like we did in Eq. (1.1). If the neutron passes the left slit, the state of the electron will be perturbed from $|e_0\rangle$ to $|e_1\rangle$, while if the neutron passes the right slit, or does not pass at all, the state of the electron is unchanged. We

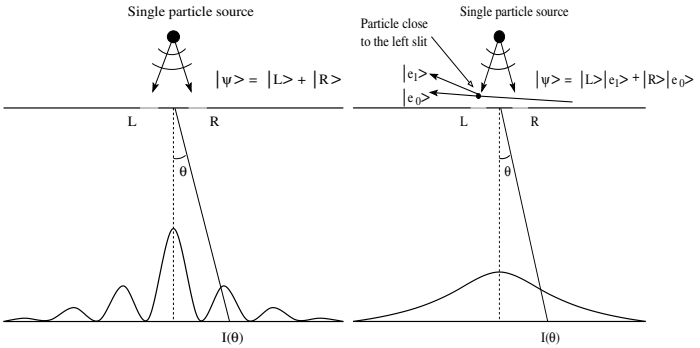


Figure 1.3: a) A single particle double slit experiment. b) The same experiment with decoherence. A single particle source emits particles uniformly in all directions. Parts of the outgoing wave incident on the slits is diffracted and passes through to the detector screen at the bottom. The wavefunction after the double slit can formally be written as a superposition of a particle traveling through the left and the right slit $|\psi\rangle = 1/\sqrt{2}\,(|\psi_L\rangle + |\psi_R\rangle)$. The particle intensity $I(\theta)$ at the detector screen is shown at the bottom of each figure. In b) the particle emitted from the source interacts and becomes entangled with another particle in the vicinity of the left slit, the interaction leads to loss of coherence and therefore reduced visibility of the interference pattern.

might write the state of the composite system as

$$\left|\psi^{n+e}\right\rangle = \frac{1}{\sqrt{2}}\left(|\psi_L\rangle\,|e_1\rangle + |\psi_R\rangle\,|e_0\rangle\right), \tag{1.3}$$

where $|\psi^{n+e}\rangle$ now denotes the state of the two particle system. Such a composite state, where we are in principle unable to specify the state of each individual particle without referring to other degrees of freedom, is called an entangled state. The neutron and the electron became entangled due to the interaction that might potentially have taken place at the left slit.

We might now try to find out whether the interference pattern of the neutron emerging from the source is affected by the electron. The interference pattern was calculated in Eq. (1.2) by taking the square of the wavefunctions describing the particle passing through the left or the right

slit according to the superposition principle,

$$I(\theta) \propto |\psi_L(\theta) + \psi_R(\theta)|^2 = |\psi_L(\theta)|^2 + |\psi_R(\theta)|^2 + \psi_L^*(\theta)\psi_R(\theta) + \psi_R^*(\theta)\psi_L(\theta). \tag{1.4}$$

The situation is, however, altered due to the electron at the left slit, even if the electron is nowhere near the detector where the neutron is measured. In order to find the intensity distribution at the detector screen, we need to use the composite wavefunction when we compute the inner product

$$\begin{aligned} I(\theta) &\propto \left|\psi^{n+e}(\theta)\right|^2 = \frac{1}{2}\left(\psi_L^{n*}(\theta)\langle e_1| + \psi_R^{n*}(\theta)\langle e_0|\right)\left(\psi_L^n(\theta)|e_1\rangle + \psi_R^n(\theta)|e_0\rangle\right) \\ &= \frac{1}{2}\left[|\psi_L^n(\theta)|^2\langle e_1|e_1\rangle + |\psi_R^n(\theta)|^2\langle e_0|e_0\rangle + \left(\psi_L^{n*}(\theta)\psi_R^n(\theta) + \psi_R^{n*}(\theta)\psi_L^n(\theta)\right)\langle e_1|e_0\rangle\right] \\ &= \frac{1}{2}\left[|\psi_L^n(\theta)|^2 + |\psi_R^n(\theta)|^2 + \left(\psi_L^{n*}(\theta)\psi_R^n(\theta) + \psi_R^{n*}(\theta)\psi_L^n(\theta)\right)\alpha\right]. \end{aligned} \tag{1.5}$$

The visibility of the interference term is here reduced by the overlap factor $\alpha = |\langle e_1|e_0\rangle|$ due to the interaction with the electron at the left slit. The situation is illustrated in Fig. 1.3 b). We say that the coherence of the neutron passing the double slit is reduced due to the interaction with the phonon.

The degradation of coherence due to interaction with uncontrolled degrees of freedom is called decoherence, and is a central concept throughout this thesis. Due to interaction, the quantum properties of the neutron in the double slit experiment is seemingly lost. The intensity pattern of Fig. 1.3 b) is consistent with a classical "particle" passing either the left *or* the right slit. The lesson can be phrased as follows: if there is *in principle* a possibility to find out which path the particle took through the double slit, by a measurement of another physical quantity, then the particle will behave as it took either the left or the right path through the the setup, rather than a coherent superposition of all possible paths at the same time.

The decoherence in quantum bits, which is the main topic of this thesis, is exactly the same concept and is qualitatively identical to decoherence in the double slit experiment. In a qubit, which is a quantum system where the dynamics is restricted to two distinct states $|0\rangle$ and $|1\rangle$, the basic states might couple to other degrees of freedom in the environment. If the interaction is such that the dynamical evolution of the environment is different conditioned upon the state of the qubit, any coherent superposition of the qubit states is degraded in the same way as the particle in the double slit experiment. As an isolated system, the qubit might be prepared in a superposition of $|0\rangle$ *and* $|1\rangle$, after interaction with the environment the coherence decays until the state of the qubit is the classical combination of either $|0\rangle$ *or* $|1\rangle$.

## 1.3 Decoherence, general formalism

In this section we will describe the formalism of decoherence used in later chapters and in paper 2, 3 and 4.

As we have seen, decoherence is the inevitable loss of quantum coherence in a system due to entanglement with other degrees of freedom. Suppose we have a quantum system, system $A$, initially prepared in the pure state $\left|\phi^A(0)\right\rangle = c_i(0)\left|i\right\rangle$, where $\left|i\right\rangle$ are the eigenvectors of an operator $\hat{O}$, i.e. the possible states we can obtain as outcomes of a measurement of this observable. If system $A$ interacts with another system, $B$, the latter will evolve in time conditioned upon the state of the former. Since quantum mechanics is a linear theory, the unitary evolution of the composite system can be written schematically as

$$\left|\phi^A(0)\right\rangle\left|\phi^B(0)\right\rangle = \sum_i c_i(0)\left|i\right\rangle\left|\phi^B(0)\right\rangle \xrightarrow{t} \sum_i c_i(t)\left|i\right\rangle\left|\phi_i^B(t)\right\rangle, \qquad (1.6)$$

where $\left|\phi_i^B(t)\right\rangle$ is the state of system $B$ at time $t$ conditioned upon that system $A$ was initially in the state $\left|i\right\rangle$. If we now form the reduced density matrix for system $A$ (see App. A.1),

$$\rho_A = \mathrm{Tr}_B\left(\rho_{AB}\right) = \sum_{ij} c_i(t)c_j(t)^*\left|i\right\rangle\left\langle j\right|\left\langle\phi_j^B(t)|\phi_i^B(t)\right\rangle, \qquad (1.7)$$

we find that the coherence between two given states $i$ and $j$ of system $A$, is given by the overlap element $\left\langle\phi_j^B(t)|\phi_i^B(t)\right\rangle$, between the states of system $B$ conditioned upon that system $A$ was initially in state $\left|i\right\rangle$ and $\left|j\right\rangle$, respectively. For two interacting systems $A$ and $B$ the dynamics of $B$ will in general depend on the state of $A$ such that $\left|\phi_i^B(t)\right\rangle$ and $\left|\phi_j^B(t)\right\rangle$ might take different trajectories in the Hilbert space of system $B$. If the two trajectories are distinct the distance between them will typically vary in time. The overlap element $\left\langle\phi_j^B(t)|\phi_i^B(t)\right\rangle$ will therefore oscillate as function of time and the coherence of system $A$ will typically decay initially, but might still be recovered at later times. In principle system $A$ might still be used as a qubit if one knows the details of the coherence oscillations and the other system $B$ does not disturb the state of $A$ in an uncontrolled fashion.

Let us now move to a more practical example where the quantum system $A$ is initially prepared in a superposition state and is weakly coupled to an environment $E$ with a large number of degrees of freedom $\epsilon_1..\epsilon_N$. System $B$ is then replaced by a general environment composed of a large number of subsystems. In similar fashion as in the previous example, the entanglement

dynamics of the composite state can in general be written as

$$\sum_i c_i \left|s_i\right\rangle \left|e_0\right\rangle \xrightarrow{t} \sum_i c_i \left|s_i\right\rangle \left|e_i\right\rangle , \tag{1.8}$$

where $|s_i\rangle$ is a complete set of basis states for system $A$ and $|e_0\rangle$ is the initial state of the environment. The set of basis states that is robust against the perturbation induced by the environment is also called pointer states [8, 9]. The reduced density matrix of system $A$ is

$$\rho_A = \mathrm{Tr}_E(\rho) = \sum_{ij} c_i(t)c_j(t)^* \left|s_i\right\rangle \left\langle s_j\right| \left\langle e_i|e_j\right\rangle . \tag{1.9}$$

We can not necessarily assume from the outset that the states $|e_i\rangle$ are mutually orthogonal such that $\langle e_i|e_j\rangle = 0$. However, we can decompose the state of the environment $|e_i\rangle = |\epsilon_{1i}\rangle \otimes |\epsilon_{2i}\rangle \otimes ... \otimes |\epsilon_{Ni}\rangle$ in the large number of degrees of freedom composing it. Since in general the coupling between the system and the environment will result in slightly different trajectories for each subsystem of the environment, we get $\langle \epsilon_i|\epsilon_j\rangle = \alpha < 1$. Even if a typical system in the environment is very weakly perturbed by the presence of the system $S$ and $\alpha$ is close to 1 the total environmental states will therefore rapidly approach orthogonality if the number of subsystems $N$ is large $\langle e_i|e_j\rangle \approx \alpha^N \approx 0$. Still, since the full dynamics is unitary, recurrences of coherence will take place if we wait sufficiently long time. The time between recurrences will however for all practical purposes become infinitely long for a large environment, composed of maybe $N \approx 10^{23}$ degrees of freedom, or even more. In addition, realistic environments can usually not be considered to be closed. In open systems, which we will discuss in more detail later, the information about the system is irreversibly lost to a thermal bath which rapidly forgets any information about the state of the system.

As a side note, we show in fact in paper 2, that the time between recurrences of coherence in a quantum two level system coupled to an environment is much higher in an environment with frustrated internal interaction, than in a noninteracting, or ordered one. Such an environment is therefore especially dangerous if our objective is to preserve the coherence of the central quantum system, and in qubit engineering this is indeed the goal of primary importance.

## 1.4 Quantum computing and the quantum bit

A quantum computer is a machine that would exploit the full complexity of the many-particle quantum wavefunction in order to solve a computational problem. It would take advantage of the additional information in a quantum state due to quantum entanglement and make use of the superposition principle. The two principles that make quantum mechanics fundamentally different from classical physics. The context for the development of the quantum computer may be clarified by comparison with a more familiar quantum technology: the laser [10]. Humans knew very well how to make light long before they invented the laser. Since ancient times we have mastered technologies such as the fire and ways to take advantage of and reflect the sunlight. Later we have seen inventions such as the lightbulb, now in all different shapes for specific applications and more modern examples such as light emitting diodes controlled by electric fields. These light sources all has one common property in common, they are all incoherent, meaning that the electromagnetic light waves is emitted at random times and from random origins within the source. The outgoing light from these sources is therefore a statistical mixture of light with an uncontrolled, or at best, uniform distribution of phases. In a laser however, the light quanta are all generated in phase, we call it *coherent emission*. This is a quantum mechanical effect, and the *coherent light* have different properties from light emitted from classical light sources. These properties are useful for thousands of applications, from laser cooling to eye surgery, most of which were not imagined by the first laser physicists. Still, lasers does not replace conventional light sources such as lamps. In the same way a quantum computer will not be a faster, bigger or smaller version of an ordinary computer. It will rather be a different kind, engineered to control coherent quantum mechanical waves for future applications which may not necessarily be evident at present time.

### 1.4.1 The quantum bit: The quantum engineers version of Schrödinger's cat

The basic building block of the quantum computer is the quantum bit, or qubit.

In a classical computer, the basic unit of information is the bit (shorthand for binary digit). In order to store information an ordinary computer uses a register composed of many classical bits, where each bit is a physical system that can be in two distinct states, 0 or 1, e.g. two positions of an electrical switch, two distinct levels of current or voltage or two di-

rections of magnetization or polarization. In analogy with this, the qubit is a quantum mechanical system which has two basis states, e.g. $|0\rangle$ and $|1\rangle$. However, since the qubit is now quantum mechanical the superposition principle applies and the qubit can in general be in either the state $|0\rangle$ or $|1\rangle$ or in a superposition the basis states $\alpha|0\rangle + \beta|1\rangle$, where $\alpha$ and $\beta$ are complex numbers. In classical physics the cat of Schrödinger is either dead or alive. In quantum mechanics it is either dead or alive or in general a combination of dead *and* alive at the same time. Qubits can in principle be realized by all coherent systems where the dynamics is restricted to two energy levels. We will come back to different realizations of qubits in the later chapters.

### 1.4.2 A concrete example: The superconductor based flux qubit

The flux qubit is a superconducting qubit, where the fundamental units are a superconducting ring, typically fabricated on a lengthscale of 100nm, containing at least one Josephson junction. The Josephson junction is an insulating barrier preventing any classical currents to pass through, but allowing quantum mechanical tunneling of charge across the barrier. The flux qubit is illustrated in Fig. 1.4.

A superconductor is a conductor where the electrons have condensed into a single macroscopic state, a coherent phase of matter described by the quantum mechanical wavefunction $\psi(\mathbf{r}, t)$, where $\mathbf{r}$ is the spatial variable, and $t$ is time. The phase transition from the normal to the superconducting state takes place at a material specific critical temperature $T_c$, where the normal electron and hole-like excitations are separated from the superconducting condensate of Cooper-pairs [11], by an energy gap $\Delta_s(T)$, favoring the superconducting phase. The Cooper pairs are the "particles" of the superconducting phase with twice the charge of the electron, they can "split" into two normal electrons if an energy $\Delta_s(T)$ is provided, but for temperatures much below the critical temperature $k_B T \ll \Delta_S(T)$ excitations to the normal phase are exponentially blocked.

The macroscopic superconducting wavefunction $\psi(\mathbf{r}, t)$ leads to two phenomena of quantum nature which are essential for the construction of the qubit. In the flux qubit, the first phenomenon is flux quantization, the requirement that the magnetic flux through the superconducting ring should be an integer number times the basic flux quantum $\Phi_0 = \frac{h}{2e}$, where $h$ is Planck's constant and $e$ is the electron charge. The magnetic flux induced by the current is proportional to the current passing through the loop, and limits the possible current states in the loop. The flux quantization arises

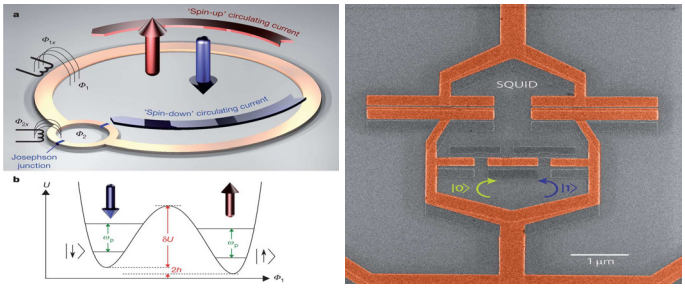


Figure 1.4: The flux qubit. To the left: Schematic visualization of the physics of a flux qubit acting as a quantum mechanical spin. The upper part shows a superconducting ring separated by two Josephson junctions in parallel. Circulating current in the ring gives rise to flux inside the loop encoding two low energy states that can exist in a superposition. In this design one has the possibility to control the external flux bias in the main loop $\Phi_1$ and in the secondary loop at the Josephson junctions $\Phi_2$. The bottom left figure shows the double well potential as a function of $\Phi_1$. When the bias flux is equal to half a flux quantum, the two states, $|\downarrow\rangle$ and $|\uparrow\rangle$, corresponding to current flowing clockwise and anti-clockwise around the loop, respectively, have similar energy. This point is called the degeneracy point. The height of the barrier is controlled by $\Phi_2$. Right figure: Electron microscope image of a real flux qubit. The superconducting loop separated by Josephson junctions is in the lower part of the figure. The upper part is circuits used for read out of the qubit state. The left figure is taken from G. Rose *et al.*, Nature 473,194198 (2011), while the right figure is taken from M. J. Biercuk Nature Physics 7, 525526 (2011)

from the criterion that the wavefunction $\psi(\mathbf{r}, t)$ should be single valued at all points on the loop. The phase $\phi(\mathbf{r}, t)$ of the wavefunction $|\psi(\mathbf{r}, t)|e^{i\phi(\mathbf{r},t)}$ can in general vary as a function of the coordinates of the loop (the current is in fact proportional to the gradient of the phase). Single valuedness of the wavefunction require that the phase can only increment by an integer number of $2\pi$ after a full revolution around the loop.

The second phenomenon is Josephson tunneling. The Josephson junction typically consists of two superconductors separated by an insulating barrier of thickness $2-3$nm, through which Cooper pairs can tunnel coher-

ently. The supercurrent through the barrier

$$I = I_0 \sin\phi \tag{1.10}$$

varies as a function of the phase difference $\phi$ between the superconducting wavefunctions on each side of the barrier. In the presence of a potential difference $V$ across the barrier, the phase difference evolve as

$$\hbar\dot{\phi} = 2eV. \tag{1.11}$$

In principle one could make a qubit from a simple LC circuit, composed of a capacitor and a inductor in series. For a dissipationless superconductor the Hamiltonian of the LC circuit is simply

$$H = \frac{q^2}{2C} + \frac{\phi^2}{2L}, \tag{1.12}$$

where $q$ is the charge on the capacitor of capacitance $C$ and $\phi$ is the flux through the loop which has inductance $L$.

The potential of this LC circuit as a function of the flux $\phi$ through the loop can be recognized as the harmonic oscillator potential, where all energy levels are equally spaced. Since qubit operations require us to manipulate the two lowest energy levels by resonant pulses without exciting higher levels, this circuit does not make a suitable qubit, a resonant pulse would trigger excitations to arbitrary high energy states. To make a controllable qubit we need a nonlinear element in order to break the harmonicity of the LC Hamiltonian given by Eq. (1.12).

The full Hamiltonian of the flux qubit with a Josephson junction reads

$$H = \frac{q^2}{2C_J} + \frac{\phi^2}{2L} - E_J \cos\left[\frac{2e}{\hbar}(\phi - \phi_{ext})\right], \tag{1.13}$$

where $q$ is now the charge on the Josephson barrier and $C_J$ is its capacitance, $\phi$ is the flux through the superconducting loop, $\phi_{ext}$ is the external flux imposed through the loop and the last term is the energy stored in the Josephson junction

$$U = \int I(t)V(t)dt = \frac{\hbar I_0}{2e}\int \sin\phi d\phi = -E_J\cos\phi \tag{1.14}$$

where $I(t)$ and $V(t)$ is given by Eqs. (1.10) and (1.11).

The potential landscape of Eq. (1.13) is a double well potential as a function of the flux coordinate, see the bottom left picture of Fig. 1.4, where the localized states in each well is named $|\downarrow\rangle$ and $|\uparrow\rangle$. These two

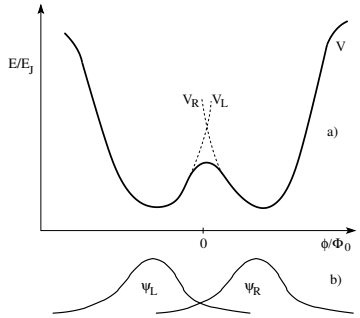


Figure 1.5: a) Double-well potential for the superconducting loop with a Josephson junction with Hamiltonian given by Eq. (1.13). b) The localized wave functions $|\psi_L\rangle$, $|\psi_L\rangle$ corresponding to the ground states in the potentials $V_L$ and $V_R$, respectively.

states differ by a single flux quantum passing through the loop. If the loop is biased by half a flux quantum $\phi_{ext} = \Phi_0/2$ the two states are degenerate.

The two states $|\downarrow\rangle$ and $|\uparrow\rangle$ might be assumed to be the ground states $|\psi_L\rangle$ and $|\psi_R\rangle$ of single well potentials $V_L$ and $V_R$ of Fig. 1.5, where $V$ is the effective double-well potential. We might now represent the Hamiltonian, Eq. (1.13), in the basis of the localized wavefunctions $|\psi_L\rangle$ and $|\psi_R\rangle$. In this representation the Hamiltonian matrix becomes

$$H = \begin{vmatrix} \langle\psi_R| H |\psi_R\rangle & \langle\psi_R| H |\psi_L\rangle \\ \langle\psi_L| H |\psi_R\rangle & \langle\psi_L| H |\psi_L\rangle \end{vmatrix}. \tag{1.15}$$

If the extension of each localized wavefunction into the barrier is small, the terms $\langle\psi_R| H |\psi_R\rangle$ and $\langle\psi_L| H |\psi_L\rangle$ can be approximated by the effective single well potentials $\langle\psi_R| V_R |\psi_R\rangle = E_R$ and $\langle\psi_L| V_L |\psi_L\rangle = E_L$, where $E_{R,L}$ is the energy of the right and left well respectively. For wells of roughly similar shape, only the relative energy difference of the two wells $E_R - E_L = \Delta$ is important.

Furthermore, if we write for the tunneling splitting element $2\langle\psi_L| H |\psi_R\rangle = \Delta_0$, the Hamiltonian, Eq. (1.13), can be expressed in the form

$$H = \frac{1}{2}\begin{vmatrix} \Delta & \Delta_0 \\ \Delta_0 & -\Delta \end{vmatrix} = \frac{1}{2}\left(\Delta\sigma_z + \Delta_0\sigma_x\right), \tag{1.16}$$

in the basis of the localized states $|\psi_L\rangle = |\downarrow\rangle$ and $|\psi_R\rangle = |\uparrow\rangle$, where $\sigma_z = \begin{pmatrix} 1 & 0 \\ 0 & -1 \end{pmatrix}$ and $\sigma_x = \begin{pmatrix} 0 & 1 \\ 1 & 0 \end{pmatrix}$ are Pauli matrices. This is the qubit Hamiltonian in the spin-$\frac{1}{2}$ formalism, since it is exactly similar to that of a spin-$\frac{1}{2}$ particle in an external magnetic field. In all the papers in this thesis, we always write Hamiltonians in the spin-$\frac{1}{2}$ representation even though the physical system is not necessarily a spin-$\frac{1}{2}$ particle. The system we consider is usually, but not necessarily, thought to be a Josephson qubit which Hamiltonian resembles that of Eq. (1.13).

### 1.4.3 Challenges to overcome

The greatest challenge to overcome in order to construct a working quantum computer is the decay of coherent superpositions of qubit states, or decoherence [12]. In order to avoid decoherence, the fundamental constituents of the quantum computer, the qubits, the gates and the wiring, need to be isolated from their environment, the rest of the universe. Any interaction between these fundamental units and other degrees of freedom will disturb the fragile quantum states encoded in the computer, resulting in leakage of information from the quantum computer to the environment.

It may seem like the slow decay of the wavefunctions due to decoherence will eventually lead to loss of the quantum information encoded in the qubits. The situation, however, is not that depressing, due to the existence of various techniques under the common name of *quantum error correction*. For a introductory review of quantum error correction see Ref. [13], while experimental realizations of this technique can be found in Refs. [14, 15, 16]. Errors in quantum computers that are beneath a critical threshold can be corrected by use of various techniques usually based on redundancy. The simplest example is simply based on storing multiple copies of the same information [12]. The main requirement for quantum computing is then that there must be possible to carry out multiple operations between the elements of the computer, the qubits, before the coherence of the wavefunction has decayed beneath the threshold for error correction.

Originally DiVincenzo [17, 18] stated a set of criteria required for the physical implementation of a fault-tolerant quantum computer. Ten years later a slightly revised set of criteria was formulated by O'Brien *et al.* [10]. We will here briefly list the main requirements.

**A scalable physical system with well characterized qubits:** We need well characterized qubits, i.e. physical systems of which the self Hamiltonian is known to a good precision, and where the dynamics is constrained

to the lowest two energy levels. In addition the computer must operate in a Hilbert space whose dimensions can grow exponentially without an exponential cost in other resources, such as space, time or energy. This point includes not only the qubits, but all the necessary components required for fabrication, including the technology used for manipulation, control and error correction.

**Initialization:** One needs to be able to initialize the qubits used as registers to an initial pure state. This is usually done either by cooling to the ground state, provided that the temperature is sufficiently low, or by a projection measurement. These two mechanisms are actually not too different from each other as one might see a projection measurement as some sort of cooling.

**Universal logic:** We need a universal set of quantum logic gates by which we can carry out unitary operations on the qubits, usually one or two at a time. An universal set of gates, is an elementary set of gates, such that any unitary operation on the Hilbert space of the quantum computer can be reduced to a finite sequence of gate operations [19]. In principle, however, quantum computers need not be made with gates. In adiabatic quantum computation, one defines the answer to a quantum mechanical problem as the ground state of a Hamiltonian. The physical system represented by the specific Hamiltonian is realized by choosing a specific set of couplings in a qubit network. The problem is then solved by adiabatically evolving the system to the ground state by slowly turning on the interactions [20].

**Long relevant decoherence times, much longer than the gate operation time:** The problem of preserving the coherence of the qubits is the most fundamental problem in quantum computing since interaction with environments can never, even in principle be reduced to zero. The works in this thesis is devoted to this problem, which therefore does not need further mentioning here.

**Correctability and readout:** It must be possible to extract the entropy of the computer in order to maintain the purity of its quantum state. To achieve this we need error correction protocols, and a possibility to correct errors before the purity of the quantum state is reduced beyond the threshold where error correction is impossible. If this is achieved the computer can in principle run accurately for infinite time. In addition we require the ability to read out, or measure, the state of the qubits. The measurement has to be sufficiently reliable, the outcomes of the measurement need

to accurately reflect the state of the qubit, see Ref. [21] for an example in a superconducting qubit. In addition, it should be fast on the timescale of the decoherence time of the qubits, and if many measurements is required as in a quantum error correction protocol, the measurements should preferably not add noise to the state of the qubit. Such measurements are called quantum non-demolition measurements [22], and also initializes the system into the measured state. One does not strictly need non demolition measurements, since multiple copies of the qubit information in a single basis can be constructed, but it is desirable in order to avoid storage of additional information.

In isolation each of these challenges are possible to overcome. For example, long coherence times can be easily achieved in trapped ions or atoms, or for nuclear spins. In these systems however, gates and scalability is the major issue. One core problem in the design of a quantum computer is that the different basic criteria above tend to be in conflict. Those parts of the system necessary to achieve rapid measurement must be turned strongly 'on' for error correction and read-out, but need to be strongly 'off' to preserve the the coherence of the qubits [17]. The central challenge in building a quantum computer is maintaining simultaneously the abilities to control the qubits, to measure them and to preserve their strong isolation from uncontrolled parts of the environment.

# Chapter 2

# Noise in qubits

In this chapter we will describe the relevant general concepts and terminology used in the study of noise in qubits, with emphasis on solids state qubits and in particular superconductor based devices. We will also give a brief overview of basic theory used to describe the noise.

A qubit might in general interact with every degree of freedom in its environment. The atoms, the molecules, the electrons and the nuclear spins, but also with collective degrees of freedom such as exitons, polarons, phonons and with the degrees of freedom of the electromagnetic field which are photons.

For specific physical realizations of qubits, however, some degrees of freedom are much more of a problem for the decoherence of the qubit than others. Usually the most important noise sources are those who couple most strongly to the qubit, but other factors such as the nature of the coupling and the frequency of the noise they generate is in many cases equally important.

In order to improve the coherence time of qubits it is crucial to know the nature of the most major noise sources in order to develop countermeasures such as better isolation from the most dangerous noise sources or protocols to minimize the impact of the noise on the qubit, such as e.g. dynamical decoupling, or control at the optimal point [23, 24, 25, 26, 27, 28].

## 2.1 Decoherence, relaxation, dephasing and the nature of the coupling to the environment

Before we proceed, it is useful to discuss different mechanisms of noise in qubits. Previously, in Sec. 1.3, we discussed the general idea of decoherence of a system due to entanglement with its environment and found that the entanglement in general reduces the coherence of the system. This is a crude picture of decoherence. If we want to construct a real qubit we need more information. On which timescale does the qubit decohere? What is the functional time dependence of the degree of coherence? Do some states decay faster than others? Those are questions that might be essential in constructing a qubit. In principle all qubits will eventually decohere, if we wait long enough, but if the decay of coherence is sufficiently slow, we might potentially correct the error by application of quantum error correction before the information is irreversibly lost [29, 30, 15, 12].

### 2.1.1 Relaxation and dephasing

The nature of the coupling to the environment is important for the qualitative features of the decoherence process. Consider for instance the following Hamiltonian for a qubit coupled to the environment through e.g. the charge on a Cooper pair box

$$\bar{H} = \frac{1}{2}\left[(\Delta\tau_z + \Delta_0\tau_x) + \nu\tau_z X\right] + H_{bath}, \tag{2.1}$$

where $\tau_\alpha$ are the Pauli matrices and the charge on the Cooper pair box is given by $\tau_z$, $\nu$ is the qubit-environment coupling parameter, $X$ is an operator of the environment sensitive to the qubit charge and $H_{bath}$ is the Hamiltonian of the environment.

Diagonalized in the eigenbasis of the qubit, the Hamiltonian, Eq. 2.1, becomes

$$H = \frac{1}{2}\left[E\sigma_z + \nu\left(\sigma_z X\cos\theta + \sigma_x X\sin\theta\right)\right] + H_{bath}, \tag{2.2}$$

where $E = \sqrt{\Delta^2 + \Delta_0^2}$, $\theta = \tan^{-1}\left(\frac{\Delta_0}{\Delta}\right)$ and $\sigma_\alpha$ are the Pauli matrices in the energy eigenbasis of the qubit. We denote the eigenstates of $\sigma_z$ by $|+\rangle$ and $|-\rangle$.

Without the coupling to the environment, the dynamics of the qubit is trivial. An arbitrary quantum state $|\psi\rangle = \alpha|+\rangle + \beta|-\rangle$ will simply

pick up a phase due to the energy splitting of the qubit, such that $|\psi(t)\rangle = \alpha e^{\frac{-iEt}{2\hbar}} |+\rangle + \beta e^{\frac{iEt}{2\hbar}} |-\rangle$. Visualized on the Bloch-sphere, see Section A.2, the qubit state will precess around the z-axis, equivalent with a spin-$\frac{1}{2}$ particle in a magnetic field. Environments coupling to the qubit in the eigenbasis of its intrinsic Hamiltonian give rise to what we call pure dephasing of the qubit. In our specific Hamiltonian given by Eq. (2.2), the qubit-environment interaction term proportional to $\cos\theta$ commutes with the intrinsic qubit Hamiltonian, $[E/2\sigma_z, \nu\cos\theta\sigma_z] = 0$, such that no transitions between the eigenstates of the qubit is induced by this term. This term give rise to decay of coherence in the qubit on a timescale $T_\phi$, and is also called longitudinal noise, due to its action parallel to the axis of the intrinsic Hamiltonian of the qubit. Since no transitions between the eigenstates occur, pure dephasing processes can not account for energy transfer between the qubit and its environment.

The effects of pure dephasing is easily explainable in the classical picture, where $X = \xi(t)$ models classical fluctuations in an environmental variable coupling to the qubit. The wavefunction of the qubit will pick up an additional component to its phase due to the fluctuations in $X$ and the solution of the Schrödinger equation is

$$|\psi(t)\rangle = \alpha e^{i(\phi(t)+\delta\phi(t))} |+\rangle + \beta e^{-i(\phi(t)+\delta\phi(t))} |-\rangle , \tag{2.3}$$

where $\phi(t) = \frac{iEt}{\hbar}$ and $\delta\phi(t) = \frac{\nu\cos\theta\int_0^t \xi(t')dt'}{2\hbar}$. The wavefunction has picked up a contribution to its relative phase $\delta\phi(t) = -\nu\cos\theta\int_0^t \xi(t')dt'$. Averaged over the individual realizations stochastic fluctuation process $\xi(t)$ one finds a decay of the phase coherence of the qubit $D(t) = \langle e^{i\delta\phi(t)}\rangle$. In the quantum picture the loss of coherence is due to the decay of the overlap between the two bath states $|E^+(t)\rangle$ and $|E^+(t)\rangle$ produced by the entangling dynamics due to the qubit being in the state $|+\rangle$ or $|-\rangle$, as explained in Sec. 1.3. For a more detailed description of the two pictures, see e.g. Ref. [31].

Interaction terms that couple to the qubit in the transverse direction to its own Hamiltonian will induce transitions between the eigenstates of the qubit. In the presence of transverse noise, such as the term $\nu\sin\theta\sigma_z X$ of Eq. (2.2), the occupation number in each of the qubit states is not conserved, i.e. the size of the coefficients $\alpha$ and $\beta$ can change in time. This term determines the characteristic time $T_1$ in which the qubit relaxes towards the thermal equilibrium state of the environment and is also called the spin-lattice relaxation time. The other characteristic one often encounter in the qubit literature is the dephasing time $T_2$, describing the timescale at which the phase information of the qubit decays.

Visualized on the Bloch sphere, see Fig. 3.2.1 where $\gamma_1 = 1/T_1$ and $\gamma_2 = 1/T_2$ and the z-axis denotes the population level of the energy eigenstates

of the qubit, the transverse noise is responsible for relaxation parallel to the z-axis while the decay in the equatorial plane takes place on a timescale given by [32]

$$\frac{1}{T_2} = \frac{1}{2T_1} + \frac{1}{T_\phi}.$$

Thus the decay perpendicular to the z-axis has a component both from the pure dephasing term and from the relaxation term. Note that these expressions are derived based on the assumption that the qubit couples weakly to the environment such that a perturbative approach can be applied. If the qubit is strongly coupled, i.e. in resonance with some degrees of freedom of the environment [33], the time evolution is governed by a complex interplay between both the longitudinal and the transverse coupling and will require more detailed treatment.

In the weak coupling limit, under the additional assumption of a Gaussian correlated noise, one finds that the the relaxation rate of the qubit is given by [34]

$$\frac{1}{T_1} = \nu \cos^2\theta S(E),$$

where $S(E)$ is the noise spectrum of the environment at the eigenfrequency of the qubit. We also have that

$$\frac{1}{T_\phi} = \nu \frac{\sin^2\theta}{2} S(0), \tag{2.4}$$

i.e. the pure dephasing rate is proportional to the noise spectrum of the environment at zero frequency. These formulas are only exact in the limit of infinite observation times $t$, for finite $t$ a distribution of frequencies are relevant to the decoherence, which is intuitively more reasonable. For pure dephasing noise in the Gaussian approximation we have [35]

$$\frac{1}{T_\phi} = 2\nu \sin^2\theta \int_{-\infty}^{\infty} \frac{\sin^2(\omega t/2)}{\omega^2} S(\omega) d\omega.$$

The message we can remember is, however, that the most important contribution to pure dephasing noise origins from the low frequency part of the noise spectrum, while the most important contribution to transverse noise origins from frequencies close to resonance with the qubit. This knowledge was used in paper 1. Typically, at least in solid state qubits, one finds that the pure dephasing time is shorter than the relaxation time, and is therefore the most important limiting factor preserving qubit coherence.

### 2.1.2 Quantum noise vs classical noise

In the literature one often makes the distinction between classical noise and quantum noise. Sometimes there might be some confusion related to these concept. Here we will briefly clarify what we mean by quantum and classical noise.

In classical physics, the study of a noisy time dependent quantity usually involves its spectral density $S(\omega)$, which is given by the autocorrelation function of the noisy quantity we are interested in. The study of quantum noise in the perturbative limit, the limit where the coupling between the noise source and e.g. the qubit is sufficiently small in order to be treated by perturbation theory, is analogous to the classical case in that we might define the quantum spectral density by the two time correlation function

$$S_{xx}(\omega) = \int_{-\infty}^{\infty} dt e^{i\omega t} \langle \hat{x}(t)\hat{x}(0)\rangle \,, \tag{2.5}$$

where $\hat{x}(t)$ is a operator representing the physical quantity giving rise to noise in the qubit.

The fundamental difference between quantum and classical noise is due to the fact that the quantum operator $\hat{x}(t)$ may not necessarily commute with itself at different times. The correlator $\langle \hat{x}(t)\hat{x}(0)\rangle$ is therefore in general complex in the quantum case, while classically it is of course always real. Classically the spectral density is always symmetric, $S(\omega) = S(-\omega)$. Quantum mechanically, however, since the correlator is now allowed to be complex, the spectral density is no longer necessarily symmetric in frequency, meaning that $|S(\omega) - S(-\omega)| \geq 0$.

For a quantum system subject to quantum noise from a noise source in thermal equilibrium, one finds from a simple golden rule calculation that the rate for transitions between the eigenstates of a qubit with frequency $\omega_{01} = \sqrt{\Delta^2 + \Delta_0^2}/\hbar$ is given by the spectral density of the noise source, $\Gamma_{01} \propto S(-\omega_{01})$ and $\Gamma_{10} \propto S(\omega_{01})$, where $\Gamma_{01}$ is the transition rate from the ground state to the first excited state and vice versa for $\Gamma_{10}$. Since the two rates are required to satisfy detailed balance the quantum noise the positive and negative frequency part of the quantum noise spectrum need to satisfy $S(\omega_{01}) = e^{\beta\hbar\omega_{01}} S(-\omega_{01})$. The quantum noise spectra is therefore in general asymmetric and the degree of asymmetry depends on the temperature of the noise source.

If the Hamiltonian describing the interaction between the quantum system and the noise source commutes with the Hamiltonian of the quantum system itself, then the noise source cannot induce direct transitions between the eigenstates of the system. It may, however, disturb the eigenfrequencies

of the system and thereby its relative phases, giving rise to pure dephasing in the qubit. In this case one finds [36] that the pure dephasing rate is given strictly by the symmetric in frequency part of the noise spectrum, i.e. by $S(-\omega_{01}) + S(\omega_{01})$. Therefore the quantum behavior of the noise source is not important for the pure dephasing rate $1/T_\phi$ of the qubit, but might be essential if we want to find the relaxation time $T_1$.

## 2.2 A brief outline of general theories describing noise in qubits

Textbooks in physics tend to describe ideal situations, where the physical system is isolated. For these systems we can, at least in some cases, write down the equations of motion for a the few degrees of freedom involved and find analytical solutions for the dynamics under appropriate physical assumptions about the system. In general, however, the systems we encounter in nature are not isolated, they always interact with their environment.

In classical physics the environmental interaction is usually unproblematic. When discussing the forces of a rigid body, or the acceleration of a car, the small details of the environment are usually unimportant compared to major mechanical forces, or can be treated by collective parameters such as temperature, wind resistance etc. In quantum physics however, the role of the environment is much more special and subtle. When a quantum system interact with an environment it looses its quantum coherence and behaves like a classical system for all practical purposes [37, 38]. Even though candidates for qubits are among the best protected quantum systems against environmental noise that we hope to technologically take advantage of, they are still open quantum systems and has to be described as such [39].

### 2.2.1 Open systems

A closed quantum system decoupled from its surrounding environment is described by unitary time evolution. In general, and open system is a quantum system $S$ which is coupled to another quantum system $E$ called the environment. It can therefore be thought to be a subsystem of the combined system $S + E$, which, in turn, might be considered to be a closed system governed by Hamiltonian dynamics. The total Hamiltonian for this system can be denoted

$$H = H_S + H_E + H_{SE}, \tag{2.6}$$

where $H_S$, $H_E$ are the internal Hamiltonian of the system and the environment, respectively, and $H_{SE}$ describes the interaction between the two systems. The environment might also be a reservoir, an environment with an infinite number of degrees of freedom. A heath-bath or bath is a reservoir in thermal equilibrium. The dynamics of the total system is given by the von Neumann equation

$$\dot{\rho}(t) = -\frac{i}{\hbar}\left[H(t), \rho(t)\right] \tag{2.7}$$

and the reduced density matrix of the system is obtained by the tracing over the degrees of freedom of the environment $\rho_s = Tr_E\{\rho\}$. In practice, however, unless the environment consist of only a few degrees of freedom, solving the exact dynamics of the total system is far too complicated. Neither are we interested in the exact details of the environmental dynamics. Therefore, when treating open systems, one generally use effective models where the action of the environment on the system is captured by a simplified model.

### 2.2.2 Spin-boson model and the Master equation

Traditionally, since one did not understand the details of the sources of decoherence in qubits, one described the environment as an ensemble of harmonic oscillators. The standard models for the harmonic oscillator bath, one develop is based on the models of Caldeira and Leggett [40, 41], and Feynman and Vernon [42]. For a review of the spin-boson models, where a quantum two-level system is coupled to a dissipative environment , see Ref. [43].

These models are usually solved by use of the Master equation, where one makes approximations in order to obtain an effective equation for the dynamics of the reduced density matrix of the system, without explicity keeping track of the details of the environment.

The most commonly used Master equations for the reduced density matrix of the system $\rho_S$ are on the form

$$\dot{\rho}_S(t) = \hat{\mathcal{L}}[\rho_S(t)] = -\frac{i}{\hbar}\left[H'_S(t), \rho_S(t)\right] + \hat{\mathcal{D}}[\rho_S(t)], \tag{2.8}$$

where $\mathcal{L}$ and $\mathcal{D}$ are superoperators acting on $\rho_S$. [39] Here the first term of the right hand side is the unitary part of the equation and the nonunitary part $\hat{\mathcal{D}}[\rho_S(t)]$ is due to decoherence. An explicit derivation of the master equation for the system studied in paper 1 is given in Appendix B.2. Generally, the Hamiltonian entering the unitary part of the equation is not

identical to the unperturbed free Hamiltonian $H_S$ of system $S$ since the environment is perturbing the free Hamiltonian, leading to a renormalization of the energy levels of $S$.

To obtain the Master equation on the form given by Eq. (2.8), one makes use of two approximations, commonly referred to as the Born-Markov approximation. If one assume that the correlation time $\tau_c$ of the environment is much shorter than the timescale for intrinsic dynamics of the qubit $1/\omega_q$, any self-correlation within the environment created by the coupling to the system will decay rapidly compared to the timescale over which the state of the system varies noticeably. This approximation, where memory effects in the environment is neglected is called the Markov approximation. Furthermore, if the coupling to the environment is sufficiently weak and the environment is a reservoir that is not altered statistically by the interaction with the environment, one might assume that the density matrix of the composite system is a product state at all times

$$\rho(t) \approx \rho_S(t) \otimes \rho_E, \tag{2.9}$$

where $\rho_E$ is constant in time.

## 2.3 Noise in solid state devices and qubits

Noise is present in every real solid state material and is therefore an intrinsic problem encountered in all kinds of devices based on solids. As an example, the voltage drop $V(t)$ across a resistor of resistance $R$ is found to fluctuate as a function of time even if the applied current is constant in time ($I(t)$ =const.). The obvious explanation for this voltage fluctuations is the thermal agitation of the charge carriers in the conductor, but also other sources might potentially contribute to the noise. In this section we will briefly describe the main mechanisms which gives rise to noise in solid state materials.

### 2.3.1 Johnson-Nyquist noise

Already in 1927 Johnson studied the intrinsic voltage fluctuations in a range of materials which was not limited to solids [44]. Johnson simply studied the intrinsic fluctuations in the voltage across the materials in equilibrium at zero bias current, in addition he measured the resistance of each sample material. It was found that the voltage fluctuations were proportional to the resistance of the material.

The results of Johnson were first interpreted by Nyquist by use of thermodynamic arguments [45], and have later been generalized in the

fluctuation-dissipation theorem [46] which states that the thermal fluctuations in equilibrium can be related to the dissipation in a non-equilibrium situation.

In an electrical circuit, such as the simple resistor considered above, the voltage fluctuations at zero bias current ($I(t) = 0$) can be described by its spectral density [47],

$$S_V(\omega) = \sqrt{\frac{2}{\pi}} \int_0^\infty C_V(\tau) \cos(\omega\tau)\, d\tau,$$
$$C_V(\tau) = \langle V(\tau)V(0)\rangle - \langle V\rangle^2 . \tag{2.10}$$

The Johnson-Nyquist formula $S_V(\omega) = 4k_BTR(\omega)$ states that the voltage fluctuations at frequency $\omega$ in equilibrium can be related to the dissipation at the same frequency $R(\omega)$. This is special case of the fluctuation dissipation theorem applied to an electrical circuit.

In most conductors one finds that resistance is approximately frequency independent for a wide range of frequencies, $R(\omega) = R(0)$ for $\omega < 10^{10}$Hz [47]. The Johnson-Nyquist formula therefore gives that this thermal noise is frequency independent (white noise) except at very high frequencies.

The Johnson-Nyquist noise is theoretically well understood and is unavoidable in any dissipative material, i.e. not in superconductors below the critical temperature. However, the magnitude of Johnson-Nyquist noise can in principle be reduced arbitrarily by reducing the temperature. At the temperatures ($T < 1$K) used in mesoscopic quantum devices such as qubits, Johnson-Nyquist noise is typically not the major issue.

### 2.3.2 Shot noise

Shot noise, also called counting noise, is intrinsic to all measurements which involves discrete quanta. Since measurements of currents or voltages inevitably involves the build up of electric charges, the discreteness of the electric charge will lead to finite current pulses at the electrodes used to measure a given sample.

Shot noise is encountered in all transport measurements, but is most important in quantum transport such as e.g. transport through tunneling barriers, quantum point contacts and quantum dots [48]. This is due to the fact that the relative importance of shot noise in a current measurement depends of the size of the current. At the low currents, which is typically used in quantum devices, the shot noise due to the finiteness of the electric charge can make a significant fluctuation is the total current.

Since the state of a qubit, e.g. the presence of a electron in a quantum dot, is typically measured by its influence on the current through a conductor interacting with the quantum dot, shot noise is important also in qubits. The discreteness of the charge through the same conductor, might also lead to fluctuations in the energy level of the quantum dot, and therefore to dephasing.

Shot noise is quite easily distinguished from Johnson-Nyquist noise since the former is temperature and frequency independent [48], while the Johnson-Nyquist noise is proportional to the temperature.

### 2.3.3 Low frequency noise: $1/f$ noise

$1/f$-noise (or flicker noise) refers to noise with a frequency power spectrum inversely proportional to the frequency $S(f) \propto 1/f$. Such a noise spectrum has been observed in a wide range of very different materials [47] and was for a long time, a fundamental problem in condensed matter physics. The physical origin of $1/f$ noise is still in many cases not understood in detail, one does not believe that there is a single universal source of $1/f$-noise explaining this noise in all systems where it is observed.

Noise with a $1/f$ spectral density is especially important in qubits due to the fact that the pure dephasing rate of the qubit is determined by the low frequency tail of the power spectrum, see Eq. (2.4). $1/f$-noise is therefore in many cases considered to be the most important issue in extending the coherence time in solid state qubits.

A wide range of different mechanisms, which we will not discuss here, have been considered in order to theoretically explain the observed $1/f$ noise [47, 49]. To a large extent, however, one agrees that $1/f$ noise is in many materials well described by an appropriate distribution of activated random processes, each with a Lorentzian spectrum

$$S(\omega) \propto \frac{\tau}{1+\omega^2\tau^2}, \tag{2.11}$$

where $\tau = 1/\gamma$ is the characteristic time of the random process.

Following Dutta and Horn, if the distribution of characteristic times is $D(\tau) \propto 1/\tau$ in a range $\tau_1 \leq \tau \leq \tau_2$ then the integrated spectral density will have the observed frequency dependence

$$S(\omega) \propto \int \frac{\tau}{1+\omega^2\tau^2} D(\tau) d\tau \propto \frac{1}{\omega}, \tag{2.12}$$

for $\tau_2^{-1} \leq \omega \leq \tau_1^{-1}$. This idea was originally presented already in 1939 by M. Surdin, see Ref. [50].

For thermally activated random processes $\tau = \tau_0 e^{E/kt}$, where $E$ is the activation energy for a given transition, the appropriate distribution of characteristic times is obtained if the energy distribution is uniform, $D(E) = const.$ for $kT\ln(\tau_1/\tau_0) \leq E \leq kT\ln(\tau_2/\tau_0)$.

The physical origins of the Lorentzian random process is well motivated in amourpous solids, or any material with amorphous regions such as surface oxide layers. In amorphous solids measurements of the heat capacity has indicated the presence of tunneling two level systems with the appropriate distribution of energy splittings $D(E)$ [49]. Other tunneling mechanisms has also been proposed, such as tunneling between the conduction band and impurity levels, however these effects can not explain the $1/f$ noise observed in metals. In many qubit design, especially those based on superconductors and Josephson junctions, the main source of decoherence is usually thought to origin from two level systems in the amorphous substrates and oxide layers used to fabricate the device. The next section will largely be devoted to this specific noise source.

# Chapter 3

# Decoherence due to quantum or classical two level systems

As mentioned in the previous chapter, a major source of noise in solid state electronic devices, and superconducting qubits in particular, are thought to origin from fluctuating two level systems.

Two level systems (TLSs) are systems which can classically exist in two distinct states. Examples of two level systems are systems where a current or voltage is allowed to switch between two set levels, a charge configuration tunneling between two metastable states and the spin degree of freedom of an electron or proton. The systems with switching current or voltage levels are usually examples of classical TLSs or fluctuators, while the electron spin usually needs to be treated quantum mechanically, as a degree of freedom described by a quantum state vector in a two-dimensional Hilbert space. The quantum TLS can exist in all possible complex superpositions of the two chosen basis states, making the problem more challenging than its classical counterpart.

In between these two extremes, the classical and the quantum TLS, we find a spectrum of systems which behaves more or less quantum mechanically depending on the interaction with its own environment, just like the qubit itself. In paper 4, we show that the quantum model for the TLS can often be reduced to an equivalent classical model that might simplify further analysis of the problem.

Decoherence of qubits due to other two level systems is relevant in all the

works presented in this thesis, especially to the papers 1, 2 and 4 where the noise source is explicitly assumed to be TLSs. In paper 3 we do not make any explicit assumptions about the nature of the noise, since the treatment is relevant for general noise. Still the most relevant origin of the noise is fluctuating TLSs.

In this text we will often refer to a qubit which interact with other TLSs. This might cause some confusion since the qubit is of course also a TLS. When referring to a TLS in this context we mean TLSs in the environment of the qubit. The qubit or quantum device is always explicitly referred to as the qubit or the central system.

## 3.1 The classical and the quantum theory for the two level system: The microscopic origin of the two level system

The microscopic source of decoherence in solid state qubits vary in different physical realizations of the qubits and in many realizations the microscopic origin of the noise is still debated in the literature. There are, however, experiments which convincingly shows direct signs of TLSs in the Josephson junction coupling to the superconducting qubit [51, 52, 53]. In addition, for example in GaAs double quantum dots, the major source of both pure dephasing and relaxation is thought to be due to the hyperfine interaction between nuclear spins in the material and the electron spin occupying the quantum dot [54, 55, 56, 57]. In these systems the microscopic understanding of the noise sources has lead to countermeasures such as polarizing the spin bath [58, 59] and optical quantum measurements which prepares the spin environment in favorable states [60]. However, there is usually multiple sources of decoherence, and phonons are also argued to be important [61] in GaAs quantum dots. These phonons couple indirectly to the electron in the quantum dot through the orbital degree of freedom of the electron, which again couple to the spin due to the spin-orbit interaction [62, 63].

While some strong experimental data convincingly points in the direction of TLSs as an important noise source, other sources of noise might still be important. The microscopic origin of the noise is often guessed based on knowledge of the materials used to fabricate the qubit, e.g. of the amorphous substrate in the Josephson junction of the superconductor based qubits [64]. But information from the decoherence of the qubit itself can also be used in order to gain information about the nature of the noise sources. In this sense the qubit is used as a spectrometer, measuring the characteristics of its environment [36, 65]. For illustrating the nature of the

noise sources in qubits, we move to an example relevant in all superconductor based qubits, and in particular for the charge qubit.

### 3.1.1 Microscopic origin of the fluctuating two level system in glasses, an example

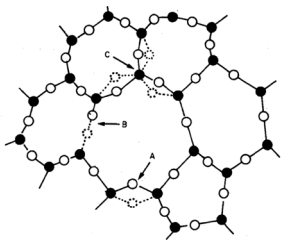


Figure 3.1: Two dimensional cut through the structure of $SiO_2$ in the amorphous phase. The atoms in positions $A$ and $B$ can tunnel between two energetically favorable positions in an effective energy landscape which resembles a double well potential(see Fig. 3.2). The potential energy of the atom in each of the wells are close, but correspond to spatially separated positions. The tunneling between the two minima can potentially lead to noise and decoherence of a qubit in the vicinity of the material. Figure is taken from Galperin *et al.* Advances in Physics Vol. 38 No. 6 p. 669-737 (1989)

Empirically one often finds a noise in qubits and other single particle tunneling devices, which has a distribution of spectral frequencies resembling a $1/f$-spectrum [66, 67, 68, 69, 70, 51], or see Refs. [47, 49, 71] for reviews. The $1/f$-spectrum points in the direction of an ensemble of TLSs with an $1/\gamma$ distribution of relaxation rates as the source of this noise [71]. In superconductor based qubits, an important source of decoherence is believed to be the tunneling of microscopic charges, such as electrons from the conduction band to impurity levels, giving rise to fluctuations in the Josephson energy of the junction. In addition, fluctuations in the critical current are thought to be due to atomic defects in the oxide barrier of the tunnel junction, see Fig. 3.1. The core features of these defects can be modeled by fluctuating TLSs, switching between two metastable states. Signatures of these TLSs have been observed in avoided level crossings in the spectroscopy of the qubit, suggesting a TLS in resonance with the

qubit, located in the tunnel junction [51, 52, 53]. Furthermore, ensembles of charged TLSs are thought to be located in the amorphous substrate used to fabricate the qubit and in the oxide layer covering electrodes [72].

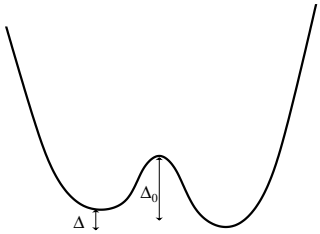


Figure 3.2: A double well potential for a tunneling system describing the 2D projection of the effective potential landscape typically encountered in amorphous solids used in qubit fabrication such as the one shown in Fig. 3.1. A particle experiencing this effective potential can quantum mechanically tunnel between the two energy minima of which are separated by a energy barrier of height $\Delta_0$. The energy difference between the minima is given by $\Delta$.

The theory describing these fluctuating TLSs was developed a long time ago in order to describe the heat capacity of glasses such as vitreous silica [73, 74, 75, 76]. In insulating crystals the heat capacity was already well known, described by the Debye theory where the low temperature behaviour is determined by acoustic phonons and has a $\propto T^3$ temperature dependence. In silica, on the other hand, there were empirical evidence of temperature dependence proportional to $T$. In addition other data of the low temperature thermal behaviour was also not in correspondence with the theory, such as the conductivity and sound velocity [77, 78, 79]. The model of TLSs in glasses was used by Phillips and Anderson *et al.* in order to explain the discrepancy [74, 75]. The model of decoherence by TLSs was developed even earlier in order to describe spectral diffusion in glasses in relation to spin resonance, where resonant spins are disturbed by other, non-resonant spins which can be modelled by the classical fluctuator model [80, 81]. In the following we will describe the physics behind the model for the TLSs encountered in glasses.

In a perfect crystal, each atom is constrained by symmetry to occupy a single potential minimum. Defects, however, might be represented as interstitial or substitutional impurity atoms or molecules moving in a multi-minima effective potential provided by its neighbours, e.g. a double well

potential as shown in Fig. 3.2. At sufficiently low temperatures the dynamics is restricted to the lowest energy states. If the potential is such that there is two potential minima reasonably close in energy, $\Delta \sim kT$, but also significantly lower than any other minima, then the dynamics is restricted to the states where the particle exists in either of the potential minima, or in the quantum analogue, a superposition of the two. The number of defects contributing at small temperatures is only a small fraction of the total, most defects are essentially immobile below the glass transition temperature [73]. If such a defect is charged, the tunneling between the minima of the potential well will give rise to noise in the electric field acting on the qubit. And even if no charge is associated with the defect, the tunneling might give rise to a deformation potential which might alter the energy levels of the qubit and therefore lead to dephasing.

### 3.1.2 The origin of the Hamiltonian used to describe the TLS

Knowing the microscopic origin of our model, we might think of it simply as a single charged particle in a potential, e.g., the double well potential of Fig. 3.2. This model can be mapped to Hamiltonian

$$H = \frac{1}{2}\left(\Delta\sigma_z + \Delta_0\sigma_x\right), \tag{3.1}$$

where $\sigma_\alpha$ are the Pauli matrices along the component $\alpha$, $\Delta$ and $\Delta_0$ are the energy splitting and the tunneling element, respectively. [73] The model is equivalent to that of a spin particle in a magnetic field. The energy splitting and the tunneling element can be calculated from the specific shape of the potential. If the tunneling element is small, then the energy splitting $\Delta$ can be found from the double well potential as shown in Fig. 3.2. The tunneling element is given by the overlap element, $\langle\psi_L|H|\psi_R\rangle$, between the wavefunctions localized in the right and left well. It is roughly given by the height of the potential barrier, as shown in Fig. 3.2, but in general it needs to be calculated from the specific shape of the potential. However, in practice we are seldom interested in the exact details of the TLS. In order to reduce the noise in qubits by countermeasures, it is important to identify what kind of systems are responsible for the noise, their number, their rough parameter distribution and perhaps most importantly, where they are located. To the best of my knowledge, it is usually difficult to justify detailed first principles calculation of parameters based on models of real materials.

The configurational defect, or for us, the TLS, does in general interact with its environment. Lattice vibrations, which quantized modes are called

phonons, might disturb the shape of the potential and the energy splitting of the two wells. Phonons, and other (quasi-)particles might also entangle with the positional degree of freedom of the particle in the well, and might cause resonant transitions between the eigenstates of $H$. Depending on the strenght and nature of the environmental interaction, the particle will behave to a larger or smaller extent as an effective classical fluctuator, switching between its two lowest metastable states. If the environmental interaction is weak, however, the TLS is governed by its Hamiltonian $H$ and behaves like a coherent quantum system, much like the qubit itself. There is, however, no sharp transition between the quantum and the classical regime, in paper 4 we discuss this transition in further detail.

### 3.1.3 Quantum model for the decoherence of the qubit by TLSs

A general quantum model of a qubit interacting with an ensemble of TLSs again interacting with their own environment can be cast in the form

$$\begin{aligned} H &= H_q + H_f + H_i + H_e + H_{fe}, \\ H_q &= \frac{1}{2}\sum_i \Lambda_i \tau_i, \qquad H_f = \frac{1}{2}\sum_i \Delta_i \sigma_i, \\ H_i &= \frac{1}{2}\sum_{ij} \xi_i \tau_i \sigma_j \qquad H_e = \sum_i \omega_i \hat{I}_i, \\ H_{fe} &= \sum_{ij} \nu_{ij} \sigma_i \hat{I}_j, \end{aligned} \tag{3.2}$$

where $q$, $f$ and $e$ denote the qubit, the TLS and the environment, respectively, $\tau_i$ and $\sigma_i$ are Pauli matrices acting in the Hilbert space of the qubit, and the TLS, respectively, and $\hat{I}_i$ are a complete set of generators in the Hilbert spece of the environment. Generally this model is not analyticaly tractable, and if the total number of degrees of freedom is greater than $\sim 20$ it is not even solvable directly by numerical techniques in the most powerful of present days computers.

Depending on what we are interested in, the model is often simplified. In this thesis we are mainly interested in the pure dephasing of the qubit. When the qubit is subject to pure dephasing, the environment can only alter the energy levels of the qubit, no relaxation processes are allowed.

The Hamiltonian, Eq. (3.2), can then be simplified to the following one

$$\begin{aligned} H &= H_q + H_f + H_i + H_e + H_{fe}, \\ H_q &= \frac{1}{2}E\tau_z, \qquad H_f = \frac{1}{2}\left(\Delta\sigma_z + \Delta_0\sigma_x\right), \\ H_i &= \frac{1}{2}\xi\tau_z\sigma_z, \end{aligned} \tag{3.3}$$

where the interaction Hamiltonian $H_i$ commutes with the self-Hamiltonian $H_q$ for the qubit, $[H_q, H_i] = 0$. One should then in principle also specify the Hamiltonian for the environment $H_e$ and the TLS-environment interaction $H_{fe}$. This is, however, not always done in practice. In place one construct effective models for the TLS, where the action of the environment on the TLS is captured by a smaller set of parameters, such as the temperature of the bath, the effective relaxation time $T_1$ and the pure dephasing time $T_2$ of the TLS. We will come back to one of these effective phenomenological models when we later discuss the Bloch-Redfield model.

### 3.1.4 Qubit decoherence by a set of classical fluctuators

In the quantum models for decoherence of qubits, decoherence is due to entanglement between the qubit and its environment. The entanglement results in the disappearance of coherence in the reduced density matrix for the qubit after the degrees of freedom of the bath is traced out. In many cases, however, as discussed in paper 4, one can neglect the transfer of quantum information from the qubit to the bath and consider the qubit subject to random classical external fields. In order to describe the noise acting on qubits due to fluctuations in glasses, one conventionally make use of the random telegraph noise model, where the external field switches randomly between two positions [82, 83, 84, 35, 71]. Telegraph noise is also called burst noise, or popcorn noise due to its abrupt nature. The model is also used for describing noise in semiconductor devices, such as MOSFETS, p-n junctions, tunnel junctions and SETs [85, 86, 87, 88].

The telegraph noise model can be described by the following Hamiltonian for the qubit

$$H_i = \frac{1}{2}(\mathbf{B} + \nu_i(t)\mathbf{g}) \cdot \vec{\sigma}, \tag{3.4}$$

where $\sigma_{x,y,z,}$ are the Pauli matrices acting in the Hilbert space of the qubit and $\mathbf{B}$ and $\mathbf{g}$ are vectors describing the self-Hamiltonian (external field) of the qubit and the effective noise field due to the fluctuator, respectively.

Conventionally one chooses the coordinate frame such that $\mathbf{B} = B\hat{z}$.The component of $\mathbf{g}$ parallell to $\mathbf{B}$ is responsible for pure dephasing of the qubit, while the perpendicular component give rise to relaxation. The noise field (or fluctuator) switches randomly between the states $\nu_i(t) = \pm 1$, with rates given by $\Gamma_{-+}$ and $\Gamma_{+-}$, where $\Gamma_{+-}dt$ gives the probability for switching from the state $\nu_i(t) = +1$ to $\nu_i(t) = -1$ in the time interval $dt$, and vice versa for $\Gamma_{-+}$. The solution for the decoherence of the qubit, can then be inferred after solving the coupled Master equations for the occupation probabilities $p_{\pm}(t)$ as a function of time, and averaging over the initial conditions for the fluctuator. [35]

If the two rates, $\Gamma_{-+}$ and $\Gamma_{+-}$, are identical, we have a symmetric telegraph process, that is the conventional model due to its simplicity. In paper 4, however, we use the non-symmetric version [89] of classical telegraph noise, in order to capture the effect of temperature. In this model, the rates are calculated by the appropriate Boltzmann weights.

### 3.1.5 Fundamental differences between the quantum and the classical models

As shown in paper 4, the quantum and the classical models for the TLS applied to the qubit decoherence problem, can give very similar decoherence rates for the qubits, as long as the decoherence rate of the TLS is large compared to its coupling strength to the qubit. The models, however, are qualitatively different. In the classical model, the presence of a single telegraph fluctuator, or a set of fluctuators simultaneously acting on the qubit, can never give rise to decoherence of the qubit. The fluctuator(s) simply give rise to a noisy external field in which the qubit will precess coherently, and the purity of the qubit state is conserved. Only after averaging over many realizations of the time evolution of the precessing qubit, one might obtain a density matrix for the qubit where the purity of the state has decayed.

In the quantum model, Eq. (3.2), no averaging is required, the loss of coherence in the qubit is solely due to the entanglement with its environment. We can make an analogy by the following picture: Imagine that our entire system (universe) is enclosed in a box. In the quantum model the picture is straightforward, we have a single box, containing the qubit, and its environment. When we turn on the interaction between the two, they evolve in time, depending on the state of each other and entangle. The purity of the composite system contained in the box is conserved, while the coherence of the qubit has decayed due to the entangling interaction. On the other hand, in the classical model, we need an ensemble of boxes,

each containing a qubit and a classical fluctuator. The fluctuator switches randomly, and the particular realization of the random walk is different in each box. The individual noise process in each box is in addition not dependent on the state of the qubit, there is no back-action in the classical model. The qubit evolve coherently and in general differently in each box. We then calculate the ensemble average over all boxes in order to obtain a statistical density matrix for the qubit. This density matrix is compared with the one obtained in the quantum model.

The classical model is therefore not in a strict sense a limiting case of the quantum model, but is a qualitatively different model. In the limit when the systems responsible for the decoherence of the qubit is decohered by their own environment at a rate much faster than their entanglement rate with the qubit, the two models predict similar density matrices for the qubit. Therefore, whether we simply lack control over classical fluctuating environments and the qubit is actually coherently precessing in each individual qubit experiments, as described in the classical model, or if the qubit is interacting with other quantum systems, is impossible to tell, since its density matrix in any case might be identical. Likely, both processes usually take place, with different strengths in different materials and designs used for qubit realizations.

## 3.2 TLSs subject to external driving and the Bloch-Redfield equation

As mentioned in the preceeding section, it is generally not useful to solve complicated quantum models, such as Eq. (3.2), where one keep track of the detailed state of the evironment in a very large Hilbert space. Such problems scale with the dimensionality of the Hilbert space, i.e. by $2^L$, where $L$ is the number of degrees of freedom in the composite system. Even for a modest size environment, $L = 10$, this problem is numerically costly (with an exception for a simulation by use of a hypotetical quantum computer). In this situation one might save time and money by applying the classical telegraph model. A problem with the classical model is, however, that it can not straightforwardly be applied if the TLSs are subject to external driving, or TLSs that are coupled strongly to the qubit relative to the coupling to its own environment. In this case we need to make another approach, such as the Bloch-Redfield approximation.

### 3.2.1 The Bloch-Redfield equation

The Bloch-Redfield equation is a phenomenological equation for the treatment of quantum systems subject to environments in thermal equilibrium. Rather than specifying the details of the environment, Bloch and Redfield constructed a model where its effect on the quantum system is taken into account by a small set of parameters. This model was originally developed in the field of magnetic resonance, where the resonance lines of magnetic spins are broadened due to environmental decoherence. [90, 91, 32]

The equation of motion for the density matrix of an isolated quantum system, e.g. a nuclear spin subject to an external magnetic field, is given by the von Neumann equation

$$\dot{\rho}_{\alpha\alpha'} = \frac{i}{\hbar}\langle\alpha|[\rho, H_0]|\alpha'\rangle, \tag{3.5}$$

where, e.g., for a spin in a magnetic field $B$, the Hamiltonian takes the form $H_0 = \mathbf{B}\cdot\sigma$, and $\alpha$ index the states of the TLS $|\pm\rangle$ in the eigenbasis of $\sigma_z$. If the spin interacts with the rest of the world, we might, rather than incorporating additional degrees of freedom in our model, as we did in Eq. (3.2), add additional terms to the von Neumann equation in order to incorporate the effective action of the environment. The resulting Bloch-Redfield equation is

$$\dot{\rho}_{\alpha\alpha'} = \frac{i}{\hbar}\langle\alpha|[\rho, H_0]|\alpha'\rangle - \sum_{\beta,\beta'} R_{\alpha\alpha',\beta\beta'}(\rho_{\beta\beta'} - \rho^{eq}_{\beta\beta'}(T)), \tag{3.6}$$

where the rates $R_{--,++} = R_{++,--} = \gamma_1$, $R_{-+,-+} = R_{+-,+-} = \gamma_2$ and all other components of $R$ vanishes. The matrix elements $\rho^{eq}_{\beta\beta'}(T)$ gives us the density matrix of the spin in thermal equilibrium, in the absence of external driving. This equilibrium matrix determines the state which the quantum system relaxes towards due to interaction with the thermal bath. In their equation, Bloch and Redfield captured the complex action of the environment by only three parameters, $\gamma_1$, $\gamma_2$ and $T$. The relaxation rate $\gamma_1 = 1/T_1$ determines the rate of relaxation towards equilibrium in the energy eigenbasis of $\rho$, while $\gamma_2 = 1/T_2$ determines the rate of decay of the off-diagonal elements of $\rho$ or the decoherence rate. The rates are visualized on the Bloch-sphere in Fig. 3.2.1.

The relaxation rates $\gamma_1$ and $\gamma_2$ can in principle be derived from e.g. the Born-Markov master equation. In Appendix B.2 we derive the rates in external driving assuming that the TLS is coupled to a bath of harmonic oscillators. Thus, if we know the nature of the environment of our TLSs, we can in principle derive the decay rates, $\gamma_1$ and $\gamma_2$, and use them as input in the Bloch-Redfield equations. In practice, however, our information

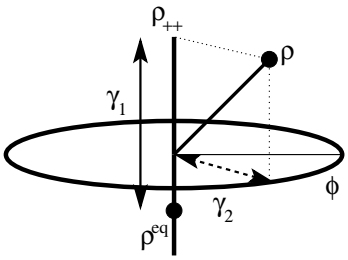


Figure 3.3: Relaxation and dephasing on the Bloch sphere. The quantum system, with density matrix $\rho$ will relax towards its equilibrium value $\rho^{eq}$ with the rates $\gamma_1 = 1/T_1$ and $\gamma_2 = 1/T_2$. The equilibrium level is determined by the temperature of the reservoir. The rate $\gamma_1$ determines the rate of relaxation along the $z$-axis, while the pure decoherence rate $\gamma_2$ determines the rate of decay perpendicular to the $z$-axis. Note that that in the absence of energy relaxation $\gamma_1 = 0$, the occupation probability of the upper level $\rho_{++}$, is conserved in time. In external driving, the motion of the density matrix on the Bloch-sphere might be extremely complex, but the action of $\gamma_1$ and $\gamma_2$ stays the same.

about the environment is usually lacking, instead the rates $\gamma_1$ and $\gamma_2$ can be inferred from experiments, such as the decay of Ramsey fringes [92, 93], free induction decay and the decay of Rabi oscillations [94]. In fact the master equation approach is not fully compatible with that of Bloch and Redfield since the former is a homogeneous set of equations while the latter is inhomogeneous. Therefore the Bloch-Redfield equations cannot be derived from first principles. In the Bloch-Redfield approach, the decay towards the equilibrium state $\rho^{eq}$ is added phenomenologically by use of a inhomogeneous term.

### 3.2.2 The statistical nature of the Bloch-Redfield equation, and two time correlation functions

The major problem encountered in paper 1, where we attempt to find the decoherence of the qubit due to TLSs subject to external driving, was to find a consistent way to evaluate the two-time correlation function of the TLS. If we know the two-time correlation function of the TLS we can find the corresponding spectral density. The spectral density is the input we

need to find the decoherence of the qubit in the lowest order perturbation theory, which is valid for weak coupling between the TLS and the qubit.

Evaluating the two-time correlation function $\langle \hat{A}(t_2)\hat{A}(t_1)\rangle$ of a measurable $\hat{A}(t)$ acting on an open quantum system is indeed not trivial, since the reduced density matrix of the system at time $t_2$ is not only dependent on the reduced density matrix at time $t_1$, but also on the detailed state of the environment, see Appendix B.1 for details. In this project, we wanted to evaluate the two-time correlation function, without having to worry about the exact details of the environment. Our tool is the Bloch-Redfield equation, which have some special properties that are important to keep in mind when evaluating statistical quantities. The Bloch-Redfield equation

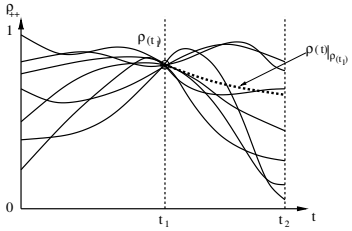


Figure 3.4: Statistical picture relevant for the interpretation of the Bloch-Redfield equation. The solution of the Bloch-Redfield equation with initial condition $\rho(t_1)$ is the ensemble average of all the individual open systems which reduced density matrices was equal to $\rho(t_1)$ at time $t_1$, their evolution history, and the detailed state of their environment is very different. If we imagine thermal equilibrium to be composed of a set of individual systems with different fluctuating trajectories of which the ensemble average equals the equilibrium density matrix $\rho^{eq}$, then the solution of the Bloch-Redfield equation with initial condition $\rho(t_1)$ is equivalent to picking out those systems that was in the state $\rho(t_1)$ at time $t_1$ from the thermal equilibrium ensemble and taking the average of all the trajectories at times $t > t_1$ for this subset.

does not treat a single open quantum system. Rather it is a statistical description of the relaxation towards equilibrium of an ensemble of systems which is initially disturbed from equilibrium by the same amount, to the state $\rho(0)$. [95, 96] The individual systems, however, might have different time evolutions before and after the initial state.

In paper 1 we did not do a fully rigorous ensemble average over the initial states at time $t_1$ in order to evaluate the two-time correlation functions of

type $\langle \hat{A}(t_2)\hat{A}(t_1)\rangle$, in place we made a classical approximation. Rigorously, we should average over the detailed distribution $p(\rho(t_1))$ of density matrices at $t_1$. However, by use of the Bloch-Redfield equation we can only know the ensemble average, i.e. the ensemble averaged density matrix. Thus we made a 'classical' approximation, where we averaged over two states on opposing sides of the Bloch-sphere with weights in accordance with the stationary solution of the Bloch-Redfield equation. The stationary state might lie outside the $z$-axis for a driven system, which was adjusted for by a coordinate transform, see App. $B$ in paper 1 for details. To the best of my knowledge a method to extract the detailed distribution of the individual density matrices for a open quantum system has not been developed and might be a interesting teoretical future project.

### 3.2.3 Two level systems subject to pulsed driving

A considerable amount of time and effort in my Ph.D. work was focused on TLSs subject to pulsed driving. Which is relevant in most real qubit experiments, since the qubit is controlled by use of external pulses. Each control pulse, does not only act on the qubit itself, but of course also on its environment. Especially if the major noise source of the qubit is other TLSs with electric or magnetic moment, systems particularly sensitive to external fields.

Unfortunatly no treatable analytic expression for the noise on a qubit due to TLSs driven by pulses was obtained during the work on this thesis. However, some results was obtained regarding the saturation of these TLSs that might give insight to the effect of pulsed driving on environmental fluctuators.

In Appendix B.3 we derive general expressions for the saturation level of a TLS subject to external AC pulses, the saturation level is the occupation level in the upper state of the TLS after an infinite sequence of pulses. Generally the occupation level is different at different times in the pulse sequence. In Fig. 3.5 we plot the occupation number in the upper state of the TLS, in steady state (i.e. after an infinite sequence of pulses), and compare with the saturation level for continuous driving at the same average intensity. We find that special combinations of field intensity and pulse length does not saturate the TLS, instead it rotates the spins an integer number of full periods, such that it is close to the ground state at the end of the pulse. This situation corresponds to the periodic decrease in steady state occupation level in the upper energy level shown in the plot. If the inverse relaxation rate $1/\gamma$ is large compared with the pulse length, the TLS will only weakly decay between the pulses, while in the opposite limit,

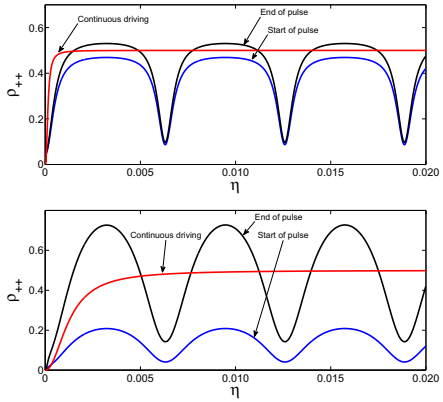


Figure 3.5: The saturation level in steady state for pulsed driving as a function of the driving strength $\eta = \frac{\mathbf{E_{ac}} \cdot \mathbf{p}}{E}$ for two different relaxation rates a) $\gamma = 1.25 \cdot 10^6$ b) $\gamma = 1.25 \cdot 10^7$. The black colored graph shows the saturation level right after the end of the pulse, while the blue graph is the saturation level right before the start of the pulse. For comparision we plot the saturation level for continuous driving with the same average intensity as for the pulse sequence, red graph. The parameters are as given in the article by John Martinis et. al. for a charge qubit [97]: $\Delta_0/\hbar = 10$GHz, dipole moment $p = 3.7$D and electric field $E_{AC} = 3 \cdot 10^3$V/m. The lenght of the pulses is $t_p = 10^8$ and the time between each pulse $t_f = 10 \cdot t_p$. The thermal equilibrium level is $\rho^{eq}_{++} = 0$.

the spins will relax to the thermal equilibrium level before the start of the next pulse.

## 3.3 Decoherence due to correlated two level systems

Until now, we have been concerned with the decoherence of a qubit due to TLSs that are again coupled to their own individual environments. In a real material, however, the TLSs communicate with each other, directly through electromagnetic or strain fields, or indirectly through other degrees

of freedom in the environment. The environments which is responsible for the decoherence of each TLS, might in many realizations be a common bath for multiple TLSs. Such conditions will result in correlations between the different TLSs responsible for the decoherence of the central qubit.

Due to the wastly increased complexity introduced by correlations, investigations of qubit decoherence due to correlated environments has been subject to relatively little research compared to the problem of uncorrelated environments. One might ask whether correlations between different sources of noise is at all important. Correlations should, of course, alter the dynamics of the noise sources, but does it really matter to the qubit whether its environments communicate or not? Furthermore, is the noise sources responsible for decoherence in qubits typically correlated, or are the coupling sufficiently weak making the commonly used formalism of individual TLSs in individual environments a very good model for all practical purposes?

### 3.3.1 Are the TLSs responsible for decoherence in qubits correlated?

In order for correlations to be important in a system of TLSs, the decoherence and relaxation of each TLS due to environments that are not directly coupled to the qubit or other TLSs is required to be weak compared to the interaction internally among the TLSs. If the decoherence of a TLSs due to an external bath is dominant, potential correlations between the TLSs will rapidly decay due to the dissipative interaction with the bath.

Until now, not much effort have been made in order to understand the importance of correlations in solid state qubit environments. What have been done is entirely theoretical modeling of qubit decoherence in different realizations of correlated baths, by use of the mean field approximation for the bath. [98, 99, 100, 101] Whether interactions among the bath spins coupld be important or not in physical realizations of qubits are largely unknown, and are at best, guesses, such as *"The effect of environmental self-interaction is almost certainly of importance in the solid state" [102].* Interaction is, however, assumed to be weak in several environments that are thought to be responsible for the decoherence of solid state qubits, such as e.g. TLSs in glasses and nuclear spins in $C^{13}$ atoms interacting with vacancy centers in diamond, [103, 104]. In these systems weak correlations certainly exists, but is not dominant compared to i.e interactions with phonons for TLSs in amorphous solids. In different qubit designs, such as nuclear spins interacting with electrons in semiconductor quantum dots [105, 106, 107, 108, 109], the exhange between nuclear spins mediated

by the central electron in the dot might be relatively strong, but ferromagnetic. We will later see that ferromagnetic environments are less dangerous with respect to decoherence compared to systems with frustrated couplings.

Superconducting flux qubits, and quantum intereference devices are the only systems known to the author where strongly interacting systems are suggested to be a major source of decoherence. [110, 111] In these systems metal-induced gap states, states on the metal-insulator insulator interface that might be localized due to disorder at the interface, [112] are thought to interact strongly with each other by competing interactions, giving rise to a frustrated environment acting on the qubit. In addition there might potentially be other important correlated environments, yet to be discovered. It might furthermore be advantageous for engineering purposes to know the effect of frustrated environments on qubit decoherence such that potential designs, where, e.g., the material is thought to contain glassy systems that could couple to the qubit, can be compared aganst other materials based on existing theory.

### 3.3.2 Frustrated environments and spin-glasses

In paper 2 we investigate the mechanisms behind the decoherence of a qubit coupled to an interacting spin system that we can tune between a spin-glass and a ferromagnet. A spin-glass is a magnetic system composed of interacting spins, with frustrated interactions. A spin glass stays in contrast to a ferromagnet, where the interaction between each spin in the sample favors all spins to align in the same direction. As an example, consider a Heisenberg Hamiltonian of the form

$$H = \sum_{ij} \Omega_{ij}^{\alpha} \sigma_i^{\alpha} \sigma_j^{\alpha} - J_{ij}^{z} \sigma_i^{z} \sigma_j^{z} \tag{3.7}$$

where $i, j$ denote individual spins in the sample, $\sigma_i^{\alpha}$ are the Pauli matrices along the $\alpha$ direction, and $\Omega_{ij}^{\alpha}$ and $J_{ij}^{z}$ denote the coupling between pairs of spin particles. If e.g. $J_{ij}^{z} = 1$ and $\Omega_{ij}^{\alpha} = 0$ for all pairs $i, j$ the system is a ferromagnet. At zero temperature this system has two degenerate ground states where all spins are aligned in the $z$ direction, and there is a distinct gap to the first exited state. This system is a permanent magnet below a critical temperature $T_c$.

We might now introduce frustrated couplings to the model. Frustrated couplings in a spin system means that the couplings between the spins works against each other, favoring different orientation of the spin. In a system with many competing interactions, no particular orientation will usually be much more favorable than any other, as opposed to the ferromagnet.

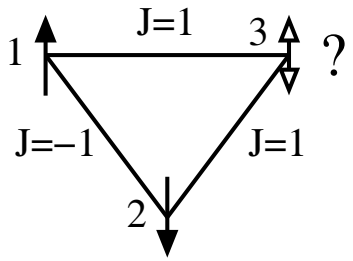


Figure 3.6: Three spin-$\frac{1}{2}$ particles in a triangle configuration. The coupling is Ising type with $J^z_{12} = -1$ and $J^z_{13} = J^z_{23} = 1$. The setup is an example of a frustrated spin system, there is no way to arrange the spins in order to completely satisfy all the internal couplings. In the situation where we have already placed spin 1 and 2 as illustrated in the figure, there is no obvious choise for the direction of the third spin.

The nature of frustrated interactions is illustrated for a simple model with only three spins in a triangle configuration in Fig. 3.6. The frustrated part of the interaction might be introduced to the model defined by Eq. (3.7), by adding a random element to the coupling between the spins. Explicitly we might introduce $\Omega_{ij} \in [-\Omega, \Omega]$ in Eq. (3.7), such that for each pair of spins, the coupling is randomly picked in the interval $[-\Omega, \Omega]$. In general we will for nonzero $\Omega$ have many competing interactions, and for $\Omega \gg J$ the ground state of Eq. (3.7) will be completely disordered, with vanishing net magnetization in the absence of external fields.

Spin-glass behaviour was first identified in noble metals (e.g. Ag, Au, Cu) weakly diluted by transition metal ions, such as Fe or Mn, other known spin glass materials are disordered magnetic metals, such as amorphous FeZr and partially disordered magnetic insulators such as $Eu_xSr_{1-x}S$. [113] However, in principle many disordered strongly interacting magnetic system are candidates that could have a spin-glass phase. As explained, a spin glass has a largely random-looking mixture of ferromagnetic and antiferromagnetic interactions. Analytical solutions for the spin glass model, is known for the infinite range Sherrington-Kirkpatrick model, [114] which is the Ising version of Eq. (3.7) with $J_{ij} = 0$. This model was solved analytically by Parisi, [115, 116, 117] in the limit of a infinite system.

The Parisi solution has some details which is interesting to us. The topology of the set of states in the spin-glass, can be described based on the "Hamming distance" $D$, [118] where $D$ is the fraction of spins needed

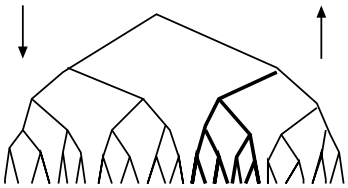

Figure 3.7: The bifurcating hierarchical three of a spin glass. The spin states are represented by the end points of the lowest branches. The Hamming distance $D$ between two states is represented by the height of the highest vertex in the lowest path connecting two states. The state overlap $q$ us greatest between states with smallest $D$. The barrier height between two states is assumed to be a increasing function of $D$. Thus, on the time scale of a given experiment only a part of the hierarchy, e.g. the part shown in thick lines, will be explored.

to reorient in order to convert one state to another. With this metric, the distances between the low-lying states of the system can be represented by a hierarchical three, see Fig. 3.7. The distance between two states is represented by a three on which the states are the end points. Spaces on which the metric $D$ have this representation is called ultrametric. Since the distance $D$ between two states is proportional to the number of spin-flips it follows that the overlap between two states $q$ is inversely related to $D$.

For us what is important is that in a spin glass, the number of states close to the ground state are very large, but the overlap between any two randomly picked such states are in general extremely small. In paper 2 we develop a picture where the decoherence of the central spin is related the overlap between the environmental state in the presence and in the absence of the central spin. In a spin glass, with many competing interactions, even a small perturbation might alter the detailed structure of the three (Fig. A.1), and its end states, such that the time evolution of the glass might be altered completely by the presence of the single spin. In a ferromagnet, however, or any ordered material, this is not the case. A small perturbation is not sufficient to break the symmetry of the ferromagnetic ground state.

As a side note it is worth mentioning that the spectrum of fluctuations in the magnetic moment $S_M(f)$ should obey a $S_M(f) \propto 1/f$ law if one assume that the characteristic time $\tau$ for transitions between the states depends exponentially on the barrier height for spin flips and that these barriers have a reasonably broad distribution. [118] Since a noise spectrum

proportional to $1/f$ is typically observed in mesoscopic circuits, spin-glasses should not be excluded as major candidates responsible for decoherence in physical realizations of solid state qubits.

# Appendices

# Appendix A

# Concepts and formalism

## A.1 The density matrix

Density matrices are used in order to treat statistical mixtures of pure quantum states. The general density matrix written in terms of the basis functions $|\psi_i\rangle$ is

$$\rho = \sum_i p_i \left|\psi_i\right\rangle \left\langle\psi_i\right|, \tag{A.1}$$

where $p_i$ is the non-negative probability to find the system in the state $|\psi_i\rangle$. Since the probabilities $p_i$ should add up to one, the density matrix of a physical system is required to have $\mathrm{Tr}(\rho) = 1$. Furthermore, the density matrix is positive definite (meaning that all the eigenvalues are positive), and Hermitian.

Systems where all the coefficients $p_i$ are zero exept one are said to be in a pure state. If we know the state of a single isolated quantum system it is in a pure state, but we might also use the same terminology when referring to an ensemble of systems where each copy of the system in that ensemble is in the same state.

We use the term mixed state to denote single systems for which we do not know the exact quantum state, or equivalently an ensemble of systems with a distribution of pure states described by $p_i$. However, the density matrix of a mixed system does not capture all the information about the system. In general, different ensembles of pure states might correspond to the same density operator. The non-uniqueness of $\rho$ implies that we cannot infer the probabilities $p_i$ in an arbitrary basis from the density matrix.

The formalism of density matrices was introduced early in the development of quantum mechanics by Landau [119] and von Neumann [120] to describe the statistical state of a quantum system. A description in terms of density matrices is needed in order to treat the nonunitary dynamics of open quantum systems, or any interacting quantum system where we are only interested in a subsystem of the full system.

Expectation values of any operator $\hat{A}$ of the system can be evaluated if the density matrix is known, by the trace formula

$$\langle A \rangle = \mathrm{Tr}(\rho A) = \sum_i p_i \langle \psi_i | A | \psi_i \rangle . \tag{A.2}$$

The density matrix therefore captures all possible information about outcomes of measurements on the same system.

The time evolution of the density matrix is described by the von Neumann equation

$$i\hbar \frac{\partial \rho}{\partial t} = [H, \rho], \tag{A.3}$$

where $H$ is the Hamiltonian of the system. The von Neumann equation is a direct generalization of the Scrödinger equation to statistical ensembles, and the two equations are physically fully equivalent describing unitary quantum evolution.

In order to describe non-unitary dynamics in open quantum systems one adds dissipative terms to the right hand side of Eq. A.3. There are several more or less rigorous ways to do this. Rigorous derivations usually involves an averaging procedure, see e.g. Ref. [40] or Ref. [32], but at some point one has to break time reversal symmetry. Dissipative terms can therefore not be derived from quantum mechanics alone and has to be introduced phenomenologically at some point in the derivation.

### A.1.1 Reduced density matrices

Reduced density matrices refer to the density matrix of a subsystem of a larger system. If the different subsystems are entangeled with each other, we can not specify the quantum state any of these subsystems without referring to the other systems. In order to speak about subsystems it is therefore convinient to introduce reduced density matrices.

To illustrate the concept, we consider two quantum systems (e.g., two qubits), prepared in the EPR-state

$$|\psi\rangle = \frac{1}{\sqrt{2}} \left( |1\rangle_1 |0\rangle_2 - |0\rangle_1 |1\rangle_2 \right),$$

where the subscripts 1 and 2 denote qubit 1 and qubit 2, respectively. Each qubit can be in two possible states, $|0\rangle$ and $|1\rangle$. The reduced density matrix of system 1 is defined by tracing over the degrees of freedom of system 2:

$$\rho_1 = \mathrm{Tr}_2 |\psi\rangle \langle\psi| = {}_2\langle 1|\psi\rangle \langle\psi|1\rangle_2 + {}_2\langle 0|\psi\rangle \langle\psi|0\rangle_2. \tag{A.4}$$

For any local observable $A = A_1 \otimes I_2$ acting only on qubit 1, the expectation value can be found by use of the trace rule applied to the reduced density matrix of system 1:

$$\langle A\rangle = \mathrm{Tr}(\rho A) = \mathrm{Tr}(\rho_1 A_1).$$

The expectation values of all local observables of a system is known as long as we know its reduced density matrix.

We note that for the two qubit system prepared in the EPR-state, the reduced density matrix of system 1 is diagonal. The reduced density matrix would be exactly the same if system 1 was prepared in an equal statistical mixture of $|0\rangle_1$ and $|1\rangle_1$. This implies that measurements of observables on system 1 alone cannot in general discriminate between pure and mixed states. Thus we can view density matrices as a mathematical tool for determining the probability distribution of possible measurements on the system without the need of specifying its exact state.

## A.2 The Bloch sphere

The Bloch sphere, is a geometrical construction that can be used used to parameterize and visualize the density matrix of both pure and mixed quantum systems. Even though the construction is commonly referred to as the Bloch sphere, mixed states will lie in the interior of the sphere. It is therefore also called the Bloch ball. The Bloch sphere was developed by Felix Bloch in order to study of nuclear induction, i.e. the precession of nuclear spins subject to a magnetic field [121], and is a well known concept used in the field of magnetic resonance. The advantage of the Bloch sphere is that it allows us to relate the evolution of a quantum state to the precession of a classical magnetic moment in a magnetic field. For the Bloch equations of motion of the classical magnetic moment in a external field, or its quantum spin-$\frac{1}{2}$ equivalent, see Ref. [32].

The density matrix of a two level quantum system can be parameterized in the following way

$$\rho = \frac{1}{2}\left(I + \alpha \cdot \sigma\right), \tag{A.5}$$

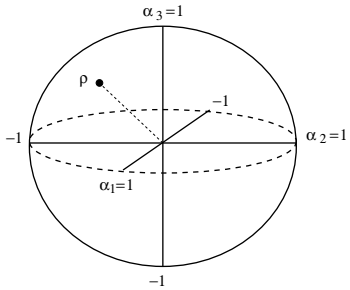


Figure A.1: The Bloch sphere. The density matrix $\rho$ of a quantum system can be visualized on the Bloch sphere when parametrized by use of the Bloch vector $\rho = \frac{1}{2}(I + \alpha \cdot \sigma)$. The density matrix is drawn on the Bloch sphere according to its overlaps $\alpha$ with the three different Pauli matrices.

where $\alpha \in \mathbb{R}^3$ is called the Bloch vector, or the coherence vector of the system.

In paper 1 we make use of a different parametrization of the density matrix, which is useful for systems driven by an external field in order to obtain differential equations which are not explicitly time dependent. In that paper we make use of the rotating wave approximation, where one neglect rapidly oscillating terms which enter the Hamiltonian of the TLS in the interaction picture. When the rotating wave approximation works, i.e. when the detuning between the driving field and the TLS eigenfrequency is small, a parameterization of the density matrix which follows the driving frequency is useful. In paper 1 the following parameterization is used,

$$\rho = \begin{pmatrix} n & f^* e^{-i\Omega t} \\ f e^{i\Omega t} & 1-n \end{pmatrix},$$

where $n = \rho_{++}$ and $f = e^{-i\Omega t}\rho_{-+}$. This parameterization can be visualized on the Bloch sphere in the reference frame rotating by frequency $\Omega$ by the following simple relations:

$$\alpha_1 = \mathrm{Re}\, f, \qquad \alpha_2 = \mathrm{Im}\, f \qquad \alpha_3 = 2(n - 1/2). \tag{A.6}$$

The geometric concept of the Bloch sphere can in principle be extended to quantum systems of arbitrarily many degrees of freedom. In paper 3 we make use of a 4-level Bloch sphere construction in order to study the effect of correlated noise in two coupled qubits.

# Appendix B

# Derivations and complementary material relevant for the first paper

## B.1 Two time correlation functions

In order to find the noise spectrum of a quantum system, it is necessary to first find the two time correlation function of the operator of interest. In this section we will show that extracting the two time correlation function from knowledge of the reduced density matrix of the system alone is not possible without further assumptions.

Assume that we want to know the two time correlation function of an operator $A$ acting on a system $S$ (e.g. in order to find perturbatively by use of the noise spectrum, the action of this system on another quantum system such as the qubit). In our case our system is not a isolated one but interacting with its environment $E$.

Before we move to two time correlation functions, we note that finding the expectation value of a single system operator is straightforward

$$\langle A \rangle = \langle A_S \otimes I_E \rangle = \mathrm{tr}_{S\otimes E}(A\rho_{tot}) = \mathrm{tr}_S\left[A\,\mathrm{tr}_E(\rho_{tot})\right] = \mathrm{tr}_s(A\rho_S) \tag{B.1}$$

where $\rho_{tot} \in S \otimes E$ is the composite density matrix of the system and the environment. The time evolution of the composite system is given by the von Neumann equation

$$\dot{\rho}_{tot} = [H, \rho_{tot}], \qquad H = H_S + H_E + H_{SE}. \tag{B.2}$$

Our goal is to calculate two time correlation functions by referring only to the reduced density matrix of the system $\rho_S$ that we have calculated by use of the non-homogeneous Bloch-Redfield equations of the form $\dot{\rho}_S = L\rho_S + l$ where $L$ is a general Lindblad super-operator, and $l$ is a non-homogeneous term which determines the equilibrium density matrix.

Proceeding, we attempt to calculate the two time correlation function for two quantum operators acting on the system at two different times (for us it is sufficient to consider two identical operators). The expression in the Heisenberg picture is

$$\langle A(t_1)A(t_2)\rangle = \mathrm{tr}_{SE}[\rho_{tot}(0)A(t_1)A(t_2)] \tag{B.3}$$

where

$$\begin{aligned} \rho_{tot}(0) &= e^{iHt_1 t}\rho_{tot}(t_1)e^{-iHt_1} \\ A(t_1) &= e^{iHt_1}A(0)e^{-iHt_1}. \end{aligned} \tag{B.4}$$

Now we can write out the correlation function Eq.(B.3) by inserting the expressions given by Eq. (B.4). We get the following expression for the two time correlation function

$$\begin{aligned} \langle A(t_1)A(t_2)\rangle &= \mathrm{tr}_{SE}\left[e^{iHt_1}\rho_{tot}(t_1)A(0)e^{iHt(t_2-t_1)}A(0)e^{-iHt_2}\right] \\ &= \mathrm{tr}_{SE}\left[A(0)e^{-iH(t_2-t_1)}\rho_{tot}(t_1)A(0)e^{iHt(t_2-t_1)}\right] \\ &= \mathrm{tr}_S\left\{A(0)tr_E\left[e^{-iH(t_2-t_1)}\rho_{tot}(t_1)A(0)e^{iHt(t_2-t_1)}\right]\right\} \end{aligned} \tag{B.5}$$

where we have used the cyclic property of the trace, and the fact that the operator $A$ act only on the system part of the total Hilbert space. From Eq. B.5 we see that in principle the full dynamics of the composite system $\rho_{tot}$, given by $H$ is required in order to extract the correlation function.

Since the quantity we need is given by the second trace of Eq. B.5, our only hope is to simplify this expression by appropriate assumptions. If we define $\tau = t_2 - t_1$ and the following operator

$$\zeta_{\rho_{tot}(t_1)A(0)}(\tau) = e^{-iH(\tau)}\rho_{tot}(t_1)A(0)e^{iHt(\tau)} \tag{B.6}$$

such that $\zeta(0) = \rho_{tot}(t_1)A(0)$. It is clear that $\zeta(\tau)$ satisfy the von Neumann equation similarly to $\rho_{tot}$, such that

$$\frac{d}{d\tau}\zeta(\tau) = -i[H, \zeta(\tau)]. \tag{B.7}$$

What we are seeking is an equation of motion for

$$v_{\rho_{tot}(t_1)A(0)}(\tau) = \mathrm{tr}_E[\zeta_{\rho_{tot}(t_1)A(0)}(\tau)] = \mathrm{tr}_E\left[e^{-iH(t_2-t_1)}\rho_{tot}(t_1)A(0)e^{iHt(t_2-t_1)}\right]. \tag{B.8}$$

But if we assume that $\zeta(\tau)$ factorizes (i.e $\zeta(\tau) = \xi(\tau) \otimes R_0$), where $R_0$ is the the equivalent of the reservoir state in thermal equilibrium, then our equations are completely analogous to our starting equations for deriving the Master equation for $\rho$. Thus we can in principle derive a Master equation for $\upsilon$ of the form

$$\frac{d}{d\tau}\upsilon_{\rho_{tot}(t_1)A(0)}(\tau) = L\upsilon_{\rho_{tot}(t_1)A_{(0)}}(\tau). \tag{B.9}$$

This equation might then be used together with Eq. B.5 in order to find an explicit expression for the two time correlation function. The disadvantage of such an approach is that we need to know when we can neglect the entanglement dynamics between the system and the environment and use the assumption of factorization. We have not been able to apply this approach in the derivation of the two-time correlation function of the driven TLS. In paper 1 we finally used a Bloch-Redfield approach together with a semi-classical assumption in order to find the noise spectrum of the TLSs in external driving.

## B.2 Decoherence due to an ensemble of oscillators using the Born-Markov Master equation

In this chapter we will show how to derive the rates we use as input in the Bloch-Redfield equation for a TLS in an external AC field amd subject to an environment of harmonic oscillators (e.g. phonons).

### B.2.1 The model

Assume we have a system ($S$) interacting with its environment ($E$). The Hamiltonian of the composite system can be written in general form

$$H = H_S + H_E + H_{SE}, \tag{B.10}$$

where $H_s$ and $H_E$ is the Hamiltonians for $S$ and $E$ respectively, and $H_{SE}$ is the interaction part. We want information about the system $S$ without requiring detailed information about the composite system $S \otimes E$. Let $\chi(t)$ be the density operator for $S \otimes E$. The reduced density operator for the system $S$ is then $\rho(t) = \mathrm{tr}_E[\chi(t)]$.

We can calculate the expectation value of any operator $\hat{O}$ in the Schrödinger picture from the knowledge of $\rho(t)$ alone, and not of the full $\chi(t)$:

$$\langle\hat{O}\rangle = \mathrm{tr}_{S\otimes E}[\hat{O}\chi(t)] = \mathrm{tr}_S[\hat{O}\,\mathrm{tr}_R(\chi(t))] = \mathrm{tr}_S[\hat{O}\rho(t)]. \tag{B.11}$$

Our objective is to obtain an equation for $\rho(t)$ where the properties of $E$ enter only as parameters.

### B.2.2 Exact von Neumann equation

We start with the von Neumann equation for our composite system

$$\dot{\chi} = \frac{1}{i\hbar}[H, \chi] \tag{B.12}$$

We then make a transform to the interaction picture, separating the motion generated by $H_S + H_E$ from that generated by the interaction $H_{SE}$. Defining

$$\tilde{\chi}(t) = e^{(i/\hbar)(H_S+H_R)t}\chi(t)e^{-(i/\hbar)(H_S+H_R)t}$$

and differentiating, by use of the Schrödinger equation, we obtain

$$\begin{aligned}\dot{\tilde{\chi}}(t) &= \frac{i}{\hbar}(H_S + H_R)\tilde{\chi} - \frac{i}{\hbar}\tilde{\chi}(H_S + H_R) + e^{(i/\hbar)(H_S+H_R)t}\dot{\chi}(t)e^{-(i/\hbar)(H_S+H_R)t} \\ &= \frac{1}{i\hbar}[\tilde{H}_{SE}(t), \tilde{\chi}],\end{aligned} \tag{B.13}$$

where

$$\tilde{H}_{SE}(t) = e^{(i/\hbar)(H_S+H_R)t}H_{SE}e^{-(i/\hbar)(H_S+H_R)t}$$

.

We proceed by integrating Eq.(B.13) giving

$$\tilde{\chi}(t) = \chi(0) + \frac{1}{i\hbar}\int_0^t dt'[\tilde{H}_{SE}(t'), \tilde{\chi}(t')],$$

and then substitute this integrated expression for $\tilde{\chi}(t)$ inside the commutator in Eq.(B.13). We obtain

$$\dot{\tilde{\chi}}(t) = \frac{1}{i\hbar}[\tilde{H}_{SE}(t), \chi(0)] - \frac{1}{\hbar^2}\int_0^t dt'[\tilde{H}_{SE}(t), [\tilde{H}_{SE}(t'), \tilde{\chi}(t')]]. \tag{B.14}$$

So far the expression is exact, we have simply rewritten Eq.(B.12) to a form which is more suitable for later approximations.

### B.2.3 Born and Markov approximations

We assume that the interaction $H_{SE}$ is turned on at $t = 0$ and that no correlations between the system and the environment exists at this initial time. Then $\chi(0) = \tilde{\chi}(0) = \rho(0)R_0$, where $R_0$ is the initial density operator

of the environment. Then, by tracing over the environmental degrees of freedom in Eq.(B.14) we obtain the master equation

$$\dot{\tilde{\rho}}(t) = -\frac{1}{\hbar^2}\int_0^t dt' \,\mathrm{tr}_R\{[\tilde{H}_{SE}(t),[\tilde{H}_{SE}(t'),\tilde{\chi}(t')]]\}, \tag{B.15}$$

where we have omitted the term $\frac{1}{i\hbar}\mathrm{tr}_E\{[\tilde{H}_{SE}(t),\chi(0)]\}$ by the assumption that $\mathrm{tr}_E\{\tilde{H}_{SE}(t)R_0\} = 0$. Furthermore, by assuming that the coupling $H_{SE}$ between $S$ and $E$ is weak and that $E$ is a large system which is approximately unaffected by its coupling to $S$, we write

$$\tilde{\chi}(t) = \tilde{\rho}(t)R_0. \tag{B.16}$$

The assumption that the composite system maintains a product state during time evolution is called the Born approximation. The Born approximation states that the system and environment is uncorrelated at all times, a rather strong approximation.

The master equation Eq.(B.15) can now be written

$$\dot{\tilde{\rho}}(t) = -\frac{1}{\hbar^2}\int_0^t dt' \,\mathrm{tr}_R\{[\tilde{H}_{SE}(t),[\tilde{H}_{SE}(t'),\tilde{\rho}(t')R_0]]\}. \tag{B.17}$$

The above equation is still nonlocal in time, since the derivative of the density matrix depends on itself at earlier times. However, by assuming that the reservoir correlation time is small compared to the time scale of significant change in the state of the system, we can replace $\tilde{\rho}(t')$ by $\tilde{\rho}(t)$. This is equivalent to the assumption that the environmental operators coupling to the system is delta correlated. The assumption that the correlation time of the environment is approaching zero, i.e., that the state of the environment only depends on the temperature, but not on its history, is a Markovian assumption for the bath. Thus we obtain our Born-Markov master equation

$$\dot{\tilde{\rho}}(t) = -\frac{1}{\hbar^2}\int_0^t dt' Tr_R\{[\tilde{H}_{SE}(t),[\tilde{H}_{SE}(t'),\tilde{\rho}(t)R_0]]\}. \tag{B.18}$$

To make this equation more explicit, we assume that we can write the interaction Hamiltonian in the diagonal form $\tilde{H}_{SE}(t) = \sum_\alpha \tilde{S}_\alpha(t)\otimes\tilde{E}_\alpha(t)$, where $\tilde{S}_\alpha(t)$ are the operators acting in the Hilbert space of the system which couples to the environment and $\tilde{E}_\alpha(t)$ are the corresponding operators acting in the environment. Thus we can write Eq.(B.17) as

$$\dot{\tilde{\rho}}(t) = -\frac{1}{\hbar^2}\int_0^t dt' \sum_{\alpha\beta} Tr_R\{[\tilde{S}_\alpha(t)\otimes\tilde{E}_\alpha(t),[\tilde{S}_\beta(t')\otimes\tilde{E}_\beta(t'),\tilde{\rho}(t')R_0]]\}. \tag{B.19}$$

We now define the environment self-correlation functions

$$C_{\alpha\beta}(t,t') = Tr_E[\tilde{E}_\alpha(t)\tilde{E}_\beta(t')R_0] = \langle E_\alpha(t)E_\beta(t')\rangle_{R_0}. \tag{B.20}$$

Assuming that the environment is in a stationary state we can write $C_{\alpha\beta}(t,t') = Tr_E[E_\alpha(t-t')E_\beta\rho_E] = C_{\alpha\beta}(t-t')$. Using this definition and writing out the double commutator Eq. (B.19) becomes

$$\begin{aligned}\dot{\tilde{\rho}}(t) = -\frac{1}{\hbar^2}\int_0^t dt' \sum_{\alpha\beta}\{&C_{\alpha\beta}(t-t')[\tilde{S}_\alpha(t)\tilde{S}_\beta(t')\tilde{\rho}(t') - \tilde{S}_\beta(t')\tilde{\rho}(t')\tilde{S}_\alpha(t')] \\ &+ C_{\beta\alpha}(t'-t)[\tilde{\rho}(t')\tilde{S}_\beta(t')\tilde{S}_\alpha(t) - \tilde{S}_\alpha(t)\tilde{\rho}(t')\tilde{S}_\beta(t')]\}.\end{aligned} \tag{B.21}$$

It is now very explicit that if the self-correlation functions $C_{\alpha\beta}(t-t')$ can be approximated by delta functions, then we can safely replace $\tilde{\rho}(t')$ by $\tilde{\rho}(t)$ If we also do the substitution $\tau = t - t'$ we can write our master equation as

$$\begin{aligned}\dot{\tilde{\rho}}(t) = -\frac{1}{\hbar^2}\int_0^t dt' \sum_{\alpha\beta}\{&C_{\alpha\beta}(\tau)[\tilde{S}_\alpha(t)\tilde{S}_\beta(t-\tau)\tilde{\rho}(t) - \tilde{S}_\beta(t-\tau)\tilde{\rho}(t)\tilde{S}_\alpha(t)] \\ &+ C_{\beta\alpha}(-\tau)[\tilde{\rho}(t)\tilde{S}_\beta(t-\tau)\tilde{S}_\alpha(t) - \tilde{S}_\alpha(t)\tilde{\rho}(t)\tilde{S}_\beta(t-\tau)]\}.\end{aligned} \tag{B.22}$$

We have now obtained a local in time master equation depending only on the reduced density matrix of the system itself.

We might proceed by carrying out a transformation back to the Scrdinger picture. By use of the following expression

$$\dot{\rho}(t) = -\frac{i}{\hbar}[H_S, \rho(t)] + e^{-iH_S t}\dot{\tilde{\rho}}(t)e^{iH_S t}, \tag{B.23}$$

and insertion of Eq.(B.19) we obtain

$$\dot{\rho}(t) = -i[H_S,\rho(t)] - \int_0^t dt' \sum_{\alpha\beta}\{C_{\alpha\beta}(\tau)[S_\alpha, S_\beta(-\tau)\rho(t)] + C_{\beta\alpha}(-\tau)[\rho(t)S_\beta(-\tau), S_\alpha]\}. \tag{B.24}$$

### B.2.4 Explicit model of a TLS subject to a harmonic oscillator bath

We are now interested in looking at how the rates $T_1$ and $T_2$ entering the Bloch Redfield equations can be derived and especially which basis they act in. In order to model a two level system acting as environment for a qubit,

but that is also itself interacting with environmental degrees of freedom, we consider a Hamiltonian model where the environmental bosons couples to the position basis of the two level fluctuators.

$$\begin{aligned} H &= H_S + H_E + H_{SE} \\ H_S &= \frac{1}{2}(\Delta\sigma_z + \Delta_0\sigma_x) \\ H_E &= \sum_i (\frac{1}{2m_i}p_i^2 + \frac{1}{2}m_i\omega_i^2 q_i^2) \\ H_{SE} &= \sigma_z \otimes \sum_i c_i q_i = \sigma_z \otimes \hat{E}. \end{aligned} \tag{B.25}$$

where $q_i$ and $p_i$ are position and momentum operators of bosonic harmonic oscillators modeling the phonon environment of the two level system. We now make a transformation to the energy eigenbasis of the fluctuator

$$\begin{aligned} H_S &= \frac{E}{2}\sigma_z \\ H_E &= \sum_i (\frac{1}{2m_i}p_i^2 + \frac{1}{2}m_i\omega_i^2 q_i^2) \\ H_{SE} &= (\frac{\Delta}{E}\sigma_z + \frac{\Delta_0}{E}\sigma_x) \otimes \sum_i c_i q_i = \sigma_z \otimes E. \end{aligned} \tag{B.26}$$

Our goal is to solve the master equation explicitly for the Hamiltonian above. First we want to determine the self correlation functions. Since the system environment coupling $H_{SE}$ is such that each system operator couples to the same environment operator we can drop the indices on the self correlation function (each index correspond to the same environment operator $E = \sum_i c_i q_i$. We thus find

$$C(\tau) = \langle E(\tau)E\rangle = \sum_{ij}\langle c_j q_j(\tau) c_i q_i\rangle = c_i^2\langle q_i(\tau)q_i\rangle, \tag{B.27}$$

where we have assumed that the different oscillators of the environment is uncorrelated (i.e, not interacting). Writing the position operators in terms of bosonic ladder operators $q_i = \sqrt{\frac{1}{2m_i\omega_i}}(a_i + a_i^\dagger)$, or in the interaction picture $q_i(\tau) = \sqrt{\frac{1}{2m_i\omega_i}}(a_i e^{-i\omega_i\tau} + a_i^\dagger e^{i\omega_i\tau})$, we can calculate the correlation function

$$\langle q_i(\tau)q_i\rangle = \frac{1}{2m_i\omega_i}\left\{\langle a_i a_i^\dagger\rangle e^{-i\omega_i\tau} + \langle a_i^\dagger a_i\rangle e^{i\omega_i\tau}\right\}, \tag{B.28}$$

where $N_i = \langle a_i^\dagger a_i \rangle$ is the mean occupation number of the $i$th oscillator. Under the assumption that the environment is in thermal equilibrium we have $N_i(T) = \frac{1}{e^{\omega/k_B T}-1}$. Thus we can write for the oscillator correlation function:

$$\begin{aligned}\langle q_i(\tau) q_i \rangle &= \tfrac{1}{2m_i\omega_i}\left\{(1+N_i(T))e^{-i\omega_i\tau} + N_i(T)e^{i\omega_i\tau}\right\} \\ &= \tfrac{1}{2m_i\omega_i}\left\{(1+2N_i(T))\cos(\omega_i\tau) - i\sin(\omega_i\tau)\right\} \\ &= \tfrac{1}{2m_i\omega_i}\left\{\coth\left(\tfrac{\omega_i}{2k_BT}\right)\cos(\omega_i\tau) - i\sin(\omega_i\tau)\right\}. \end{aligned} \tag{B.29}$$

Inserting Eq. B.67 into Eq. B.27. We can now express the full environment self correlation function as

$$C(\tau) = \sum_i \frac{c_i^2}{2m_i\omega_i}\left\{\coth\left(\frac{\omega_i}{2k_BT}\right)\cos(\omega_i\tau) - i\sin(\omega_i\tau)\right\} = \vartheta(\tau) - i\eta(\tau), \tag{B.30}$$

where

$$\vartheta(\tau) = \sum_i \frac{c_i^2}{2m_i\omega_i}\coth\left(\frac{\omega_i}{2k_BT}\right)\cos(\omega_i\tau) \tag{B.31}$$

$$= \int_0^\infty d\omega J(\omega)\coth\left(\frac{\omega}{2k_BT}\right)\cos(\omega_i\tau) \tag{B.32}$$

and

$$\eta(\tau) = \sum_i \frac{c_i^2}{2m_i\omega_i}\sin(\omega_i\tau) \tag{B.33}$$

$$= \int_0^\infty d\omega J(\omega)\sin(\omega\tau). \tag{B.34}$$

The functions $\vartheta(\tau)$ and $\eta(\tau)$ are called the noise kernel and the dissipation kernel, respectively. The spectral function entering the expressions is defined by $J(\omega) = \sum_i \frac{c_i^2}{2m_i\omega_i}\delta(\omega-\omega_i)$.

We can now re-express our master equation Eq.(B.24) in terms of these new functions, inserting the explicit operators from our Hamiltonian. Our final equation takes the form

$$\begin{aligned}\dot\rho(t) = &-\frac{i}{\hbar}[H_S, \rho(t)] \\ &- \sum_{\alpha\beta}\int_0^t d\tau\{\vartheta(\tau)[\sigma_\alpha, [\sigma_\beta(-\tau), \rho(t)]] - i\eta(\tau)[\sigma_\alpha, \{\sigma_\beta(-\tau), \rho(t)\}_+]\}.\end{aligned} \tag{B.35}$$

### B.2.5 The equations of motion

We are now ready to find the equations of motion of our two level system using the parameters of our model Hamiltonian Eq.(B.26). In order to calculate the commutators of Eq.(B.35) we have to find the time evolution of the operators $\sigma_\alpha$ in the Heisenberg picture. We have

$$\sigma_z(t) = e^{\frac{iH_S t}{\hbar}} \sigma_z e^{\frac{-iH_S t}{\hbar}} = \sigma_z \tag{B.36}$$

and

$$\sigma_x(t) = e^{\frac{iEt\sigma_z}{2\hbar}} \sigma_z e^{\frac{-iEt\sigma_z}{2\hbar}}, \tag{B.37}$$

and by use of the Baker-Hausdorf lemma we obtain

$$\sigma_x(t) = \sigma_x + (it)[H_S, \sigma_x] - \frac{(it)^2}{2!}[H_S, [H_S, \sigma_x]] - \frac{(it)^3}{3!}[H_S, [H_S, [H_S, \sigma_x]]]]. \tag{B.38}$$

Inserting for $H_S$ we find

$$\sigma_x(-\tau) = \sigma_x \cos(\omega\tau) + \sigma_y \sin(\omega\tau) \tag{B.39}$$

If we parametrize the density matrix by use of the Bloch vector $\mathbf{m}$ as follows

$$\rho(t) = \frac{1}{2}(I + m_x\sigma_x + m_y\sigma_y + m_z\sigma_z), \tag{B.40}$$

we can express the commutators and the anticommutators on the simple form:

$$\begin{aligned}
[\sigma_z, \rho] &= i\sigma_y m_x - i\sigma_x m_y \\
([\sigma_x, \rho] &= i\sigma_z m_y \cos(\omega\tau) - i\sigma_y m_z \cos(\omega\tau) \\
&\quad - i\sigma_z m_x \sin(\omega\tau) + i\sigma_x m_z \sin(\omega\tau) \\
\{\sigma_z, \rho\}_+ &= \sigma_z + m_z \\
\{\sigma_x, \rho\}_+ &= \sigma_x + m_z
\end{aligned} \tag{B.41}$$

and the double commutators are

$$\begin{aligned}
[\sigma_z, [\sigma_z, \rho]] &= 2\sigma_x m_x + 2\sigma_y m_y \\
[\sigma_x, [\sigma_z, \rho]] &= -2\sigma_z m_x \\
[\sigma_x, [\sigma_x, \rho]] &= 2\sigma_y m_y \cos(\omega\tau) + 2\sigma_z m_z \cos(\omega\tau) - 2\sigma_y m_x \sin(\omega\tau) \\
[\sigma_z, [\sigma_x, \rho]] &= -2\sigma_x m_z \cos(\omega\tau) - 2\sigma_y m_z \sin(\omega\tau) \\
[\sigma_z, \{\sigma_z, \rho\}_+] &= 0 \\
[\sigma_x, \{\sigma_z, \rho\}_+] &= -2i\sigma_y \\
[\sigma_x, \{\sigma_x, \rho\}_+] &= 0 \\
[\sigma_z, \{\sigma_x, \rho\}_+] &= 2i\sigma_y
\end{aligned} \tag{B.42}$$

We can now insert this expression into our master equation Eq.(B.35), where we have introduced the frequency $\omega = \frac{E}{\hbar}$. On component form the equations of motion for the density matrix is then

$$\begin{aligned}
\dot{m}_x(t) &= m_x(t)\frac{\Delta^2}{E^2}A - m_y(t)\omega + m_z(t)\frac{\Delta\Delta_0}{E^2}A_c \\
\dot{m}_y(t) &= m_x(t)(\omega - \frac{\Delta\Delta_0}{E^2}A_s) + m_y(t)(\frac{\Delta^2}{E^2}A + \frac{\Delta_0^2}{E^2}A_c) - m_z(t)\frac{\Delta\Delta_0}{E^2}A_s \\
\dot{m}_z(t) &= -m_x(t)\frac{\Delta\Delta_0}{E^2} + m_z(t)\frac{\Delta_0^2}{E^2}A_c,
\end{aligned} \tag{B.43}$$

where we have introduced

$$A = 2\int_0^\infty \int_0^\infty d\omega' d\tau J(\omega') \cosh\left(\frac{\omega'}{2k_bT}\right)\cos(\omega'\tau) \tag{B.44}$$

$$A_c = 2\int_0^\infty \int_0^\infty d\omega' d\tau J(\omega') \cosh\left(\frac{\omega'}{2k_bT}\right)\cos(\omega'\tau)\cos(\omega\tau) \tag{B.45}$$

$$A_s = 2\int_0^\infty \int_0^\infty d\omega' d\tau J(\omega') \cosh\left(\frac{\omega'}{2k_bT}\right)\cos(\omega'\tau)\sin(\omega\tau) \tag{B.46}$$

we can write our equations of motion on the final simple matrix form

$$\dot{\vec{m}}(t) = \begin{bmatrix} \frac{\Delta^2}{E^2}A & -\omega + \frac{\Delta\Delta_0}{E^2}A_s & \frac{\Delta\Delta_0}{E^2}A_c \\ \omega - \frac{\Delta\Delta_0}{E^2}A_s & \frac{\Delta^2}{E^2}A + \frac{\Delta_0^2}{E^2}A_c & \frac{\Delta\Delta_0}{E^2}A_s \\ \frac{\Delta\Delta_0}{E^2}A_c & 0 & \frac{\Delta_0^2}{E^2}A_c \end{bmatrix} \cdot \vec{m}(t). \tag{B.47}$$

Our fluctuator coupled to the environment by the interaction term $H_{SE} = \frac{1}{E}(\Delta\sigma_z + \Delta_0\sigma_x) \otimes \hat{E}$ As we can see from Eq. B.47, the $\sigma_z$ term in the environment coupling is alone responsible for the decoherence in the x-y plane while the $\sigma_x$ term is responsibele for decoherence in the y-z plane on the Bloch sphere (i.e., this term causes relaxation along the z axis, meaning energy decay). But we also see cross terms depending on the presence of both terms in the fluctuator environment coupling. However, if we assume that the TLS operators in which couples to the environment each couple to independent environmental degrees of freedom, then these cross-terms vanishes. We find that by making this assumption we get decay rates which resembles the $1/T_1$ and $1/T_2$ of the Bloch Redfield equations. However, the equations themselves are different. We can se from the above Master equation is homogeneous, while the Bloch-Redfield equation is non-homogeneous. We can therefore not derive the Bloch-Redfield equation direcly from the master equation.

## B.3 Two level system subject to a pulsed driving field

We will in this section derive the solution of the Bloch-Redfield equation for a TLS subject to pulsed driving. We consider a TLS interacting with a general environment responsible for relaxation and pure dephasing. We assume weak coupling to the qubit, so that it can be neglected when solving the equations of motion for the TLS.

The Hamiltonian in the rotating wave approximation is as in paper 3:

$$H_{RWA} = \frac{1}{2}E\sigma_z - \frac{\eta\Delta_0}{2}\left(e^{-i\Omega t}|+\rangle\langle -| + e^{i\Omega t}|-\rangle\langle +|\right). \tag{B.48}$$

With the above Hamiltonian the explicit Bloch-Redfield equations are

$$\begin{aligned}\frac{d\rho_{++}}{dt} &= \frac{i\eta\Delta_0}{2\hbar}\left(e^{-i\Omega t}\rho_{-+} - e^{i\Omega t}\rho_{+-}\right) - \frac{1}{T_1}\left(\rho_{++} - \rho_{++}^{eq}\right)\\ \frac{d\rho_{-+}}{dt} &= \frac{iE}{\hbar}\rho_{-+} + \frac{i\eta\Delta_0}{2\hbar}e^{i\Omega t}(2\rho_{++} - 1) - \frac{1}{T_2}\rho_{-+}.\end{aligned} \tag{B.49}$$

In order to avoid the explicit time dependence we make the transformation $n = \rho_{++} - \rho_{++}^{eq}$, $f = e^{-i\Omega t}\rho_{-+}$ and $f^* = e^{i\Omega t}\rho_{+-}$. We also introduce the Rabi frequency $A = \eta\Delta_0/\hbar$ and the deviation from resonance $z = E/\hbar - \Omega$. As in the paper we assume symmetric coupling to the environment, $1/T_1 = 1/T_2 = \gamma$. This approximation is not valid in general, but is a fair approximation in many solid state systems. A general inequality $T_2 \leq 2T_1$ can be derived from the master equation.

The above equations of motion, Eq. (B.49), can be cast in the following form

$$\begin{aligned}\dot{n} &= -A\,\mathrm{Im}\,f - \gamma n\\ \mathrm{Im}\,\dot{f} &= A(n + n_{eq} - \frac{1}{2}) - \gamma\,\mathrm{Im}\,f + z\,\mathrm{Re}\,f\\ \mathrm{Re}\,\dot{f} &= -z\,\mathrm{Im}\,f - \gamma\,\mathrm{Re}\,f.\end{aligned} \tag{B.50}$$

We solve the equations by Laplace transformation (using the shorthand notation $\mathrm{Re}\,f = r$, $\mathrm{Im}\,f = i$)

$$\begin{aligned}sN - n_0 &= -AI - \gamma N\\ sI - i_o &= A(N + \frac{n_{eq} - 1/2}{s}) - \gamma I + zR\\ sR - r_0 &= -zI + \gamma R,\end{aligned} \tag{B.51}$$

where $N$, $R$ and $I$ are the Laplace transforms of $n$, $r$ and $i$, respectively.

By algebraic manipulations we obtain

$$\begin{aligned}
N &= \frac{n_0((s+\gamma)^2+z^2) - zAr_0}{(s+\gamma)((s+\gamma)^2+z^2+A^2)} - \frac{Ai_0}{(s+\gamma)^2+z^2+A^2} \\
&\quad - \frac{-A^2(n_{eq}-1/2)}{s((s+\gamma)^2+z^2+A)} \\
I &= \frac{i_0(s+\gamma)+zr_0+An_0}{(s+\gamma)^2+z^2+A^2} - \frac{-A^(n_{eq}-1/2)(s+\gamma)}{s((s+\gamma)^2+z^2+A)} \\
R &= \frac{-zA(\frac{n_0}{s+\gamma}+\frac{n_{eq}-1/2}{s}) - zi_0}{(s+\gamma)^2+z^2+A^2} + \frac{r_0((s+\gamma)^2+A^2)}{(s+\gamma)((s+\gamma)^2+A^2+z^2)}. \qquad \text{(B.52)}
\end{aligned}$$

These equations can be transformed back by the inverse Laplace transform.

We now look at the solution during and after a single driving pulse. We call the time of the pulse $t_p$ and the time of free evolution after the pulse $t_f$ Using that the time evolution in the absence of the driving field is simply $n(t_f) = n_0 e^{-\gamma t_f}$ and $f(tf) = f_0 e^{(-\gamma+iz)tf}$, we obtain the following time evolution when considering a single pulse of time $t_p$ followed by a successive free evolution lasting a time $t_f$,

$$\begin{aligned}
n(t_p+t_f) =& \frac{n_0 e^{-\gamma(t_p+t_f)}}{z^2+A^2}(A^2\cos(\sqrt{z^2+A^2}t_p)+z^2) \\
&- \frac{A}{\sqrt{A^2+z^2}} i_0 e^{-\gamma(t_p+t_f)}\sin(\sqrt{z^2+A^2}t_p) \\
&- \frac{zAr_0}{A^2+z^2} e^{-\gamma(t_p+t_f)}\left(1-\cos(\sqrt{z^2+A^2}t_p)\right) \\
&- \frac{A^2(n_{eq}-1/2)}{\gamma^2+z^2+A^2} e^{-\gamma t_f}\Big[1-e^{-\gamma t_p}\Big(\cos(\sqrt{z^2+A^2}t_p) \\
&+ \frac{\gamma}{\sqrt{z^2+A^2}}\sin(\sqrt{z^2+A^2}t_p)\Big)\Big] \qquad \text{(B.53)}
\end{aligned}$$

The evolution of the real part of the density matrix element $f$ is

$$\begin{aligned}
r(t_p+t_f) = &\cos(zt_f)\Big\{\frac{e^{-\gamma(t_p+t_f)}}{z^2+A^2}[-zAn_0(1-\cos(\sqrt{z^2+A^2}t_p))+r_0(A^2+z^2\cos(\sqrt{A^2+z^2}t_p))]\\
&-\frac{zi_0}{\sqrt{z^2+A^2}}e^{-\gamma(t_p+t_f)}\sin(\sqrt{z^2+A^2}t_p)\\
&-\frac{zA(n_{eq}-1/2)}{\gamma^2+z^2+A^2}e^{-\gamma t_f}[1-e^{-\gamma t_p}(\cos(\sqrt{z^2+A^2}t_p)+\frac{\gamma}{\sqrt{z^2+A^2}}\sin(\sqrt{z^2+A^2}t_p))]\Big\}\\
&-\sin(zt_f)\Big\{\frac{e^{-\gamma(t_p+t_f)}}{\sqrt{z^2+A^2}}[An_0\sin(\sqrt{z^2+A^2}t_p)+zr_0\sin(\sqrt{A^2+z^2}t_p)]\\
&+i_0e^{-\gamma(t_p+t_f)}\sin(\sqrt{z^2+A^2}t_p)\\
&+\frac{\gamma A(n_{eq}-1/2)}{\gamma^2+z^2+A^2}e^{-\gamma t_f}[1-e^{-\gamma tp}(\cos(\sqrt{z^2+A^2}tp)-\frac{\sqrt{z^2+A^2}}{\gamma}\sin(\sqrt{z^2+A^2}tp))]\Big\}.
\end{aligned} \tag{B.54}$$

And for the imaginary part we obtain

$$\begin{aligned}
i(t_p+t_f) = &\cos(zt_f)\Big\{\frac{e^{-\gamma(t_p+t_f)}}{\sqrt{z^2+A^2}}[An_0\sin(\sqrt{z^2+A^2}t_p)+zr_0\sin(\sqrt{A^2+z^2}t_p)]\\
&+i_0e^{-\gamma(t_p+t_f)}\sin(\sqrt{z^2+A^2}t_p)\\
&+\frac{\gamma A(n_{eq}-1/2)}{\gamma^2+z^2+A^2}e^{-\gamma t_f}[1-e^{-\gamma tp}(\cos(\sqrt{z^2+A^2}tp)-\frac{\sqrt{z^2+A^2}}{\gamma}\sin(\sqrt{z^2+A^2}tp))]\Big\}\\
&+\sin(zt_f)\Big\{\frac{e^{-\gamma(t_p+t_f)}}{z^2+A^2}[-zAn_0(1-\cos(\sqrt{z^2+A^2}t_p))+r_0(A^2+z^2\cos(\sqrt{A^2+z^2}t_p))]\\
&-\frac{zi_0}{\sqrt{z^2+A^2}}e^{-\gamma(t_p+t_f)}\sin(\sqrt{z^2+A^2}t_p)\\
&-\frac{zA(n_{eq}-1/2)}{\gamma^2+z^2+A^2}e^{-\gamma t_f}[1-e^{-\gamma t_p}(\cos(\sqrt{z^2+A^2}t_p)+\frac{\gamma}{\sqrt{z^2+A^2}}\sin(\sqrt{z^2+A^2}t_p))]\Big\}.
\end{aligned} \tag{B.55}$$

In the limit $t_f \to 0$, the solution reduce to the expression given in Eqs. (8) and (9) in paper 1.

### B.3.1 Derivation for pulses, for general $T_1$ and $T_2$, assuming resonance

In this section we are interested in the saturation level of the density matrix for a driven TLS, in general the driving might be pulsed. We here want to loosen the assumption that the decoherence is symmetric, i.e. that

$\gamma = 1/T_1 = 1/T_2$. This makes solution much more complicated, but we can obtain a solution if we assume that the driving is resonant with the eigenfrequency of the TLS, $\omega = \Omega$.

The equations of motion we consider is identical to Eq. B.49, where we set the detuning to zero, $z = 0$ We find the following set of eigenvectors (here we use the notation $N = \frac{\eta \Delta_0}{\hbar}$)

$$\begin{aligned}
\lambda_1 &= \frac{-1}{T_2}, & x_1 &= \begin{bmatrix} 0 \\ 1 \\ 0 \end{bmatrix} \\
\lambda_2 &= -\frac{1}{T_1} - \frac{1}{2T_2} + \phi, & x_2 &= \begin{bmatrix} -\frac{1}{T_1} + \frac{1}{2T_2} + \phi \\ 0 \\ N \end{bmatrix} \\
\lambda_3 &= -\frac{1}{T_1} - \frac{1}{2T_2} - \phi, & x_3 &= \begin{bmatrix} -\frac{1}{T_1} + \frac{1}{2T_2} - \phi \\ 0 \\ N \end{bmatrix},
\end{aligned} \tag{B.56}$$

where $\phi = \sqrt{(\frac{1}{2T_2} - \frac{1}{T_1})^2 - N^2}$.

The homogeneous solution is

$$y_h = c_1 e^{\lambda_1 t} \vec{x}_1 + c_2 e^{\lambda_2 t} \vec{x}_2 + c_3 e^{\lambda_3 t} \vec{x}_3 \tag{B.57}$$

and the particular solution is

$$y_p = \begin{bmatrix} \frac{1}{2} + \frac{\rho_{++}^{eq} - 1/2}{1 + \frac{I}{I_c}} \\ 0 \\ T_2 N \frac{\rho_{++}^{eq} - 1/2}{1 + \frac{I}{I_c}} \end{bmatrix}$$

where the saturation level of the density matrix is denoted $I/I_c = \frac{T_1 T_2}{2} N^2$. We also introduce $A = -\frac{1}{T_1} + \frac{1}{2T_2} + \sqrt{(\frac{1}{2T_2} - \frac{1}{T_1})^2 - N^2}$ and $B = -\frac{1}{T_1} + \frac{1}{2T_2} - \sqrt{(\frac{1}{2T_2} - \frac{1}{T_1})^2 - N^2}$. The general solution of the Bloch-Redfield equations transformed back to the non-rotating reference system can now be

written

$$\begin{aligned}
\rho_{++}(t) &= Ac_2e^{\lambda_2 t} + Bc_3e^{\lambda_3 t} + \frac{1}{2} + \frac{\rho_{++}^{eq}}{1+I/Ic},\\
\mathrm{Re}\,\rho_{-+}(t) &= c_1e^{\lambda_1 t}\cos(\Omega t) - N\left(c_2e^{\lambda_2 t} + c_3e^{\lambda_3 t} + T_2\frac{\rho_{++}^{eq}}{1+I/Ic}\right)\sin(\Omega t),\\
\mathrm{Im}\,\rho_{-+}(t) &= c_1e^{\lambda_1 t}\sin(\Omega t) + N\left(c_2e^{\lambda_2 t} + c_3e^{\lambda_3 t} + T_2\frac{\rho_{++}^{eq}}{1+I/Ic}\right)\cos(\Omega t).
\end{aligned} \tag{B.58}$$

We need to determine the coefficients $c_1$, $c_2$ and $c_3$ in order to solve the initial value problem. In the following we also introduce the notation $R = \frac{\rho_{++}^{eq}}{1+I/Ic}$. The initial values are

$$\begin{aligned}
\rho_{++}(0) &= Ac_2 + Bc_3 + \frac{1}{2} + R = z,\\
\mathrm{Re}\,\rho_{-+}(0) &= c_1 = x,\\
\mathrm{Im}\,\rho_{-+}(0) &= N(c_2 + c_3 + 1/2 + T_2R) = y,
\end{aligned} \tag{B.59}$$

and by inverting the equations we obtain

$$\begin{aligned}
c_1 &= x,\\
c_2 &= (z - \frac{yB}{N} - \frac{1}{2} - R(1-T_2B))\frac{1}{B-A},\\
c_3 &= (z - \frac{yA}{N} - \frac{1}{2} - R(1-T_2A))\frac{1}{A-B}.
\end{aligned} \tag{B.60}$$

We can then write down the final solution in the presence of external field

$$\begin{aligned}
\rho_{++}(t_p) &= e^{\lambda_2 t_p}\frac{A}{A-B}[z - \frac{yB}{N} - \frac{1}{2} - R(1-T_2B)]\\
&\quad + e^{\lambda_3 t_p}\frac{B}{B-A}[z - \frac{yA}{N} - \frac{1}{2} - R(1-T_2A)] + \frac{1}{2} + R,\\
\mathrm{Re}\,\rho_{-+}(t_p) &= xe^{\lambda_1 t_p}\cos(\Omega t_p) - \Big\{e^{\lambda_2 t_p}\frac{N}{A-B}[z - \frac{yB}{N} - \frac{1}{2} - R(1-T_2B)]\\
&\quad + e^{\lambda_3 t_p}\frac{N}{B-A}[z - \frac{yA}{N} - \frac{1}{2} - R(1-T_2A)] + T_2NR\Big\}\sin(\Omega t_p),\\
\mathrm{Im}\,\rho_{-+}(t_p) &= xe^{\lambda_1 t_p}\sin(\Omega t_p) + \Big\{e^{\lambda_2 t_p}\frac{N}{A-B}[z - \frac{yB}{N} - \frac{1}{2} - R(1-T_2B)]\\
&\quad + e^{\lambda_3 t_p}\frac{N}{B-A}[z - \frac{yA}{N} - \frac{1}{2} - R(1-T_2A)] + T_2NR\Big\}\cos(\Omega t_p).
\end{aligned} \tag{B.61}$$

The solution of the Bloch-Redfield equations Eq. (B.49) in the absence of external field is far more trivial.

$$\begin{aligned}\rho_{++}(t_f) &= ze^{\frac{-2t_f}{T_1}} + \rho_{++}^{eq}(1 - e^{\frac{-2t_f}{T_1}}),\\ \mathrm{Re}\,\rho_{-+}(t_f) &= xe^{\frac{-t_f}{T_2}}\cos(\omega t_f) - ye^{\frac{-t_f}{T_2}}\sin(\omega t_f),\\ \mathrm{Im}\,\rho_{-+}(t_f) &= xe^{\frac{-t_f}{T_2}}\sin(\omega t_f) + ye^{\frac{-t_f}{T_2}}\cos(\omega t_f).\end{aligned} \tag{B.62}$$

Since we are mainly interested in saturation of the qubit rather than the transient behavior, we want to find the steady state solution of the two-level system density matrix when subjected to a infinite sequence of pulses. We write the time evolution of the density matrix as follows

$$\rho(t = t_p + t_f) = P(t_f)M(t_p)\rho + P(t_f)m(t_p) + p(t_f) = U\rho + u.$$

Since we have already found the time evolution of $\rho$ we can read off the matrices $M$ and $P$ directly

$$M(t_p) = \begin{bmatrix} \frac{Ae^{\lambda_2 t_p} - Be^{\lambda_3 t_p}}{A-B} & 0 & -\frac{AB(e^{\lambda_2 t_p} - e^{\lambda_3 t_p})}{N(A-B)} \\ -\frac{N\sin(\Omega t_p)(e^{\lambda_2 t_p} - e^{\lambda_3 t_p})}{(A-B)} & \cos(\Omega t_p)e^{\lambda_1 t_p} & -\frac{\sin(\Omega t_p)(Ae^{\lambda_2 t_p} - Be^{\lambda_3 t_p})}{(A-B)} \\ -\frac{N\cos(\Omega t_p)(e^{\lambda_2 t_p} - e^{\lambda_3 t_p})}{(A-B)} & \sin(\Omega t_p)e^{\lambda_1 t_p} & -\frac{\cos(\Omega t_p)(Ae^{\lambda_2 t_p} - Be^{\lambda_3 t_p})}{(A-B)} \end{bmatrix} \tag{B.63}$$

and

$$m(t_p) = \begin{bmatrix} \frac{Ae^{\lambda_2 t_p}(-\frac{1}{2} - R(1-T_2B)) + Be^{\lambda_3 t_p}(-\frac{1}{2} - R(1-T_2A))}{A-B}) + \frac{1}{2} + R \\ -\frac{N\sin(\Omega t_p)}{A-B}[e^{\lambda_2 t_p}(-\frac{1}{2} - R(1-T_2B)) + e^{\lambda_3 t_p}(-\frac{1}{2} - R(1-T_2A)) + T_2R] \\ \frac{N\cos(\Omega t_p)}{A-B}[e^{\lambda_2 t_p}(-\frac{1}{2} - R(1-T_2B)) + e^{\lambda_3 t_p}(-\frac{1}{2} - R(1-T_2A)) + T_2R] \end{bmatrix}. \tag{B.64}$$

In the absence of the driving field we have

$$P(t_f) = \begin{bmatrix} e^{\frac{-2t_f}{T_1}} & 0 & 0 \\ 0 & \cos(\omega t_f)e^{\frac{-t_f}{T_2}} & -\sin(\omega t_f)e^{\frac{-t_f}{T_2}} \\ 0 & \sin(\omega t_f)e^{\frac{-t_f}{T_2}} & \cos(\omega t_f)e^{\frac{-t_f}{T_2}} \end{bmatrix} \tag{B.65}$$

and

$$p(t_f) = \begin{bmatrix} \rho_{++}^{eq}(1 - e^{\frac{2t_f}{T_1}}) \\ 0 \\ 0. \end{bmatrix} \tag{B.66}$$

We are now looking for the full time evolution of a infinite sequence of pulses. The density matrix $\rho$ after the $n$-th combined pulse-free evolution sequence is

$$\rho_{n+1} = PM\rho_n + Pm + p.$$

By substituting $\rho_n = u_n + c$ we get

$$u_{n+1} + c = PMu_n + PMc + Pm + p.$$

If we then choose

$$c = (1 - PM)^{-1}(Pm + p), \tag{B.67}$$

we obtain that

$$\rho_n = c + u_n = c + (PM)^n u_0.$$

In practice we have a damped system for the parameter interval we are interested in and thus $(PM)^n$ goes to zero for large $n$.

It remains to compute $U = PM$ and $Pm + p$ (we write $\omega = \Omega$ since our calculation already assumes resonance). We get

$$U(t_f + t_p) = \begin{bmatrix} e^{\frac{-2t_f}{T_1}} \frac{Ae^{\lambda_2 t_p} + Be^{\lambda_3 t_p}}{A-B} & 0 & -e^{\frac{-2t_f}{T_1}} \frac{AB(e^{\lambda_2 t_p} - e^{\lambda_3 t_p})}{N(A-B)} \\ -e^{\frac{-t_f}{T_2}} \frac{N \sin(\Omega(t_p+t_f))(e^{\lambda_2 t_p} - e^{\lambda_3 t_p})}{(A-B)} & e^{\frac{-t_f}{T_2}} \cos(\Omega(t_p + t_f))e^{\lambda_1 t_p} & -e^{\frac{-t_f}{T_2}} \frac{\sin(\Omega(t_p+t_f))(Ae^{\lambda_2 t_p} - Be^{\lambda_3 t_p})}{(A-B)} \\ -e^{\frac{-t_f}{T_2}} \frac{N \cos(\Omega(t_p+t_f))(e^{\lambda_2 t_p} - e^{\lambda_3 t_p})}{(A-B)} & e^{\frac{-t_f}{T_2}} \sin(\Omega(t_p + t_f))e^{\lambda_1 t_p} & -e^{\frac{-t_f}{T_2}} \frac{\cos(\Omega(t_p+t_f))(Ae^{\lambda_2 t_p} - Be^{\lambda_3 t_p})}{(A-B)} \end{bmatrix} \tag{B.68}$$

and

$$P(t_f)m(t_p) + p(t_f) = \begin{bmatrix} e^{\frac{-2t_f}{T_1}} [\frac{Ae^{\lambda_2 t_p}(-\frac{1}{2} - R(1-T_2B)) + Be^{\lambda_3 t_p}(-\frac{1}{2} - R(1-T_2B))}{A-B}) + \frac{1}{2} + R] + \rho_{++}^{eq}(1 - e^{\frac{2t_f}{T_1}}) \\ -e^{\frac{-t_f}{T_2}} \frac{N \sin(\Omega(t_p+t_f))}{A-B} [e^{\lambda_2 t_p}(-\frac{1}{2} - R(1-T_2B)) + Be^{\lambda_3 t_p}(-\frac{1}{2} - R(1-T_2A)) + T_2R] \\ -e^{\frac{-t_f}{T_2}} \frac{N \cos(\Omega(t_p+tf))}{A-B} [e^{\lambda_2 t_p}(-\frac{1}{2} - R(1-T_2B)) + Be^{\lambda_3 t_p}(-\frac{1}{2} - R(1-T_2A)) + T_2R] \end{bmatrix}. \tag{B.69}$$

We have finally obtained all the expressions we need in order to find the saturation level of the TLS in steady state, given by

$$\rho(t \to \infty) = c,$$

where $c$ is given by Eq. (B.67).

### B.3.2 Realistic pulses: averaging over the length of the pulse

In the preceeding analysis of this section, we assumed a fixed time $t_p$ for the driving pulse. The fixed pulse time give rise to sharp resonance dips in the saturation level of the TLS as a function of the driving strength $\eta$, see Fig. 3.5. For realistic pulse generators we expect that we are not able to generate perfectly sharp square pulses. To account for the finite rise time and the randomness in the onset of the square pulse we might average over a distribution of pulses of slightly different lengths $t_p$.

The simplest assumption for the distribution of pulse lengths is the Gaussian distribution

$$f(t) = e^{-\frac{(t-\bar{t}_p)^2}{2\sigma^2}}, \tag{B.70}$$

where $\bar{t}_p$ is the mean pulse length and $\sigma$ is the standard deviation in the length of the pulse.

By use of the Gaussian distribution, Eq. (B.70), we can compute the ensemble averaged versions of the propagators during the pulse given by Eqs. (B.63) and (B.64). We define the ensemble average by

$$\langle U(t_p)\rangle_{t_p} = \frac{\int_{-\infty}^{\infty} dt_p e^{\frac{-(t_p-\bar{t}_p)^2}{2\sigma^2}} U(t_p)}{\int_{-\infty}^{\infty} dt_p e^{\frac{-(t_p-\bar{t}_p)^2}{2\sigma^2}}} \tag{B.71}$$

and obtain the following expressions for the pulse length averaged propa-

gators:

$$
\begin{aligned}
\langle M_{11}(t_p)\rangle_{t_p} &= \frac{Ae^{\frac{\sigma^2\lambda_2^2}{2}+\lambda_2\bar{t}_p} - Be^{\frac{\sigma^2\lambda_3^2}{2}+\lambda_3\bar{t}_p}}{A-B},\\
\langle M_{12}(t_p)\rangle_{t_p} &= 0,\\
\langle M_{13}(t_p)\rangle_{t_p} &= -\frac{AB(e^{\frac{\sigma^2\lambda_2^2}{2}+\lambda_2\bar{t}_p} - e^{\frac{\sigma^2\lambda_3^2}{2}+\lambda_3\bar{t}_p})}{N(A-B)},\\
\langle M_{21}(t_p)\rangle_{t_p} &= -\frac{N\left[\sin(\Omega(\bar{t}_p+\lambda_2\sigma^2))e^{\frac{\sigma^2\lambda_2^2}{2}+\lambda_2\bar{t}_p} - \sin(\Omega(\bar{t}_p+\lambda_3\sigma^2))e^{\frac{\sigma^2\lambda_3^2}{2}+\lambda_3\bar{t}_p}\right]}{(A-B)},\\
\langle M_{22}(t_p)\rangle_{t_p} &= \cos(\Omega(\bar{t}_p+\lambda_1\sigma^2))e^{\frac{\sigma^2\lambda_1^2}{2}+\lambda_1\bar{t}_p},\\
\langle M_{23}(t_p)\rangle_{t_p} &= -\frac{A\sin(\Omega(\bar{t}_p+\lambda_2\sigma^2))e^{\frac{\sigma^2\lambda_2^2}{2}+\lambda_2\bar{t}_p} - B\sin(\Omega(\bar{t}_p+\lambda_3\sigma^2))e^{\frac{\sigma^2\lambda_3^2}{2}+\lambda_3\bar{t}_p}}{(A-B)},\\
\langle M_{31}(t_p)\rangle_{t_p} &= -\frac{N\left[\cos(\Omega(\bar{t}_p+\lambda_2\sigma^2))e^{\frac{\sigma^2\lambda_2^2}{2}+\lambda_2\bar{t}_p} - \cos(\Omega(\bar{t}_p+\lambda_3\sigma^2))e^{\frac{\sigma^2\lambda_3^2}{2}+\lambda_3\bar{t}_p}\right]}{(A-B)},\\
\langle M_{32}(t_p)\rangle_{t_p} &= \sin(\Omega(\bar{t}_p+\lambda_1\sigma^2))e^{\frac{\sigma^2\lambda_1^2}{2}+\lambda_1\bar{t}_p},\\
\langle M_{33}(t_p)\rangle_{t_p} &= -\frac{A\cos(\Omega(\bar{t}_p+\lambda_2\sigma^2))e^{\frac{\sigma^2\lambda_2^2}{2}+\lambda_2\bar{t}_p} - B\cos(\Omega(\bar{t}_p+\lambda_3\sigma^2))e^{\frac{\sigma^2\lambda_3^2}{2}+\lambda_3\bar{t}_p}}{(A-B)}.
\end{aligned}
\tag{B.72}
$$

and

$$
\begin{aligned}
\langle m_1(t_p)\rangle_{t_p} &= \frac{Ae^{\frac{\sigma^2\lambda_2^2}{2}+\lambda_2\bar{t}_p}(-\frac{1}{2}-R(1-T_2B) + Be^{\frac{\sigma^2\lambda_3^2}{2}+\lambda_3\bar{t}_p}(-\frac{1}{2}-R(1-T_2A)}{A-B}) + \frac{1}{2} + R,\\
\langle m_2(t_p)\rangle_{t_p} &= -\frac{N}{A-B}[\sin(\Omega(\bar{t}_p+\lambda_2\sigma^2)e^{\frac{\sigma^2\lambda_2^2}{2}+\lambda_2 t_p}(-\frac{1}{2}-R(1-T_2B))\\
&\quad + \sin(\Omega(\bar{t}_p+\lambda_3\sigma^2)e^{\frac{\sigma^2\lambda_3^2}{2}+\lambda_2 t_p}(-\frac{1}{2}-R(1-T_2A)) + T_2R],\\
\langle m_3(t_p)\rangle_{t_p} &= \frac{N}{A-B}[\cos(\Omega(\bar{t}_p+\lambda_2\sigma^2)e^{\frac{\sigma^2\lambda_2^2}{2}+\lambda_2 t_p}(-\frac{1}{2}-R(1-T_2B))\\
&\quad + \cos(\Omega(\bar{t}_p+\lambda_3\sigma^2)e^{\frac{\sigma^2\lambda_3^2}{2}+\lambda_2 t_p}(-\frac{1}{2}-R(1-T_2A)) + T_2R].
\end{aligned}
\tag{B.73}
$$

From these expressions we can compute the averaged expressions for the quantities $U(t_f+t_p)$ and $P(t_f)m(t_p)+p(t_f)$ of Eqs. (B.68) and (B.69).

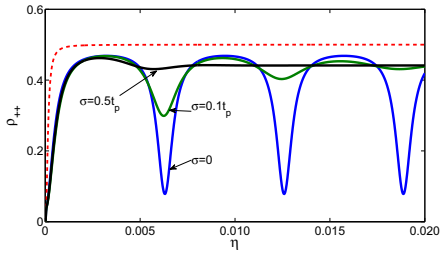


Figure B.1: The saturation level of the TLS in steady state for pulsed driving as a function of the driving strength $\eta = \frac{\mathbf{E_{ac}}\cdot\mathbf{p}}{E}$ for relaxation rates $\gamma = 1.25 \cdot 10^6$. The solid graphs shows the saturation level of the TLS in steady state at the onset of the next pulse for different Gaussian distributions of pulse lengths. The saturation level for continuous driving with the same average intensity as for the pulse sequence is plotted for comparision, red dashed graph. The standard deviation in the distribution, Eq. (B.70), is a) blue graph: $\sigma = 0$, b) green graph: $\sigma = 0.1t_p$ and c) black graph$\sigma = 0.5t_p$. The parameters are as given in the article by John Martinis et. al. for a charge qubit [97]: $\Delta_0/\hbar = 10$GHz, dipole moment $p = 3.7$D and electric field $E_{AC} = 3 \cdot 10^3$V/m. The average lenght of the pulses is $\bar{t}_p = 10^8$ and the time between each pulse $t_f = 10 \cdot t_p$. The thermal equilibrium level is $\rho^{eq}_{++} = 0$.

The expression, Eq. (B.67), then gives us the density matrix in steady state $\rho(t \to \infty)$ averaged over the length of the pulses. As an example, the saturation level in steady state for three different values of $\sigma$ is plotted in Fig. B.1. We see that the sharp resonance peaks are smeared out as the pulse length becomes less sharp. However, the results are not significantly altered until $\sigma$ is of the order of a few percent of $t_p$ which could in principle be avoided by a state of the art pulse generator.

# Appendix C

# Complementary derivations for the third paper

In this chapter we will give supplementary derivations, that were not given explicitly in the paper.

## C.1 The time evolution operator

The time evolution operator is defined by

$$U = e^{-\frac{i}{\hbar}H_0 t} = S e^{-\frac{i}{\hbar}Dt} S^{-1},$$

where $S$ is the eigenvector matrix of $H_0$ and $D$ is the eigenvalue matrix. With

$$S = \begin{pmatrix} \eta_- + \eta_+ & \eta_+ - \eta_- & -\gamma_+ - \gamma_- & \gamma_+ - \gamma_- \\ \eta_- - \eta_+ & \eta_+ + \eta_- & +\gamma_+ - \gamma_- & \gamma_+ + \gamma_- \\ \eta_- - \eta_+ & \eta_+ + \eta_- & -\gamma_+ + \gamma_- & -\gamma_+ - \gamma_- \\ \eta_- + \eta_+ & \eta_+ - \eta_- & +\gamma_+ + \gamma_- & -\gamma_+ + \gamma_- \end{pmatrix}, \tag{C.1}$$

$$e^{-\frac{i}{\hbar}Dt} = \begin{pmatrix} e^{-\frac{i}{\hbar}\Omega t} & 0 & 0 & 0 \\ 0 & e^{\frac{i}{\hbar}\Omega t} & 0 & 0 \\ 0 & 0 & e^{-\frac{i}{\hbar}\epsilon t} & 0 \\ 0 & 0 & 0 & e^{\frac{i}{\hbar}\epsilon t} \end{pmatrix} \tag{C.2}$$

and $S^{-1} = S^T$, we obtain for the matrix elements of $U$:

$$
\begin{aligned}
U_{11} &= (\eta_+^2 + \eta_-^2)\frac{\cos\Omega t}{2} - i\eta_+\eta_- \sin\Omega t + (\gamma_+^2 + \gamma_-^2)\frac{\cos\Omega t}{2} - i\gamma_+\gamma_- \sin\Omega t \\
U_{12} &= i(\eta_+^2 - \eta_-^2)\frac{\sin\Omega t}{2} + (\gamma_+^2 - \gamma_-^2)\frac{\sin\Omega t}{2} \\
U_{13} &= i(\eta_+^2 - \eta_-^2)\frac{\sin\Omega t}{2} - (\gamma_+^2 - \gamma_-^2)\frac{\sin\Omega t}{2} \\
U_{14} &= (\eta_+^2 + \eta_-^2)\frac{\cos\Omega t}{2} - i\eta_+\eta_- \sin\Omega t - (\gamma_+^2 + \gamma_-^2)\frac{\cos\Omega t}{2} + i\gamma_+\gamma_- \sin\Omega t \\
U_{22} &= (\eta_+^2 + \eta_-^2)\frac{\cos\Omega t}{2} + i\eta_+\eta_- \sin\Omega t + (\gamma_+^2 + \gamma_-^2)\frac{\cos\Omega t}{2} + i\gamma_+\gamma_- \sin\Omega t \\
U_{23} &= (\eta_+^2 + \eta_-^2)\frac{\cos\Omega t}{2} + i\eta_+\eta_- \sin\Omega t - (\gamma_+^2 + \gamma_-^2)\frac{\cos\Omega t}{2} - i\gamma_+\gamma_- \sin\Omega t \\
U_{24} &= i(\eta_+^2 - \eta_-^2)\frac{\sin\Omega t}{2} - (\gamma_+^2 - \gamma_-^2)\frac{\sin\Omega t}{2} \\
U_{33} &= (\eta_+^2 + \eta_-^2)\frac{\cos\Omega t}{2} + i\eta_+\eta_- \sin\Omega t - (\gamma_+^2 + \gamma_-^2)\frac{\cos\Omega t}{2} + i\gamma_+\gamma_- \sin\Omega t \\
U_{34} &= i(\eta_+^2 - \eta_-^2)\frac{\sin\Omega t}{2} + (\gamma_+^2 - \gamma_-^2)\frac{\sin\Omega t}{2} \\
U_{33} &= (\eta_+^2 + \eta_-^2)\frac{\cos\Omega t}{2} - i\eta_+\eta_- \sin\Omega t - (\gamma_+^2 + \gamma_-^2)\frac{\cos\Omega t}{2} - i\gamma_+\gamma_- \sin\Omega t.
\end{aligned}
\tag{C.3}
$$

Here we have given the upper triangle of the symmetric matrix $U$, and used $\hbar = 1$ units.

## C.2 Solutions for the Bloch vector in the stationary path approximation

In the stationary path approximation we have tabulated the decay of the Bloch vector for different initial states. The table can be found on page 4 in the third paper and is computed by use of the formula

$$
\alpha_{15}(t) = \sqrt{\frac{3}{2}} - \sqrt{\frac{3}{2} - \sum_{i=1}^{14} \alpha_i^2(t)} \approx \sqrt{\frac{1}{6}} \sum_{i=1}^{14} \alpha_i^2(t). \tag{C.4}
$$

The decay of the mean square of the different components is in the paper only given for the initial state $|\psi_0\rangle = |01\rangle - |10\rangle$. Here we give the solutions for the components for the last three tabulated initial states.

For the initial state $|\psi\rangle = |01\rangle + |10\rangle$ we have

$$\begin{aligned}
\langle\alpha_9^2(t)\rangle &= \langle\alpha_{13}^2(t)\rangle = \frac{\langle\sigma\xi^2\rangle}{8}\Big[\frac{1-\cos\omega_- t}{\omega_-} + \frac{1-\cos\omega_+ t}{\omega_+}\Big]^2 \\
\langle\alpha_{10}^2(t)\rangle &= \langle\alpha_{14}^2(t)\rangle = \frac{\langle\sigma\xi^2\rangle}{8}\Big[\frac{\sin\omega_- t}{\omega_-} - \frac{\sin\omega_+ t}{\omega_+}\Big]^2 \\
\langle\alpha_{11}^2(t)\rangle &= \frac{\langle\delta\xi^2\rangle}{4}\Big[\frac{1-\cos\omega_- t}{\omega_-} - \frac{1-\cos\omega_+ t}{\omega_+}\Big]^2 \\
\langle\alpha_{12}^2(t)\rangle &= \frac{\langle\delta\xi^2\rangle}{4}\Big[\frac{\sin\omega_- t}{\omega_-} + \frac{\sin\omega_+ t}{\omega_+}\Big]^2 .
\end{aligned} \tag{C.5}$$

We observe that the Bloch vector in this case diffusion is enhanced along the $\lambda_9$, $\lambda_{10}$, $\lambda_{13}$ and $\lambda_{14}$ components if the noise is correlated.While it is diminished for anticorrelated noise, in contrast to what was found for the initial state $|\psi\rangle = |01\rangle - |10\rangle$, where the noise vanished for all components in the presence of fully correlated noise.

For the initial state $|\psi\rangle = |00\rangle + |11\rangle$ we get

$$\begin{aligned}
\langle\alpha_9^2(t)\rangle &= \langle\alpha_{11}^2(t)\rangle = \frac{\langle\delta\xi^2\rangle}{8}\Big[\frac{1-\cos\omega_- t}{\omega_-} + \frac{1-\cos\omega_+ t}{\omega_+}\Big]^2 \\
\langle\alpha_{10}^2(t)\rangle &= \langle\alpha_{12}^2(t)\rangle = \frac{\langle\delta\xi^2\rangle}{8}\Big[\frac{\sin\omega_- t}{\omega_-} - \frac{\sin\omega_+ t}{\omega_+}\Big]^2 \\
\langle\alpha_{13}^2(t)\rangle &= \frac{\langle\sigma\xi^2\rangle}{4}\Big[\frac{1-\cos\omega_- t}{\omega_-} - \frac{1-\cos\omega_+ t}{\omega_+}\Big]^2 \\
\langle\alpha_{14}^2(t)\rangle &= \frac{\langle\sigma\xi^2\rangle}{4}\Big[\frac{\sin\omega_- t}{\omega_-} + \frac{\sin\omega_+ t}{\omega_+}\Big]^2 ,
\end{aligned} \tag{C.6}$$

while for the state $|\psi\rangle = |00\rangle - |11\rangle$ we find

$$\begin{aligned}
\langle\alpha_9^2(t)\rangle &= \langle\alpha_{10}^2(t)\rangle = \frac{\langle\sigma\xi^2\rangle}{8}\Big[\frac{1-\cos\omega_- t}{\omega_-} + \frac{1-\cos\omega_+ t}{\omega_+}\Big]^2 \\
\langle\alpha_{10}^2(t)\rangle &= \langle\alpha_{12}^2(t)\rangle = \frac{\langle\sigma\xi^2\rangle}{8}\Big[\frac{\sin\omega_- t}{\omega_-} - \frac{\sin\omega_+ t}{\omega_+}\Big]^2 \\
\langle\alpha_{13}^2(t)\rangle &= \frac{\langle\sigma\xi^2\rangle}{4}\Big[\frac{1-\cos\omega_- t}{\omega_-} - \frac{1-\cos\omega_+ t}{\omega_+}\Big]^2 \\
\langle\alpha_{14}^2(t)\rangle &= \frac{\langle\sigma\xi^2\rangle}{4}\Big[\frac{\sin\omega_- t}{\omega_-} + \frac{\sin\omega_+ t}{\omega_+}\Big]^2 .
\end{aligned} \tag{C.7}$$

It is evident that for fully anticorrelated noise $\langle \sigma \xi^2 \rangle = 0$, the noise vanishes along all directions.

## C.3 Solution for intermediate times

In the article we give only parts of the derivation of our expression for $\Gamma$ and only for the initial state $|\psi_0\rangle = |01\rangle$.

Here we will go through the solution for the initial state $|\psi_0\rangle = |01\rangle - |10\rangle$:

The transformation

$$\rho = S^{-1}\rho' S, \quad V''(t) = S^{-1}V'(t)S, \tag{C.8}$$

to the frame where the initial state lies on the south pole of the Bloch sphere along the $\lambda_{15}$ axis is carried out by the transformation matrix

$$S = \frac{1}{\sqrt{2}} \begin{pmatrix} \sqrt{2} & 0 & 0 & 0 \\ 0 & -1 & 0 & -1 \\ 0 & -1 & 0 & 1 \\ 0 & 0 & \sqrt{2} & 0 \end{pmatrix}. \tag{C.9}$$

By use of this transform and the equation

$$\dot{\alpha}_i(t) \approx f_{ij15}\beta_j(t)m_{15}(0), \tag{C.10}$$

we obtain the following equations of motions along the 6-dimensional tangent subspace of the Bloch sphere.

$$
\begin{aligned}
\dot{\alpha}_9(t) &= \mathrm{Im}\,\frac{V'_{12}-V'_{13}}{\sqrt{2}} = \frac{\xi_1(t)}{\sqrt{2}}[\lambda_1\sin\omega_- t+\lambda_2\sin\omega_+ t]\\
&\quad -\frac{\xi_2(t)}{\sqrt{2}}[\lambda_2\sin\omega_- t+\lambda_1\sin\omega_+ t]\\
\dot{\alpha}_{10}(t) &= \mathrm{Re}\,\frac{V'_{12}-V'_{13}}{\sqrt{2}} = \frac{\xi_1(t)}{\sqrt{2}}[-(\mu_{1-}+\mu_{2-})(\cos\omega_- t+\cos\omega_+ t)]\\
&\quad +\frac{\xi_2(t)}{\sqrt{2}}[-(\mu_{1-}-\mu_{2-})(\cos\omega_- t+\cos\omega_+ t)]\\
\dot{\alpha}_{11}(t) &= \mathrm{Im}\,V'_{23} = (\xi_1(t)-\xi_2(t))[(\mu_{1+}+\mu_{2+})\sin\omega_- t+(\mu_{1+}-\mu_{2+})\sin\omega_+ t]\\
\dot{\alpha}_{12}(t) &= \mathrm{Re}(V'_{33}-V'_{22}) = \xi_1(t)[-(\eta_-\gamma_-+\eta_+\gamma_+)^2\cos\omega_- t-(\eta_-\gamma_+-\eta_+\gamma_-)^2\cos\omega_+ t]\\
&\quad +\xi_2(t)[-(\eta_-\gamma_++\eta_+\gamma_-)^2\cos\omega_- t+(\eta_-\gamma_--\eta_+\gamma_+)^2\cos\omega_+ t]\\
\dot{\alpha}_{13}(t) &= \mathrm{Im}\,\frac{V'_{12}-V'_{13}}{\sqrt{2}} = \frac{\xi_1(t)}{\sqrt{2}}[\lambda_1\sin\omega_- t+\lambda_2\sin\omega_+ t]\\
&\quad -\frac{\xi_2(t)}{\sqrt{2}}[\lambda_2\sin\omega_- t+\lambda_1\sin\omega_+ t]\\
\dot{\alpha}_{14}(t) &= \mathrm{Re}\,\frac{V'_{12}-V'_{13}}{\sqrt{2}} = \frac{\xi_1(t)}{\sqrt{2}}[-(\mu_{1-}+\mu_{2-})(\cos\omega_- t+\cos\omega_+ t)]\\
&\quad +\frac{\xi_2(t)}{\sqrt{2}}[-(\mu_{1-}-\mu_{2-})(\cos\omega_- t+\cos\omega_+ t)]. \qquad \text{(C.11)}
\end{aligned}
$$

For the mean square of the components we obtain

$$
\begin{aligned}
\langle\alpha_9^2(t)\rangle &= \frac{1}{2}\int_0^t dt_1\int_0^t dt_2\langle\xi_1(t_1)\xi_1(t_2)\rangle[\lambda_1^2\sin\omega_- t_1\sin\omega_- t_2\\
&\quad +\lambda_2^2\sin\omega_+ t_1\sin\omega_+ t_2+\lambda_1\lambda_2(\sin\omega_- t_1\sin\omega_+ t_2+\sin\omega_+ t_1\sin\omega_- t_2)]\\
&\quad +\langle\xi_2(t_1)\xi_2(t_2)\rangle[\lambda_1^2\sin\omega_- t_1\sin\omega_- t_2\\
&\quad +\lambda_2^2\sin\omega_+ t_1\sin\omega_+ t_2+\lambda_1\lambda_2(\sin\omega_- t_1\sin\omega_+ t_2+\sin\omega_+ t_1\sin\omega_- t_2)]\\
&\quad -\langle\xi_1(t_1)\xi_2(t_2)\rangle[\lambda_1\lambda_2(\sin\omega_- t_1\sin\omega_- t_2+\sin\omega_+ t_1\sin\omega_+ t_2)+\lambda_1^2\sin\omega_- t_1\sin\omega_+ t_2\\
&\quad +\lambda_2^2\sin\omega_+ t_1\sin\omega_- t_2]\\
&\quad -\langle\xi_2(t_1)\xi_1(t_2)\rangle[\lambda_1\lambda_2(\sin\omega_- t_1\sin\omega_- t_2+\sin\omega_+ t_1\sin\omega_+ t_2)+\lambda_2^2\sin\omega_- t_1\sin\omega_+ t_2\\
&\quad +\lambda_1^2\sin\omega_+ t_1\sin\omega_- t_2], \qquad \text{(C.12)}
\end{aligned}
$$

and by use of time translation invariance, the transformation $\tau = t_2 - t_1$ and $T = (t_1+t_2)/2$, and by assuming that the correlation time is much

shorter than the observation time $t \gg \tau_c$ we get

$$\begin{aligned}\langle\alpha_9^2(t)\rangle = \frac{1}{4}\int_0^t dT \int_{-\infty}^{\infty} d\tau \langle\xi_1(\tau)\xi_1(0)\rangle[\lambda_1^2(\cos\omega_-\tau - \cos\omega_- 2T) + \lambda_2^2(\cos\omega_+\tau - \cos\omega_+ 2T)\\ + \lambda_1\lambda_2(-\cos(\Omega\tau + 2\epsilon T) - \cos(\epsilon\tau + 2\Omega T) + \cos(\Omega\tau - 2\epsilon T) + \cos(\epsilon\tau - 2\Omega T))]\\ + \langle\xi_2(\tau)\xi_2(0)\rangle[\lambda_2^2(\cos\omega_-\tau - \cos\omega_- 2T) + \lambda_1^2(\cos\omega_+\tau - \cos\omega_+ 2T)\\ + \lambda_1\lambda_2(-\cos(\Omega\tau + 2\epsilon T) - \cos(\epsilon\tau + 2\Omega T) + \cos(\Omega\tau - 2\epsilon T) + \cos(\epsilon\tau - 2\Omega T))]\\ - 2\langle\xi_1(\tau)\xi_2(0)\rangle[\lambda_1\lambda_2(\cos\omega_-\tau - \cos\omega_- 2T + \cos\omega_+\tau - \cos\omega_+ 2T)\\ + \lambda_1^2(-\cos(\Omega\tau + 2\epsilon T) - \cos(\epsilon\tau + 2\Omega T)) + \lambda_2^2(\cos(\Omega\tau - 2\epsilon T) + \cos(\epsilon\tau - 2\Omega T))].\end{aligned} \tag{C.13}$$

As long as we observe over a time much longer than the oscillation frequencies of the two qubit-system $t \gg \max\{\Omega^{-1}, \epsilon^{-1}\omega_\pm^{-1}\}$, the terms that oscillates in $T$ can be neglected. Carrying out the integrals we obtain the final expression

$$\begin{aligned}\langle\alpha_9^2(t)\rangle = \frac{t}{4}\Big[\lambda_1^2(S_{11}(\omega_-) + S_{22}(\omega_+)) + \lambda_2^2(S_{11}(\omega_+) + S_{22}(\omega_-))\\ - 2\lambda_1\lambda_2(S_{12}(\omega_-) + S_{12}(\omega_+))\Big],\end{aligned} \tag{C.14}$$

where

$$S_{ij}(\omega) = \int_{-\infty}^{\infty} d\tau \langle\xi_i(\tau)\xi_j(0)\rangle\cos(\tau). \tag{C.15}$$

For the five other components we get the following expression by a similar derivation.

$$\begin{aligned}\langle\alpha_{10}^2(t)\rangle &= \frac{t}{4}\Big[(\mu_{1-} + \mu_{2-})^2(S_{11}(\omega_-) + S_{11}(\omega_+)) + (\mu_{1-} - \mu_{2-})^2(S_{22}(\omega_-) + S_{22}(\omega_+))\\ &\quad - 2(\mu_{1-}^2 - \mu_{2-}^2)(S_{12}(\omega_-) + S_{12}(\omega_+))\Big]\\ \langle\alpha_{11}^2(t)\rangle &= \frac{t}{4}\Big[(\mu_{1+} + \mu_{2+})^2(S_{11}(\omega_-) + S_{22}(\omega_-) - 2S_{12}(\omega_-)) + (\mu_{1+} - \mu_{2+})^2(S_{11}(\omega_+) + S_{22}(\omega_+) - 2S_{12}(\omega_+))\Big]\\ \langle\alpha_{12}^2(t)\rangle &= \frac{t}{4}\Big[(\eta_-\gamma_- + \eta_+\gamma_+)^4 S_{11}(\omega_-) + (\eta_-\gamma_+ - \eta_+\gamma_-)^4 S_{11}(\omega_+)\\ &\quad + (\eta_-\gamma_+ + \eta_+\gamma_-)^4 S_{22}(\omega_-) + (\eta_-\gamma_- - \eta_+\gamma_+)^4 S_{22}(\omega_+)\\ &\quad - 2(\eta_-\gamma_+ + \eta_+\gamma_-)^2(\eta_-\gamma_- + \eta_+\gamma_+)^2 S_{12}(\omega_-) - 2(\eta_-\gamma_+ - \eta_+\gamma_-)^2(\eta_-\gamma_- - \eta_+\gamma_+)^2 S_{12}(\omega_+)\Big]\\ \langle\alpha_{13}^2(t)\rangle &= \langle\alpha_9^2(t)\rangle\\ \langle\alpha_{14}^2(t)\rangle &= \langle\alpha_{10}^2(t)\rangle.\end{aligned} \tag{C.16}$$

We observe that the diffusion along the components, $\langle\alpha_{12}^2(t)\rangle$ and $\langle\alpha_{13}^2(t)\rangle$, is reduced in the presence of correlated noise sources. The component along $\lambda_{12}$ vanishes strictly for fully correlated noise, while the component along $\lambda_{13}$ vanishes if and only if the two qubits are at the co-resonance points. The diffusion along the four other components are reduced in the presence of anticorrelated noise sources, and enhances in the presence of correlated sources.

For the initial state $|\psi_0\rangle = |00\rangle$, the differential equations in the six directions is:

$$\begin{aligned}
\dot{\alpha}_9 &= (\xi_1(t) - \xi_2(t))\big[(\mu_{2+} + \mu_{1+})\sin\omega_- t \\
&\quad + (\mu_{2+} - \mu_{1+})\sin\omega_+ t\big] \\
\dot{\alpha}_{10} &= 0 \\
\dot{\alpha}_{11} &= \xi_1(t)\big[\lambda_1\sin\omega_- t + \lambda_2\sin\omega_+ t\big] \\
\dot{\alpha}_{12} &= \xi_1(t)\big[(\mu_{1-} + \mu_{2-})(\cos\omega_- t - \cos\omega_- t)\big] \\
\dot{\alpha}_{13} &= \xi_2(t)\big[\lambda_2\sin\omega_- t + \lambda_1\sin\omega_+ t\big] \\
\dot{\alpha}_{14} &= \xi_2(t)\big[(\mu_{1-} - \mu_{2-})(-\cos\omega_- t + \cos\omega_+ t)\big].
\end{aligned} \tag{C.17}$$

Already from this expression we see that only one out of the six directions available for dephasing motion is sensitive to correlations in the noise. The other components are only dependent on one of the noise sources. In this initial state, the noise along the $\lambda_{10}$ component vanishes regardless of correlations.

# Bibliography


[1] Aspect A, Grangier P and Roger G 1981 *Phys. Rev. Lett.* **47**(7) 460–463

[2] Ansmann M, Wang H, Bialczak R C, Hofheinz Maxand Lucero E, Neeley M, O'Connell A D, Sank D, Weides M, Wenner J, Cleland A N and Martinis J M 2009 *Nature* **461**(7263) 504–506

[3] Bohr N 1928 *nature* **121** 580–590

[4] Bohr N 1935 *Phys. Rev.* **48**(8) 696–702

[5] Bassi A and Ghirardi G 2003 *Physics Reports* **379** 257 – 426

[6] Arndt M, Nairz O, Vos-Andreae J, Keller C, van der Zouw G and Zeilinger A 1999 *Nature* **401**(6754) 680–682

[7] Feynman R P, edited by, Leighton R and Sands M 1965 *The Feynman Lectures on Physics, Volume III.* (Addison-Wesley, Massachusetts, USA)

[8] Zurek W H 1981 *Phys. Rev. D* **24**(6) 1516–1525

[9] Zurek W H 1982 *Phys. Rev. D* **26**(8) 1862–1880

[10] Ladd T D, Jelezko F, Laflamme R, Nakamura Y, Monroe C and O/'Brien J L 2010 *Nature* **464**(4) 45

[11] Cooper L N 1956 *Phys. Rev.* **104**(4) 1189–1190

[12] Nielsen M A and L C I 2000 *Quantum Computation and Quantum Information* (Cambridge University Press)

[13] Knill E, Laflamme R, Ashikhmin A, Barnum H, Viola L and Zurek W H 2001 Introduction to quantum error correction Tech. rep. Los Alamos Science

[14] Cory D G, Price M D, Maas W, Knill E, Laflamme R, Zurek W H, Havel T F and Somaroo S S 1998 *Phys. Rev. Lett.* **81**(10) 2152–2155

[15] Schindler P, Barreiro J T, Monz T, Nebendahl V, Nigg D, Chwalla M, Hennrich M and Blatt R 2011 *Science* **332** 1059–1061

[16] Reed M D, DiCarlo L, Nigg S E, Sun L, Frunzio L, Girvin S M and Schoelkopf R J 2011 *Nature* **482**(7385) 382–385

[17] Loss D and DiVincenzo D P 1998 *Phys. Rev. A* **57**(1) 120–126

[18] DiVincenzo D P 2000 *Fortschritte der Physik* **48** 771–783

[19] Barenco A, Bennett C H, Cleve R, DiVincenzo D P, Margolus N, Shor P, Sleator T, Smolin J A and Weinfurter H 1995 *Phys. Rev. A* **52**(5) 3457–3467

[20] Mizel A, Lidar D A and Mitchell M 2007 *Phys. Rev. Lett.* **99**(7) 070502

[21] Astafiev O, Pashkin Y A, Yamamoto T, Nakamura Y and Tsai J S 2004 *Phys. Rev. B* **69**(18) 180507

[22] Braginsky V B and Khalili F Y 1996 *Rev. Mod. Phys.* **68**(1) 1–11

[23] Rebentrost P, Serban I, Schulte-Herbrüggen T and Wilhelm F K 2009 *Phys. Rev. Lett.* **102** 090401

[24] Makhlin Y and Shnirman A 2004 *Phys. Rev. Lett.* **92**(17) 178301

[25] Viola L and Lloyd S 1998 *Phys. Rev. A* **58**(4) 2733–2744

[26] Uhrig G S 2007 *Phys. Rev. Lett.* **98**(10) 100504

[27] Uhrig G S 2009 *Phys. Rev. Lett.* **102**(12) 120502

[28] Biercuk M J, Uys H, VanDevender A P, Shiga N, Itano W M and Bollinger J J 2009 *Nature* **458**(7241) 996

[29] Shor P W 1995 *Phys. Rev. A* **52**(4) R2493–R2496

[30] Reed M D, DiCarlo L, Nigg S E, Sun L, Frunzio L, Girvin S M and Schoelkopf R J 2011 *Nature* **482**(7385) 382

[31] Stern A, Aharonov Y and Imry Y 1990 *Phys. Rev. A* **41**(7) 3436–3448

[32] Schlichter C P 1990 *Principles of Magnetic Resonance* (Springer-Verlag)

[33] Müller C, Shnirman A and Makhlin Y 2009 *Phys. Rev. B* **80**(13) 134517

[34] Wilhelm F, Storcz M, Hartmann U and Geller M 2007 Superconducting qubits ii: Decoherence *Manipulating Quantum Coherence in Solid State Systems* (*NATO Science Series* vol 244) ed Flatt M and ifrea I (Springer Netherlands) pp 195–232 ISBN 978-1-4020-6137-0

[35] Bergli J, Galperin Y M and Altshuler B L 2009 *New Journal of Physics* **11** 025002

[36] Clerk A A, Devoret M H, Girvin S M, Marquardt F and Schoelkopf R J 2010 *Rev. Mod. Phys.* **82**(2) 1155–1208

[37] Zurek W H 2003 *Rev. Mod. Phys.* **75**(3) 715–775

[38] Schlosshauer M 2005 *Rev. Mod. Phys.* **76**(4) 1267–1305

[39] Breuer H P and Petruccione F 2002 *The theory of open quantum systems* (Oxford Univ. Press)

[40] Caldeira A and Leggett A 1983 *Physica A: Statistical Mechanics and its Applications* **121** 587 – 616

[41] Caldeira A O and Leggett A J 1981 *Phys. Rev. Lett.* **46**(4) 211–214

[42] Feynman R and Jr F V 1963 *Annals of Physics* **24** 118 – 173 ISSN 0003-4916

[43] Leggett A J, Chakravarty S, Dorsey A T, Fisher M P A, Garg A and Zwerger W 1987 *Rev. Mod. Phys.* **59**(1) 1–85

[44] Johnson J B 1928 *Phys. Rev.* **32**(1) 97–109

[45] Nyquist H 1928 *Phys. Rev.* **32**(1) 110–113

[46] Callen H B and Welton T A 1951 *Phys. Rev.* **83**(1) 34–40

[47] Dutta P and Horn P M 1981 *Rev. Mod. Phys.* **53**(3) 497–516

[48] Hffner H, Roos C and Blatt R 2008 *Physics Reports* **469** 155 – 203 ISSN 0370-1573

[49] Weissman M B 1988 *Rev. Mod. Phys.* **60**(2) 537–571

[50] Surdin M 1939 *J. Phys. Radium* **10** 188–189

[51] Simmonds R W, Lang K M, Hite D A, Nam S, Pappas D P and Martinis J M 2004 *Phys. Rev. Lett.* **93**(7) 077003

[52] Cooper K B, Steffen M, McDermott R, Simmonds R W, Oh S, Hite D A, Pappas D P and Martinis J M 2004 *Phys. Rev. Lett.* **93**(18) 180401

[53] Oh S, Cicak K, Kline J S, Sillanpää M A, Osborn K D, Whittaker J D, Simmonds R W and Pappas D P 2006 *Phys. Rev. B* **74**(10) 100502

[54] Khaetskii A V, Loss D and Glazman L 2002 *Phys. Rev. Lett.* **88**(18) 186802

[55] Paget D, Lampel G, Sapoval B and Safarov V I 1977 *Phys. Rev. B* **15**(12) 5780–5796

[56] Coish W A, Loss D, Yuzbashyan E A and Altshuler B L 2007 *Journal of Applied Physics* **101** 081715 (pages 5)

[57] Coish W A and Loss D 2004 *Phys. Rev. B* **70**(19) 195340

[58] Burkard G, Loss D and DiVincenzo D P 1999 *Phys. Rev. B* **59**(3) 2070–2078

[59] Petta J R, Taylor J M, Johnson A C, Yacoby A, Lukin M D, Marcus C M, Hanson M P and Gossard A C 2008 *Phys. Rev. Lett.* **100**(6) 067601

[60] Stepanenko D, Burkard G, Giedke G and Imamoglu A 2006 *Phys. Rev. Lett.* **96**(13) 136401

[61] Khaetskii A V and Nazarov Y V 2001 *Phys. Rev. B* **64**(12) 125316

[62] Khaetskii A V and Nazarov Y V 2000 *Phys. Rev. B* **61**(19) 12639–12642

[63] Amasha S, MacLean K, Radu I P, Zumbühl D M, Kastner M A, Hanson M P and Gossard A C 2008 *Phys. Rev. Lett.* **100**(4) 046803

[64] Phillips A G 1981 *Amorphous Solids* (Springer-Verlag)

[65] Shnirman A, Schn G, Martin I and Makhlin Y 2011 Josephson qubits as probes of $1/f$ noise *CFN Lectures on Functional Nanostructures - Volume 2* (*Lecture Notes in Physics* vol 820) ed Vojta M, Rthig C and Schn G (Springer Berlin / Heidelberg) pp 75–85 ISBN 978-3-642-14375-5

[66] Zorin A B, Ahlers F J, Niemeyer J, Weimann T, Wolf H, Krupenin V A and Lotkhov S V 1996 *Phys. Rev. B* **53**(20) 13682–13687

[67] Nakamura Y, Pashkin Y A, Yamamoto T and Tsai J S 2002 *Phys. Rev. Lett.* **88**(4) 047901

[68] de Sousa R, Whaley K B, Hecht T, von Delft J and Wilhelm F K 2009 *Phys. Rev. B* **80**(9) 094515

[69] Van Harlingen D J, Robertson T L, Plourde B L T, Reichardt P A, Crane T A and Clarke J 2004 *Phys. Rev. B* **70**(6) 064517

[70] Wellstood F C, Urbina C and Clarke J 2004 *Applied Physics Letters* **85** 5296–5298

[71] Kogan S 1996 *Electronic noise and fluctuations in solids* (Cambridge Univ. Press)

[72] Bergli J, Galperin Y M and Altshuler B L 2009 *New Journal of Physics* **11** 025002

[73] Phillips W A 1987 *Reports on Progress in Physics* **50** 1657

[74] Phillips W A 1972 *Journal of Low Temperature Physics* **7**(3) 351–360 ISSN 0022-2291

[75] Anderson P W, I H B and M V C 1972 *Philosophical Magazine* **25**(1) 1–9

[76] Anderson A C 1986 *Phys. Rev. B* **34**(2) 1317–1318

[77] Jones D P, Thomas N and Phillips W A 1978 *Philosophical Magazine Part B* **38** 271–288

[78] Vacher R and Pelous J 1976 *Phys. Rev. B* **14**(2) 823–828

[79] Zaitlin M P and Anderson A C 1975 *Phys. Rev. B* **12**(10) 4475–4486

[80] Klauder J R and Anderson P W 1962 *Phys. Rev.* **125**(3) 912–932

[81] Black J L and Halperin B I 1977 *Phys. Rev. B* **16**(6) 2879–2895

[82] Paladino E, Faoro L, Falci G and Fazio R 2002 *Phys. Rev. Lett.* **88**(22) 228304

[83] Itakura T and Tokura Y 2003 *Phys. Rev. B* **67**(19) 195320

[84] Galperin Y M, Altshuler B L and Shantsev D V 2004 Low-frequency noise as a source of dephasing of a qubit *Fundamental Problems of Mesoscopic Physics* (*NATO Science Series* vol 154) (Springer Netherlands) pp 141–165

[85] Galperin Y M and Gurevich V L 1991 *Phys. Rev. B* **43**(16) 12900–12905

[86] Lundin N I and Galperin Y M 2001 *Phys. Rev. B* **63**(9) 094505

[87] Ralls K S, Skocpol W J, Jackel L D, Howard R E, Fetter L A, Epworth R W and Tennant D M 1984 *Phys. Rev. Lett.* **52**(3) 228–231

[88] Hung K, Ko P, Hu C and Cheng Y 1990 *Electron Device Letters, IEEE* **11** 90 –92 ISSN 0741-3106

[89] Jung Y, Barkai E and Silbey R J 2002 *Chemical Physics* **284** 181 – 194 ISSN 0301-0104

[90] Wangsness R K and Bloch F 1953 *Phys. Rev.* **89** 728–739

[91] Redfield A G 1957 *IBM J.Res. Dev.* **1**

[92] Ramsey N F 1950 *Phys. Rev.* **78**(6) 695–699

[93] Metcalfe M, Boaknin E, Manucharyan V, Vijay R, Siddiqi I, Rigetti C, Frunzio L, Schoelkopf R J and Devoret M H 2007 *Phys. Rev. B* **76**(17) 174516

[94] Ithier G, Collin E, Joyez P, Meeson P J, Vion D, Esteve D, Chiarello F, Shnirman A, Makhlin Y, Schriefl J and Schön G 2005 *Phys. Rev. B* **72**(13) 134519

[95] Lax M 1960 *Rev. Mod. Phys.* **32** 25–64

[96] Lax M 1963 *Phys. Rev.* **129** 2342–2348

[97] Constantin M, Yu C C and Martinis J M 2009 *Phys. Rev. B* **79** 094520

[98] Winograd E A, Rozenberg M J and Chitra R 2009 *Phys. Rev. B* **80**(21) 214429

[99] Camalet S and Chitra R 2007 *Phys. Rev. B* **75**(9) 094434

[100] Paganelli S, de Pasquale F and Giampaolo S M 2002 *Phys. Rev. A* **66**(5) 052317

[101] Camalet S and Chitra R 2007 *Phys. Rev. Lett.* **99**(26) 267202

[102] Tessieri L and Wilkie J 2003 *Journal of Physics A: Mathematical and General* **36** 12305

[103] Gaebel T, MDomhan, Popa I, Wittmann C, Neumann P, Jelezko F, Rabeau J R, Stavrias N, Greentree A D, Prawer S, Meijer J, Twamley J, Hemmer P R and Wrachtrup J 2006 *Nature Physics* **2** 408–413

[104] Hanson R, Dobrovitski V V, Feiguin A E, Gywat O and Awschalom D D 2008 *Science* **320** 352–355

[105] Ladd T D, Press D, De Greve K, McMahon P L, Friess B, Schneider C, Kamp M, Höfling S, Forchel A and Yamamoto Y 2010 *Phys. Rev. Lett.* **105**(10) 107401

[106] Hanson R, Kouwenhoven L P, Petta J R, Tarucha S and Vandersypen L M K 2007 *Rev. Mod. Phys.* **79**(4) 1217–1265

[107] Coish W A and Loss D 2004 *Phys. Rev. B* **70**(19) 195340

[108] Tsyplyatyev O and Loss D 2011 *Phys. Rev. Lett.* **106**(10) 106803

[109] Taylor J M, Petta J R, Johnson A C, Yacoby A, Marcus C M and Lukin M D 2007 *Phys. Rev. B* **76**(3) 035315

[110] Choi S, Lee D H, Louie S G and Clarke J 2009 *Phys. Rev. Lett.* **103**(19) 197001

[111] Gustavsson S, Bylander J, Yan F, Oliver W D, Yoshihara F and Nakamura Y 2011 *Phys. Rev. B* **84**(1) 014525

[112] Louie S G and Cohen M L 1976 *Phys. Rev. B* **13**(6) 2461–2469

[113] Binder K and Young A P 1986 *Rev. Mod. Phys.* **58**(4) 801–976

[114] Sherrington D and Kirkpatrick S 1975 *Phys. Rev. Lett.* **35**(26) 1792–1796

[115] Parisi G 1979 *Physics Letters A* **73** 203 – 205

[116] Parisi G 1979 *Phys. Rev. Lett.* **43**(23) 1754–1756

[117] Parisi G 1980 *Journal of Physics A: Mathematical and General* **13** 1101

[118] Weissman M B 1993 *Rev. Mod. Phys.* **65**(3) 829–839

[119] Landau L 1927 *Zeitschrift fr Physik A Hadrons and Nuclei* **45**(5-6) 430–441

[120] von Neumann J 1932 *Mathematische Grundlagen der Quantenmechanik* (Springer, Berlin)

[121] Bloch F 1946 *Phys. Rev.* **70**(7-8) 460–474

# Part II

# Papers

## Summary of the papers

In this section I will give a brief summary, as well as the motivation behind the research leading up to each of the papers of this thesis. The common theme in the papers is the study of qubits, or other quantum systems, interacting with noisy environments which leads to decoherence in the quantum system. This is a central problem in the field of quantum computing specifically and in mesoscale and nanoscale physics in general.

### Paper 1

In paper 1 we study the effects of an external AC driving field acting on the two level systems (TLSs) that are thought to be the main contributors to decoherence in many different designs of qubits. This study is motivated by both experimental and theoretical indications that fluctuating TLS in the amorphous substrate used to fabricate superconducting qubits are the major source of dephasing noise in these qubits. Reducing the impact of the noise produced by these sources has the potential to significantly extend the coherence time of the qubit. External driving og the qubit itself is already used in order to control and manipulate the qubit state. Part of the motivation behind this work is to understand how these control pulses alter the noise produced by the environmental TLSs in the substrate. Additional material where we study the effect of sequences of driving pulses on the environmental TLSs can be found in Appendix B. The other motivation is the prospect of using additional external driving fields which only affect the environment of the qubit, in order to reduce the impact of environmental noise on the qubit. This can be done by applying a driving field which is sufficiently detuned from the qubit frequency in order to avoid significant impact on the qubit.

There are two main results in this paper. First we show how external driving saturates the near resonant environmental TLS and how it shifts the noise spectrum of a single environmental TLS from low to high frequencies. The shift in the spectrum has the potential to reduce the dephasing noise on the qubit. Secondly, we study the effect of driving on a realistic ensemble of TLSs present in the substrate. We find that driving at high frequencies will have little impact or increase the environmental noise on the qubit, while driving at low frequencies has the potential to shift the spectrum of the part of the ensemble which is responsible fot the major negative impact on the qubit away from the low frequency region to frequencies that has less impact of the qubit. This seems to be a promising method to reduce dephasing noise in qubits and could seemingly relatively easily be tested in a future experiment.

While the work of this paper is directed towards applications for superconducting qubits, it is in principle equally relevant for all qubits or quantum devices where the primary decoherence mechanism is due to environmental TLSs. A natural extension of this paper would be to study the effect of the driven TLSs on the qubit beyond the perturbative limit used here. This is important in order to understand the influence on the qubit from TLSs which due to the driving has their frequency spectrum shifted towards the qubit frequency.

## Paper 2

In Paper 2 we study the mechanisms behind the enhanced decoherence found for environments which has frustrated competing interactions. The motivation behind the work leading to this paper was a series of theoretical papers showing rapid and much more stable loss of coherence for a central quantum system if it was coupled to a frustrated environment compared to an environment without competing interactions, e.g. a ferromagnetic or antiferromagnetic environment or an environment without any internal interaction. We wanted to understand the mechanism which led to this enhanced decoherence due to frustration.

In order to study the effect of frustration we create a model where a central spin interacts with a spin environment, where we can continuously tune the degree of frustration in the internal coupling of the environment. In agreement with previous works, we find the efficiency of decoherence to be strongest for the frustrated environment. An explanation of this fact in terms of the energy level statistics of the environment is given and supported by numerical calculations, according to which stronger level repulsion leads to more decoherence. We also discuss the possibility of enhancing the coherence time of the qubit by applying an external magnetic field, which acts by reducing the degree of frustration in the spin environment.

In this paper we contribute theoretical insight on the mechanisms behind decoherence in the little studied field of a central spin subject to an environment with frustrated couplings. This is a general work, which in principle apply to any two level system subject to an environment of interacting quantum systems. The to my knowlegde only present day relevant application of theory on this field is in flux qubits, where a major source of decoherence is thought to origin from surface states which might potentially have frustrated coupling, see reference [22] in the paper. The nature of the internal couplings of the decoherence inducing environments of qubits and other quantum devices is, however, in many cases relatively poorly understood. Since it is now clear that mutually competing internal

environment couplings might drastically increase the decoherence rate of the central quantum system, it is likely that quantum engineers could use this knowledge when designing coherent quantum devices and qubits in order to avoid selecting materials containing systems which could potentially act as frustrated environments for the device.

## Paper 3

In paper 3 we study the effects of correlated noise in coupled qubits. In order to construct a working quantum computer one require both coherent qubits and a way to make them interact and carry out computations. We might assume that in order to have a large number of qubits and gates on a chip, their spatial separation has to be small. For such a system it is likely that parts of the noisy environments might be shared between different qubits resulting in correlated noise in the quantum computer. Such correlated noise acting on two or more qubits might have very different properties with respect to decoherence compared to uncorrelated noise. This fact has already been known for some time due to the general algebraic theory of decoherence free subspaces, a theory determining the subspaces of a general multi-qubit Hamiltonian which are immune to correlated noise. In this work we are interested in the effect of correlated noise acting multi-qubit systems not necessarily prepared in its potential decoherence free subspace(s).

Most physicist working on quantum computing would likely agree that in order to establish large scale quantum computing one require efficient ways to correct unavoidable errors. The so called "threshold" theorem in quantum computing states that, once the error rate per qubit per gate is below a certain value, estimated as $10^{-4}$ - $10^{-6}$, indefinitely long quantum computation becomes feasible, see [M. I. Dyakonov, Future Trends in Microelectronics. Up the Nano Creek. p. 4-18 (2007)]. However, this threshold has been questioned in the same above mentioned paper due to the presence of correlated errors in the quantum computer. With this in mind, the author even questions if a large scale quantum computer is at all realizeable. The present work can be looked at as a small first step on the road of answering this question.

In order to study the effects of correlation it is likely that essential insight might be gained from the study of the simplest case of two coupled qubits. In this work we develop a geometric approach based on a generalized Bloch-vector construction where we can study analytically the effect of correlations in the noise sources on the decoherence rate of the coupled qubits. We find that the degree of correlation or anticorrelation in the noise acting on the two qubits can enhance or reduce the decoherence rate to a large extent if

the two qubit Hamiltonian has a high degree of symmetry. In the absence of symmetry in the Hamiltonian, the effect of correlations are weak. It is likely, however, that qubits fabricated on the same chip used for quantum computing applications will be based on the same design, which depending on the realization of the gates might result in multi qubit Hamiltonians with high degree of symmetry.

Our results show that correlations between the noise sources might be both beneficial and detrimental based on the protocol used to carry out computations. If one encode the computer be use of basis states that are in decoherence free subspaces, or parts of the Hilbert space which is weakly influenced by correlated noise the coherence time might be dramatically extended relative to the same system subject to uncorrelated sources. Other basis states will show the opposite behavior. This knowlege might have several applications in qubit, gate and protocol design as one progresses towards the next goal in the quantum computing programme, to make several coherent qubits which can communicate together to solve complex computational problems.

## Paper 4

In this paper we study the difference in the decoherence rate of a qubit coupled to either a quantum two level system again coupled to its own environment or a classical fluctuator modeled by a random telegraph process. This study is motivated by the fact that decoherence in qubits due to two level fluctuators is often theoretically described by use of a model where the qubit is subject to classical random telegraph noise. We belive that this model is valid if the TLSs in the qubits environment are decohered by their own environment on a timescale that is much faster than the timescale of the decoherence of the qubit itself. In this situation the TLSs should behave classically and be treatable by the telegraph noise model. However, it is important to have a clear understanding of the limits of this model. Previously this limit was investigated in Refs. [28] and [29] in the paper. In these studies it was found that the classical and the quantum model converged in the limit of high temperatures. The problem with the previously studied models was that their model did not allow to study separately the effect of the decoherence rate, the relaxation rate and the temperature of the TLS since they were all included in the same parameter, the temperature. In our work we constructed a model for the quantum TLS where all the environmental parameters could be varied independently. Our results shows that the difference between the quantum and the classical model depends on the ratio between the qubit-TLS coupling and the decoherence rate of

the TLS in its pointer state basis. The basis which is stable with respect to interaction with the environment.

The model we study is obtained from the study of TLSs in amorphous glasses, which is relevant for most realizations of solid state qubits. The result, that it is the decoherence rate in the pointer basis of a quantum system which limits the replacement of a full quantum model by a simpler classical one, might potentially extend to more general environments, however this require further research in order to be confirmed.

This paper emerged as a result of the master thesis of Henry J. Wold. My contribution to this paper was to analyze and interpret the results of Wold, to reproduce the numerical results and to write the paper itself.

# 1

# Effects of external driving on the coherence time of a Josephson junction qubit in a bath of two-level fluctuators

Håkon Brox,[1] Joakim Bergli,[1] and Yuri M. Galperin[1,2,3]
[1]*Department of Physics, University of Oslo, PO Box 1048 Blindern, N-0316 Oslo, Norway*
[2]*Centre for Advanced Study, Drammensveien 78, N-0271 Oslo, Norway*
[3]*A. F. Ioffe Physico-Technical Institute of Russian Academy of Sciences, 194021 St. Petersburg, Russia*
(Received 30 September 2011; published 12 December 2011)

We study the effect of external driving on the two-level systems (TLSs) assumed to be a major obstacle in increasing the coherence time of solid-state Josephson junction qubits. We find, by use of a Bloch-Redfield approach, that external driving has two major effects on the TLS. The first is increased fluctuations between the two states of the TLS; the significance of this effect compared to thermal fluctuations depends on the energy splitting of the TLS compared to temperature. The second effect is a reduction in the intensity of the noise spectrum at low frequencies, and at the same time an increase in intensity around the renormalized Rabi frequency of the TLS and the driving frequency and at beatings between these two frequencies. Finally, we study the ensemble-averaged noise spectrum for a typical distribution of TLSs known to give origin to $1/f$ noise. We find that strong driving leads to reduced noise at low frequencies, and therefore to an increased dephasing time $T_2^Q$ of the qubit. However, this effect is exponentially suppressed when the driving frequency is large compared to temperature, as we typically find for Josephson qubits. We suggest that external driving at frequencies much lower than the qubit frequency might be used in order to enhance the the qubit coherence time.

DOI: 10.1103/PhysRevB.84.245416 PACS number(s): 85.25.Cp, 03.67.Lx, 03.65.Yz, 74.78.−w

## I. INTRODUCTION

The most fundamental problem that has to be overcome in order to produce a quantum computer is the isolation of its basic elements, the quantum bits (qubits), from its environment. Entanglement with uncontrollable degrees of freedom is responsible for the decay of coherent superpositions of qubit states. The result is irreversible loss of the quantum information required for operation of the device. Superconducting qubits based on the Josephson junction are leading candidates in the design of a quantum computer. They have low losses, are easily controllable by microwave pulses, and can be fabricated by use of established integrated circuit technology. Recent progress in extending the decoherence time of the qubits has been achieved by identification of the sources of noise and their respective natures. This knowledge has lead to the development of countermeasures such as better isolation, as well as protocols to minimize the negative impact of the noise; see, e.g., Refs. 1–3, or Ref. 4 for a review of earlier results.

Bistable two-level systems (TLSs) existing in the tunneling junction and in the amorphous substrate used to fabricate the qubit are thought to be the most important source of decoherence in Josephson junction qubits;[5–11] see also Ref. 12 for a review. These TLSs are assumed to give rise to the observed $1/f$ noise spectra in Josephson qubits. It is known that control and manipulation of Josephson qubits by use of microwave pulses unavoidably leads to driving of TLSs in the vicinity of the qubit. While different theories of $1/f$ noise and their consequences have been studied in great detail, the effect of driving has with one exception been neglected.

Recently, the influence of external driving on the noise spectra of such TLSs was investigated in Ref. 13. In Ref. 13 Constantin *et al.* calculated the saturation of a TLS in external driving. However, they did not take into account the effect of driving on the dynamics of the TLS. It was found that the noise at low frequencies was unchanged by driving, while the noise at high frequencies was weakly reduced. In this paper we calculate the noise spectra from a single TLS and an ensemble of driven TLSs, taking also into account the effect of driving on dynamics of the TLS. We obtain results that differ qualitatively from those obtained in Ref. 13.

The picture we arrive at is the following: In a general environment, e.g., a disordered substrate, there will be TLSs with a wide distribution of energy splittings $E$ and relaxation rates $\gamma$. Given a driving field of frequency $\Omega$, we can divide the fluctuators into two groups: those who are far from resonance and very weakly perturbed by the driving field (group I), and those who are close to resonance with the driving field (group II). We find that the TLSs belonging to group II are strongly affected by the driving provided that the driving amplitude is large compared to the relaxation rate of the TLSs. The response to the driving can roughly be described by two effects. The first is saturation of the fluctuators. A two-level fluctuator with large energy splitting compared to temperature, $E \gg k_B T$, will in the absence of driving be frozen in the ground state, with a very small probability of switching to the exited state. By driving this fluctuator with a frequency close to resonance, the probability of excitation will increase and by increasing the driving intensity the probability for the fluctuator to be found in the upper state versus the lower state will eventually be similar; thus the TLS is saturated. A driven fluctuator will thus fluctuate (much) more rapidly between its upper and lower state. Therefore the noise from this fluctuator will increase. The second effect caused by driving is a reduction of the noise spectrum,

$$S_0(\omega) \propto \frac{\gamma}{\gamma^2+\omega^2}\frac{1}{\cosh^2(E/2k_BT)}, \tag{1}$$

at frequencies centered around $\omega = 0$, and at the same time increased noise at higher frequencies. The driving results in

 

several new peaks in the noise spectrum. Most pronounced are the peaks centered at the renormalized Rabi frequency $A'$, at the driving frequency $\Omega$, and at beatings between these two frequencies. We find that the net effect of strong driving is a suppressed noise spectrum at low frequencies.

A typical substrate used for fabrication of qubits is often assumed to contain TLSs with a distribution of relaxation rates $\propto 1/\gamma$ and a smooth distribution of energy splittings, which can be approximated as uniform.[6,12,14] This distribution is known to give rise to $1/f$ noise at low frequencies.[15] For such an ensemble of fluctuators, the low-frequency noise is strongly dominated by the fluctuators with small relaxation rates. Driving at high frequencies resonant with the energy splitting of the qubit, $\hbar\Omega \approx E_Q$ where $E_Q > k_BT$ (the energy splitting needs to be large compared to temperature, in order to avoid thermal transitions between its eigenstates), will result in a significant response only from the fluctuators near resonance with the driving field. In the absence of driving, this subset of fluctuators (group II) are frozen out and contribute only marginally to the ensemble-averaged noise spectra, which are dominated by the fluctuators with small energy splittings, $E \leqslant k_BT$. Thus suppression of the low-frequency noise from group II by strong driving only weakly influences the full ensemble-produced noise spectra at low frequencies, but strongly increases the noise at higher frequencies.

However, our results show that while external driving at qubit frequency for typical ensembles of fluctuators will not have significant impact on the low-frequency noise, external low-frequency driving might significantly suppress it. Driving at low frequencies will effect the fluctuators that contribute most strongly to the dephasing-producing noise felt by the qubit (i.e., those with small energy splitting, $E$). These TLSs are only weakly influenced by the saturation effect since their ratio $E/k_BT$ is low and correspondingly the population level in the upper state is already high in the absence of driving. Therefore, the net effect of driving on the low-$E$ fluctuators is almost entirely a shift in the frequency spectra from low to high frequencies. To us this seems like a promising method to reduce pure dephasing noise and thereby increase $T_2^Q$ for the qubit. It is, however, important to note that the high-frequency noise will be increased, specifically around the Rabi frequency of the driven fluctuators as well as around the driving frequency. One should therefore make sure that these frequencies lie sufficiently far from the eigenfrequency of the qubit in order to avoid decreasing $T_1^Q$. In this paper we will focus on the low-frequency noise; the noise at frequencies close to the qubit splitting need to be treated separately (see Refs. 16–18).

The rest of this paper is divided into the following sections. In Sec. II we will describe our model of a TLS in an external field and the assumptions behind it. Thereafter in Sec. III we will derive an expression for the noise spectrum from a single TLS and look at different limiting cases. In Sec. IV we will derive an expression for the ensemble-averaged noise in the case of strong driving, for a particular distribution of TLS parameters $P(E,\gamma) \propto 1/\gamma$. In Sec. V we will discuss the effect of the driven TLSs on the central qubit. Finally, the results will be discussed in Sec. VI.

## II. MODEL

In this section we will study the dynamics of TLSs (fluctuators) subject to an external ac electric field, $\mathbf{E}_{ac}$, and a thermal environment. The nature of the two-level systems we are interested in can, e.g., be considered to be bistable fluctuators tunneling between distinct charge configurations, leading to charge noise in the qubit. These charge fluctuators might be attributed to tunneling of charges between either localized impurity states, between localized impurity states and metallic electrodes, or between different charge configurations in a dielectric material.[10,19] We model the charge configurations associated with each state of a given TLS by its effective dipole moment $\mathbf{p}$. In order to capture the action of the environment (e.g., thermal phonons) responsible for relaxation and decoherence of the TLS, we apply the Bloch-Redfield approach.[20–22] We assume that the interaction between different TLSs is weak compared to the coupling to the thermal bath, such that eventual correlations between the TLSs are neglected. Furthermore we assume that the TLSs couple sufficiently weakly to the qubit compared to other degrees of freedom in the environment that neglect of the qubit is justified when studying the dynamics of the TLS. This allows us to use a perturbative approach when treating the effect of the TLS(s) on the qubit.

### A. Hamiltonian

Our Hamiltonian for the TLSs closely follows that of Ref. 13. A fluctuator, e.g., a particle in a double well potential with associated dipole moment $\mathbf{p}$, can be modeled as a two-level system with tunneling matrix element $\Delta_0$ and asymmetry energy $\Delta$. The Hamiltonian of this TLS in an applied electric field $\mathbf{E}_{ac}$ is then $\bar{H}(t) = \bar{H}_0 + \bar{H}_1(t)$, where $\bar{H}_0 = \frac{1}{2}(\Delta\tau_z + \Delta_0\tau_x)$ and $\bar{H}_1(t) = -\tau_z\mathbf{p}\mathbf{E}_{ac}(t)$. Here $\tau_{x,z}$ are the Pauli matrices and $\mathbf{E}_{ac}(t) = \mathbf{E}_{ac}\cos\Omega t$ is an ac electric field of angular frequency $\Omega$ coupling to the electric dipole moment of the TLS. Furthermore, the TLS interacts with the qubit through $\bar{H}_{F-Q}$ and couples to the environment through $\bar{H}_{F-\mathrm{env}}$.

By diagonalization of $\bar{H}_0$, the Hamiltonian in the energy eigenbasis becomes

$$\begin{aligned} H &= H_0 + H_1(t) + H_{F-Q} + H_{F-\mathrm{env}}, \\ H_0 &= \frac{1}{2}E\sigma_z, \\ H_1(t) &= -\eta(\Delta\sigma_z + \Delta_0\sigma_x)\cos\Omega t, \\ H_{F-Q} &= v\mu_z \otimes \tau_z = v\mu_z \otimes \left(\frac{\Delta}{E}\sigma_z + \frac{\Delta_0}{E}\sigma_x\right), \end{aligned} \tag{2}$$

where $E = \sqrt{\Delta^2 + \Delta_0^2}$ and $\eta = \mathbf{p}\mathbf{E}_{ac}/E$. The matrices $\mu_z$ and $\sigma_{x,z}$ are Pauli matrices acting in the eigenbasis of the qubit and the TLS, respectively and $v$ is the qubit-fluctuator coupling parameter. The TLS-qubit coupling will be neglected when treating the dynamics of the TLS, assuming it is weak compared to other terms. But it is, of course, important with regard to the decoherence of the qubit. We note that the situation when the qubit and the TLS have very close splittings is an exception. Then the interaction is strong. See, e.g., Refs. 16–18.

Rather than specifying the explicit nature of the coupling to the environment, $H_{F-\mathrm{env}}$, we make use of the Bloch-Redfield equation, where the environment enters as damping terms, seeking to relax the density matrix toward its thermal equilibrium value. The Bloch-Redfield equations for the density matrix elements of the two-level system in the eigenbasis of $H_0$ are[20]

$$\dot{\rho}_{\alpha\alpha'} = \frac{i}{\hbar}\langle\alpha|[\rho,H]|\alpha'\rangle + \sum_{\beta,\beta'} R_{\alpha\alpha',\beta\beta'}\left(\rho_{\beta\beta'} - \rho^{\mathrm{eq}}_{\beta\beta'}\right). \quad (3)$$

The rates $R_{--,++} = R_{++,--} \equiv T_1^{-1}$ and $R_{-+,-+} = R_{+-,+-} \equiv T_2^{-1}$ can be derived from perturbation theory,[20] and the equilibrium density matrix, $\rho^{\mathrm{eq}}_{\beta,\beta'}(T)$, is introduced phenomenologically in order to achieve relaxation toward thermal equilibrium.

By use of the rotating wave approximation, we can simplify the first two terms of our Hamiltonian, Eq. (2), obtaining

$$H_{RWA} = \frac{1}{2}E\sigma_z - \frac{\eta\Delta_0}{2}(e^{-i\Omega t}|+\rangle\langle -| + e^{i\Omega t}|-\rangle\langle +|). \quad (4)$$

Inserting into the Bloch-Redfield equation Eq. (3) we find that the time evolution of the elements of the density matrix is governed by the following set of differential equations:

$$\begin{aligned}\frac{d\rho_{++}}{dt} &= \frac{i\eta\Delta_0}{2\hbar}(e^{-i\Omega t}\rho_{-+} - e^{i\Omega t}\rho_{+-}) - \frac{1}{T_1}(\rho_{++} - \rho^{\mathrm{eq}}_{++}),\\ \frac{d\rho_{-+}}{dt} &= \frac{iE}{\hbar}\rho_{-+} + \frac{i\eta\Delta_0}{2\hbar}e^{i\Omega t}(2\rho_{++} - 1) - \frac{1}{T_2}\rho_{-+}\,.\end{aligned} \quad (5)$$

Here we note that $\rho_{+-} = \rho^{\dagger}_{-+}$ and $\rho_{--} = 1 - \rho_{++}$. To avoid the explicit time dependence we make the transformation $f = e^{-i\Omega t}\rho_{-+}$ and $f^* = e^{i\Omega t}\rho_{+-}$. We also introduce the Rabi frequency $A = \eta\Delta_0/\hbar$ and the deviation from resonance $z = E/\hbar - \Omega$. Furthermore we make the approximation for the relaxation rates $\gamma = 1/T_1 = 1/T_2$. While not valid in general, this approximation is believed to be valid when the decoherence is isotropic.[23] The general relationship $T_2 \leqslant 2T_1$ can be derived from the master equation approach.[20,24] Thus by making this simplifying assumption, asymmetry of the relaxation behavior of the TLS is left out. However, we believe that these details are not of crucial importance for the results derived concerning the qubit's decoherence due to the TLSs.

## III. SINGLE TLS

In this section we will first solve the equations of motion for a single TLS and then proceed to find its noise spectrum. This we will analyze later when we study the influence of the TLS(s) on the qubit. Using the notations $N = \rho_{++}$, $\mathrm{Re}\, f = R$, and $\mathrm{Im}\, f = I$, one can cast the Bloch-Redfield equation, Eq. (5), in the form

$$\begin{aligned}\dot{N} &= -AI - \gamma(N - N_{\mathrm{eq}}),\\ \dot{I} &= A(N - 1/2) - \gamma I + zR\,,\\ \dot{R} &= -zI - \gamma R\,.\end{aligned} \quad (6)$$

The solution of Eqs. (6) can be written as

$$\begin{pmatrix} N(t)\\ R(t)\\ I(t)\end{pmatrix} = \Lambda(t)\begin{pmatrix} N_0\\ R_0\\ I_0\end{pmatrix} + \boldsymbol{\kappa}, \quad (7)$$

where $N_0$, $R_0$, and $I_0$ are the initial values of $N$, $R$, and $I$, respectively. The solution of the homogeneous part of the equation is given by

$$\Lambda = e^{-\gamma t}\begin{pmatrix} \frac{A^2\cos A't + z^2}{A'^2} & \frac{zA(\cos A't - 1)}{A'^2} & -\frac{A\sin A't}{A'}\\ \frac{zA(\cos A't - 1)}{A'^2} & \cos A't & -\frac{z\sin A't}{A'}\\ \frac{A\sin A't}{A'} & \frac{z\sin A't}{A'} & \cos A't\end{pmatrix}, \quad (8)$$

where $A' = \sqrt{A^2 + z^2}$ is the renormalized Rabi frequency. The particular solution is given by

$$\boldsymbol{\kappa} = \begin{pmatrix} N_{\mathrm{eq}} + \frac{A^2\left(N_{\mathrm{eq}} - \frac{1}{2}\right)}{\gamma^2 + A'^2}\left[e^{-\gamma t}\left(\cos A't + \frac{\gamma\sin A't}{A'}\right) - 1\right]\\ \frac{zA\left(N_{\mathrm{eq}} - \frac{1}{2}\right)}{\gamma^2 + A'^2}\left[e^{-\gamma t}\left(\cos A't + \frac{\gamma\sin A't}{A'}\right) - 1\right]\\ \frac{\gamma A\left(N_{\mathrm{eq}} - \frac{1}{2}\right)}{\gamma^2 + A'^2}\left[1 - e^{-\gamma t}\left(\cos A't - \frac{A'\sin A't}{\gamma}\right)\right]\end{pmatrix}. \quad (9)$$

We note that by setting $t \to \infty$ in Eq. (9) it is possible to directly read out the steady-state solution.

### A. Noise spectrum from a single TLS

Given the above-specified qubit-TLS coupling, Eq. (2), the TLS is only responsible for pure dephasing of the qubit ($T_2$ processes) and cannot induce transitions between the eigenstates of the $\mu_z$ operator. The dynamics of the TLS leads to uncontrolled fluctuations in the energy splitting of the qubit, leading to an uncertainty in its phase. Alternatively, it leads to entanglement both directly to the fluctuators and indirectly to the environment of the fluctuators. In this article we will analyze the effect of the fluctuators on the qubit through the two-time correlation function of the operator responsible for the noise in the qubit energy splitting.[25] We define it as

$$\begin{aligned}G(t_1,t_2) &= \langle[q(t_2) - \bar{q}(t_2)]\,[q(t_1) - \bar{q}(t_1)]\rangle\\ &= \sum_j \langle q(t_2) - \bar{q}(t_2)\rangle|_{q_j(t_1) - \bar{q}(t_1)}\\ &\quad\times [q_j(t_1) - \bar{q}(t_1)]P[q_j(t_1) - \bar{q}(t_1)].\end{aligned} \quad (10)$$

Here $q_j(t)$ is a realization of a measurement at time $t$ of the operator $v\tau_z$, giving the variation in the qubit's energy splitting due to its interaction with a TLS, while $\bar{q}(t) = \langle q(t)\rangle = \sum_j q_j(t)P[q_j(t)]$ is the ensemble average of $q(t)$, and $P[q(t)]$ is the probability distribution of $q$ at time $t$. The Bloch-Redfield equations, Eq. (6), give the average time evolution of an ensemble of systems with the same initial condition, averaged over the details of the uncontrolled decoherence processes. Thus we find that $\langle q(t)\rangle|_{q_j}$ is simply the solution of the Bloch-Redfield equations, given the initial value $q_j$. More explicitly, we find the following expression:

$$\langle q(t)\rangle|_{q_j} = \frac{2v}{E}\{\Delta N(t) - \Delta_0[R(t)\cos\Omega t - I(t)\sin\Omega t]\}, \quad (11)$$

where the initial condition $q_j$ is written in terms of the initial values $N_0$, $R_0$, and $I_0$. The corresponding expression

for $\bar{q}(t)$ is

$$\bar{q}(t) = \frac{2v}{E}\left[\Delta N_{\rm ss} - \Delta_0\left(R_{\rm ss}\cos\Omega t - I_{\rm ss}\sin\Omega t\right)\right], \qquad (12)$$

where $N_{\rm ss}$, $R_{\rm ss}$, and $I_{\rm ss}$ are the steady-state limits for $N(t)$, $R(t)$, and $I(t)$, respectively, obtained from Eq. (7) at $t \to \infty$.

Thus we find that the correlator defined by Eq. (10) depends on the phase of the driving field at both $t_1$ and $t_2$. In a qubit experiment, where $t_1$ and $t_2$ are the initialization and measurement time, respectively, we assume that we do not have sufficient control over the phase of the driving field at initialization time and therefore average over the initial phase of the driving field. The details of this procedure are given in Appendix A.

The details of the procedure used to calculate the two-time correlation function, Eq. (10), by use of the Bloch-Redfield formalism are described in detail in Appendix B. The full procedure includes a coordinate transform, and in the following we give an outline of the procedure. First we find the density matrix in the steady state that we might visualize as a point within the Bloch sphere. Next, we note that in an external field the steady-state solution can in general lie anywhere in the Bloch sphere and not necessarily along the $z$ axis. Therefore, it is necessary to transform to the coordinate system where the steady-state solution lies along the $z$ axis. The angles defining this transform are given by the steady-state solution of Eqs. (6)–(8) and are illustrated in Fig. 1. The angles $\theta$ and $\phi$ are defined by the relations

$$\tan\theta = \frac{\sqrt{R_{\rm ss}^2 + I_{\rm ss}^2}}{1 - 2N_{\rm ss}}, \quad \tan\phi = \frac{R_{\rm ss}}{I_{\rm ss}}. \qquad (13)$$

The details of this transform and its application to the evaluation of the two-time correlation function is described in Appendix B. Since the off-diagonal elements of the density matrix vanish in this choice of basis, we are allowed to use the states $|-'\rangle$ and $|+'\rangle$ in the rotated basis as initial states, weighted by the mean population levels obtained from the density matrix in the steady state, that gives us $P[q]$.

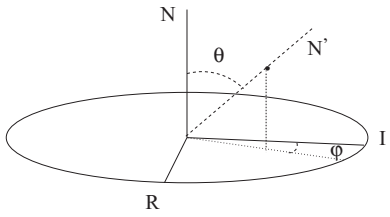


FIG. 1. The coordinate transform used in order to diagonalize the density matrix. Here $N$, $R$, and $I$ are the parameters determining the density matrix in the energy eigenbasis of the TLS, while $N'$, $R'$, and $I'$ denote the same parameters in the rotated frame defined by Eqs. (13). The frame is defined such that the off-diagonal elements of the density matrix vanish in steady state; i.e., $R'_{\rm ss} = I'_{\rm ss} = 0$. In external driving, the steady-state values of the off-diagonal elements of the density matrix are in general nonzero. The transform is used in order to make use of the average procedure described in Appendix B. In the absence of driving the two frames coincide.

In the absence of external driving the density matrix in the equilibrium will always lie along the $z$ axis and the ensemble average of $R$ and $I$ vanishes. Thus we do not require the coordinate transform. In this particular case, after introducing $\tau = t_2 - t_1$, the explicit expression for the two-time correlation function given by Eq. (10) is

$$\begin{aligned} G(t_1,t_2) &= \frac{4\Delta^2 v^2}{E^2}\langle[N(t_2) - N_{\rm eq}][N(t_1) - N_{\rm eq}]\rangle \\ &= \frac{4\Delta^2 v^2}{E^2}\lambda_{11}(\tau)N_{\rm eq}(1 - N_{\rm eq}). \end{aligned} \qquad (14)$$

Here $\lambda_{11}(\tau)$ denotes the 11 elements of $\Lambda(\tau)$ given by Eq. (8). The dependence of $N(t_2)$ on the initial values $R(t_1)$ and $I(t_1)$ vanish in the absence of external driving. We can therefore in this simple case write the propagator $\Lambda(\tau)$ as a scalar function $\lambda_{11}(\tau)$.

In the general case, when driving is included, we find

$$G(t_1,t_2) \propto f(\tau,A,\gamma,z)N'_{\rm ss}(1 - N'_{\rm ss}). \qquad (15)$$

Here $f(\tau,A,\gamma,z)$ describes the dynamics of the density matrix, while $N'_{\rm ss}$ is the population of the upper level in the rotated frame, illustrated in Fig. 1. We have

$$N'_{\rm ss}(1 - N'_{\rm ss}) = N_{\rm ss}(1 - N_{\rm ss}) + g(A,\gamma,z)\left(N_{\rm ss} - 1/2\right)^2, \qquad (16)$$

where $g(A,\gamma,z)$ describes the details of steady-state density matrix [$g(A,\gamma,z) = 0$ if $R_{\rm ss} = I_{\rm ss} = 0$]. See Eqs. (B7) and (B8) for details.

From the correlation function, Eq. (10), we can compute the contribution of a single TLS to the noise spectrum acting on the qubit. The spectrum is given by the expression

$$S(\omega) = \sqrt{\frac{2}{\pi}}\int_{-\infty}^{\infty} e^{i\omega\tau}G(|\tau|,0)\,d\tau, \qquad (17)$$

where we took into account that the correlation function $G(t_1,t_2)$ is translation invariant after the averaging procedure described in Appendix B. We note that the irreversible Bloch-Redfield equations require the measurement time to succeed the preparation time; therefore we need the absolute value of $|\tau|$ in the definition. From the full spectrum at arbitrary frequency, given by Eq. (C1) in Appendix C, we obtain in the limit $\Omega > \gamma$ the following expression for $S(\omega)$:

$$\begin{aligned} S(\omega) = 8\sqrt{\frac{2}{\pi}}\left(\frac{v\Delta}{EA'}\right)^2 N'_{\rm ss}(1 - N'_{\rm ss})\Bigg\{a_1 L(\omega) \\ + \sum_{\pm}\left[a_2 L(\omega \pm A') \pm a_3\frac{\omega \pm A'}{\gamma}L(\omega \pm A')\right]\Bigg\}, \end{aligned} \qquad (18)$$

where $L(\omega) = \gamma/(\gamma^2 + \omega^2)$,

$$\begin{aligned} a_1 &= z^2\cos^2\theta - zA\sin\theta\cos\theta\cos\phi, \\ a_2 &= A^2\cos^2\theta + zA\sin\theta\cos\theta\sin\phi, \\ a_3 &= AA'\sin\theta\cos\theta\cos\phi. \end{aligned}$$

In this limit, the spectrum only contains peaks at zero frequency $\omega = 0$ and at the Rabi frequency $A'$.

### B. Low-frequency noise

In the remaining part of this article we are interested in the noise at low frequency and how it is changed by the external driving. The reason behind this focus is that the noise at low frequencies has been identified as the dominant source of pure dephasing in Josephson junction qubits. It is known that for the Gaussian noise and diagonal qubit fluctuator coupling, the off-diagonal elements of the qubit density matrix relax (in the case of the free induction decay) at a rate (see, e.g., Ref. 12)

$$\frac{1}{T_2^Q} \propto \int_{-\infty}^{\infty} \frac{\sin^2(\omega t/2)}{\omega^2} S(\omega)\, d\omega. \tag{19}$$

For long measurement times this distribution becomes narrow, such that the pure dephasing rate of the qubit is given by $1/T_2^Q = \pi S(0)$ when $t \to \infty$. However, for realistic measurements with finite measurement times, the dephasing rate is determined by the noise spectrum in a finite domain of low frequencies centered at $\omega = 0$. In the following, we will first derive expressions for the low-frequency contribution to $S(\omega)$ due to a single TLS in the absence of external driving ($A \to 0$) and in the case of strong driving ($A \gg \gamma$). These expressions will later be used to derive the low-frequency noise spectrum for a specific distribution of driven TLSs.

From Eq. (18) we find a crossover from a regime where the driving contributes as a weak perturbative effect to a regime strongly dependent on the driving; the crossover takes place around $A \approx |z|$, given that $A \gg \gamma$. We proceed by deriving the limiting expressions in the resonant region $|z| \ll A$ and in the off-resonant region $|z| \gg A$. Using the expression $N_{\rm eq} = (e^{E/kT} + 1)^{-1}$ and Eq. (18) we get in the off-resonant regime $|z| \gg A$

$$S^{(\rm or)}_{A\gg\gamma}(\omega) \approx \sqrt{\frac{8}{\pi}} \left(\frac{v\Delta}{E}\right)^2 \frac{L(\omega)}{\cosh^2(E/2kT)} \times \left[\left(1 - \frac{5A^2}{4z^2}\right) + \frac{7A^2}{4z^2} \sinh^2 \frac{E}{2kT}\right]. \tag{20}$$

As follows from the above expression, the driving only weakly [$\propto (A/z)^2 \ll 1$] affects the fluctuators that are far from resonance.

The corresponding leading contribution to the noise spectrum in the resonant regime $|z| < A$ is

$$S^{(\rm res)}_{A\gg\gamma}(\omega) \approx 5\sqrt{\frac{2}{\pi}} \left(\frac{v\Delta}{E}\right)^2 \frac{\gamma}{A^2} \tag{21}$$

for $\omega < A$ and $\gamma, A < \Omega$. From the full spectrum Eq. (C1), together with Eq. (16) for the population of the density matrix, we can identify two main effects of external driving on the TLS noise spectra. The first effect is the altered equilibrium population of the density matrix due to driving. We can, by use of Eq. (9), express the occupation of the density matrix in steady state by

$$N_{\rm ss} = \frac{1}{2} + \frac{N_{\rm eq} - 1/2}{1 + (A^2/\gamma) L(z)}, \tag{22}$$

as previously found in Ref. 13.

External driving results in saturation of the steady-state density matrix when $A \approx \gamma$ for $|z| \ll \gamma$ and when $A \approx |z|$ for $|z| \gg \gamma$. This saturation contributes to the increased fluctuation rate between the upper and lower level of the TLS, see Fig. 2, and therefore this effect contributes to a higher intensity of the noise at all frequencies (which was not found in Ref. 13). This is especially true for TLSs where the energy splitting is large compared to temperature, meaning that the noise is very weak in thermal equilibrium since the system spends almost all its time in the ground state (see Fig. 3). There is, however, another very pronounced effect, not caught by the model of Ref. 13. The full noise spectrum of the driven TLS Eq. (C1) is composed of several peaks. At low frequencies the most pronounced are the one centered around $\omega = 0$ and the two peaks centered around the renormalized Rabi frequency, $\omega = \pm A'$; see Fig. 2. From the last term of Eq. (18) we see that the intensity around the $\omega \approx 0$ peak is reduced when the Rabi frequency $A$ becomes comparable in magnitude to the deviation from resonance $z$. Thus we have a shift in

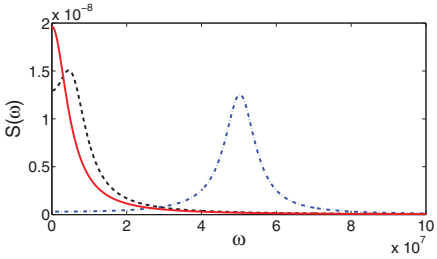


FIG. 2. (Color online) Noise spectrum induced by a single TLS for $A = 0$ (solid line), $5 \times 10^6$ Hz (dashed line), and $5 \times 10^7$ Hz (dash-dotted line). We see that with this choice of parameters, driving reduces the noise at zero frequency but enhances the noise at higher frequencies. The peak at the renormalized Rabi frequency, $A'$, is the most pronounced. Peaks at higher frequencies are suppressed as long as $A \ll \Omega$. The parameters used in the figure are $T = 0.2$ K, $\Omega = E/\hbar = 10^{10}$ Hz, $\gamma = 5 \times 10^6$ s$^{-1}$, and $\gamma_0 = 10^7$ s$^{-1}$.

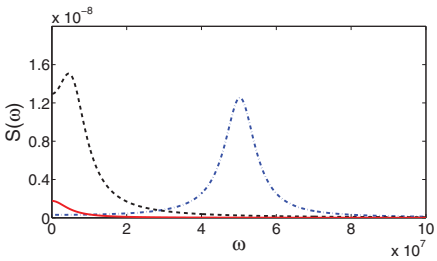


FIG. 3. (Color online) Noise spectrum induced by a single TLS, with the same parameters as used in Fig. 2, but at lower temperature $T = 0.05$ K. At this temperature, the noise is weak in the absence of the driving (solid line) since the fluctuator is frozen in its ground state, $N_{\rm eq} \approx 0.01$. Here the main effect of driving with strength $A = 5 \times 10^6$ Hz (dashed) is to increase the probability of excitation leading to increased noise at all frequencies. When the strength of the driving is $A = 5 \times 10^7$ Hz (dash-dotted) the noise spectrum is shifted sufficiently away from $\omega = 0$ toward $\omega = A'$ such that the effect of increased fluctuations is offset by the shift in the spectrum. Thus the noise at $\omega = 0$ is reduced.

the intensity from low frequencies to frequencies around the Rabi frequency. This shift might be beneficial in reducing the low-frequency noise responsible for pure dephasing of the qubit.[11] In a simplified picture the total noise at a given frequency as a response to external driving can therefore be regarded as a result of two competing mechanisms, the increased fluctuations due to increased population in the upper level of the TLS, and the shift in the spectrum from low to high frequencies. At sufficiently strong driving this shift leads to a reduction in the low-frequency ($\omega \lesssim \gamma$) contribution to the noise spectrum from a TLS with $E \lesssim kT$ as

$$\frac{S(\omega \lesssim \gamma)^{(\mathrm{res})}_{A \gg \gamma}}{S(\omega \lesssim \gamma)_0} = \frac{5\gamma^2}{2A^2}. \tag{23}$$

## IV. ENSEMBLE OF TLSs

In this section we will analyze the noise from an ensemble of the fluctuators studied in the preceding section. Our purpose is to roughly estimate the effect of external driving on the noise spectrum for a realistic Josephson junction qubit experiment. We will more specifically assume the following distribution of the TLS parameters. First, we note again that our calculations are based on the assumption that the dynamics of the fluctuators are independent of the state of the qubit. Furthermore, we assume in the following that the strength of the fluctuator-qubit coupling $v$ is uncorrelated with the relaxation rate $\gamma$ and the energy $E$. Assuming that $\Delta_0$ is an exponential function of an almost uniformly distributed parameter, such as tunnel barrier height,[12,26,27] the distribution of the TLS parameters becomes

$$P(\Delta, \Delta_0) = P_{\mathrm{TLS}}/\Delta_0, \tag{24}$$

where $P_{\mathrm{TLS}}$ is proportional to the density of states per unit energy and volume. This distribution is already widely used in models of decoherence in qubits, where it is known to give origin to the $1/\omega$ dependence of the noise spectrum at low frequencies.

Since in the following it is more convenient to work with the relaxation rate $\gamma$ and the unperturbed fluctuator energy $E$, we recast Eq. (24) by use of the relationship $\gamma = \gamma_0(E)(\Delta_0/E)^2$, where $\gamma_0(E)$ is the maximum relaxation rate for a fluctuator of energy $E$, obtaining

$$P(E,\gamma) = \frac{P_{\mathrm{TLS}}}{\gamma\sqrt{1-\gamma/\gamma_0(E)}}, \tag{25}$$

for $\gamma \in [\gamma_{\min}, \gamma_0(E)]$. The distribution has to be cut at the relaxation rate $\gamma_{\min}$ of the slowest fluctuator. However, we find that the noise spectra at frequencies $\omega \gg \gamma_{\min}$, and therefore measurements carried out with the measurement time $\tau = 1/\omega \ll 1/\gamma_{\min}$, are not sensitive to the cutoff. The maximal relaxation rate $\gamma_0$ is a power-law function of the energy $E$. Since in the following we restrict ourselves to order-of-magnitude estimates we will replace $\gamma_0(E)$ by a constant rate, $\gamma_0 \approx \gamma_0(kT)$. Our calculations (see Appendix D) show that using this assumption the noise spectrum depends only weakly on $\gamma_0$.

Before we proceed to evaluation of ensemble integrals it is convenient to introduce a new variable

$$a = A/\sqrt{\gamma} = \mathbf{E}_{ac}\mathbf{p}/\hbar\sqrt{\gamma_0}. \tag{26}$$

This variable is independent of $\gamma$ and can be treated like a constant when integrating over distributions of TLSs.

If we assume that the qubit-fluctuator coupling $v$ is uncorrelated with $\gamma$ and $E$, and by using that the single fluctuator spectrum is $\propto v^2$, we can express the ensemble-averaged noise spectrum by

$$\bar{S}_a(\omega) = \langle v^2 \rangle \int_0^{E_{\max}} \int_{\gamma_{\min}}^{\gamma_0} S_a(\omega, E, \gamma) P(E,\gamma)\, d\gamma dE. \tag{27}$$

Here we have introduced the notation $\langle v^2 \rangle = \int_{v_{\min}}^{v_{\max}} v^2 P(v) dv$, where $P(v)$ is the distribution of the qubit-fluctuator coupling $v$. By use of the given distribution of TLSs, Eq. (25), and the expression for the noise in zero driving, Eq. (20), we can evaluate the ensemble-averaged noise in the case of no driving ($a = 0$). The detailed calculation is given in Appendix D. Using the relationship $\Delta^2/E^2 = 1 - \gamma/\gamma_0$ between the relaxation rates and the fluctuator potential parameters[12] we find that the averaged spectral density is given by

$$\bar{S}_0(\omega) \approx \sqrt{\frac{8}{\pi}} \langle v^2 \rangle kT\, P_{\mathrm{TLS}} \begin{cases} \omega^{-1}, & \gamma_{\min} < \omega < \gamma_0, \\ \gamma_{\min}^{-1}, & \omega \lesssim \gamma_{\min}. \end{cases} \tag{28}$$

We conclude that without driving we obtain noise $\propto 1/\omega$ for the interval $\gamma_{\min} < \omega < \gamma_0$ that turns over to a constant value for $\omega < \gamma_{\min}$.

Next we proceed to strong driving, which we have defined by $a^2 > \gamma_0$. In order to evaluate the noise in this regime we split the domain of integration into two parts (see Fig. 4): the resonant domain $a^2\gamma > z^2$ (group II), where the fluctuators are strongly affected by the external field $\mathbf{E}_{ac}$, and the off-resonant domain $a^2\gamma < z^2$ (group I), where the fluctuators only weakly respond to the driving field. We approximate the full integral by using the asymptotic limits given by the undriven noise spectra, Eq. (20), in the off-resonant domain, while the strong driving limit is given by Eq. (21). The total ensemble-averaged

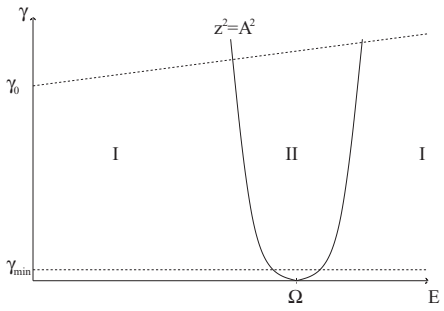


FIG. 4. The full TLS parameter domain. The TLSs inside the parabola $(\Omega - E/\hbar)^2 \leqslant A^2$, group II, are resonant with the applied field. For driving frequencies $\Omega > kT/\hbar$ the major contribution to noise originates from low-$E$ fluctuators belonging to group I outside the resonant sector. The contribution to the noise due to these fluctuators is not changed significantly by driving at frequencies much higher than their energy splittings $E$.

noise spectra for frequencies in the interval $\gamma_{\min} < \omega < \gamma_0$ is (see Appendix D for details of derivation)

$$\bar{S}_{a^2>\gamma}(\omega) \approx \sqrt{\frac{8}{\pi}}\langle v^2\rangle P_{\rm TLS}\left(\frac{k_BT}{\omega} - \frac{4\hbar a}{\cosh^2\frac{\hbar\Omega}{2kT}}\frac{1}{\sqrt{\omega}}\right) \quad (29)$$

for $\hbar a\sqrt{\omega} \ll kT$ and $\sqrt{\gamma_0} < a < \Omega/\sqrt{\gamma_0}$. Again, at $\omega \lesssim \gamma_{\min}$ the frequency $\omega$ in this expression should be replaced by $\gamma_{\min}$.

From this result, we find a correction to the $1/\omega$ noise. This correction, being $\propto\omega^{-1/2}$, is due to suppression of the noise from TLSs that are close to resonance with the driving field $\Omega$. The driving therefore leads to a reduction in the noise at intermediate and low frequencies. The derivation of the expressions Eqs. (29) and a similar one for $\omega \lesssim \gamma_{\min}$ are a good approximation only as long as $a \ll kT/\hbar\sqrt{\gamma_{\min}}$. As long as this criterion holds, we find that the correction term is small relative to the first term, even if the ratio $\hbar\Omega/kT$ is small and the term $\cosh^2(\hbar\Omega/2kT)$ approaches unity. If, however, we increase $a$ beyond this inequality, we expect that the correction term will increase until it approaches the first term in magnitude. The physics is as follows. When we increase $a$ we increase the number of fluctuators belonging to group II, at the cost of group I by increasing the width of the parabola $z^2 = A^2$ in Fig. 4 until all fluctuators are resonant with the field. Thus the number of fluctuators responding to the driving field is increased and since each fluctuator within the resonant sector will have its noise spectrum shifted toward higher frequencies, the noise at low frequencies will be reduced until it approaches zero for very large fields.

## V. DECOHERENCE OF THE QUBIT

In this section we will describe the decoherence of the qubit due to the driven TLSs in its environment. We will illustrate the effect from driven TLSs by use of an example with a specific but motivated distribution of TLS parameters. We will still assume that the qubit couples diagonally to the TLSs. The coupling was previously specified to be $H_{F-Q} = v_i\mu_z \otimes \tau_z$. Given this coupling the TLSs only have a pure dephasing effect due to renormalization of the qubit level splitting, and direct transitions between the levels of the qubit ($T_1$ processes) cannot be induced by our two-level fluctuators.

Above we have assumed that the TLSs-qubit coupling $v_i$ is not correlated with $\gamma$ and $E$. However, one has to keep in mind that different distributions of $v_i$ might have significant impact upon the dephasing of the qubit. For in-depth treatment of different ensembles of fluctuators, as well as non-Gaussian noise statistics, we refer to Refs. 10,12,28, and 29. Since we are in this paper primarily interested in the effect of external driving, we assume that all fluctuators couple to the qubit with the same strength $v$.

In the standard Gaussian approximation, the pure dephasing time $T_2$ for long times $t$ is approximately given by $T_2^{-1} = \pi S(0)$, where $S(0)$ is the noise spectrum at zero frequency.[12] Using this formula, together with Eq. (D10) for the noise at frequencies $\omega < \gamma_{\min}$, we obtain the following expression for the dephasing time of the qubit:

$$\frac{1}{T_2} \approx \sqrt{8\pi}\langle v^2\rangle P_{\rm TLS}\left(\frac{k_BT}{\gamma_{\min}} - \frac{4\hbar a}{\sqrt{\gamma_{\min}}\cosh^2\frac{\hbar\Omega}{2kT}}\right), \quad (30)$$

valid for $\hbar a\sqrt{\gamma_{\min}} \ll kT$ and $\sqrt{\gamma_0} < a < \Omega/\sqrt{\gamma_0}$.

From this expression we see that if $\hbar\Omega > kT$, then the function $\cosh^2(\hbar\Omega/2kT) \approx e^{\hbar\Omega/kT}$. We find in this case that the relative reduction in the noise spectrum due to driving is $\hbar a\sqrt{\gamma_{\min}}/kTe^{\hbar\Omega/kT}$. Thus the correction is exponentially suppressed at low temperatures. However, we notice that if the driving frequency is reduced, i.e., if one introduce a driving field at a frequency $\hbar\Omega \leqslant k_BT$ much lower than the qubit frequency, the hyperbolic function approaches unity, $\cosh^2(\hbar\Omega/2kT) \approx 1$. In this regime the derivation (see Appendix D for details) is no longer limited by the inequality $\hbar a\sqrt{\gamma_{\min}} \ll kT$. Thus the relative correction $\hbar a\sqrt{\gamma_{\min}}/kT$ might become significant, and the driving might significantly reduce the noise at zero frequency.

## VI. DISCUSSION

Our main result in this paper is that for Josephson junction qubits where the dominant noise source is TLSs interacting with the qubit, external driving has two main effects. The first is increased fluctuations of the TLS, contributing to increased noise at all frequencies. This effect is significant if the energy splitting of the fluctuator is small compared to temperature. The second effect is a reduction in the noise spectrum at low frequencies and at the same time increased noise at high frequencies, especially at the renormalized Rabi frequency $A'$.

For a typical ensemble of fluctuators characterized by the distribution $P(\Delta,\Delta_0) \propto 1/\Delta_0$ we find that external driving at high frequencies (e.g., the qubit frequency) leads to reduced noise spectra at low to intermediate frequencies, which again results in an enhanced qubit dephasing time $T_2^Q$. For a typical distribution of TLSs, $P(E,\gamma) \propto 1/\gamma$, the effect is weak since the driving only reduces the noise from TLSs with energy splittings close to resonance with the driving field (group II). For driving fields $\hbar\Omega > kT$, the resonant fluctuators (group II) contribute only weakly to the noise also in the absence of driving. In this case, both the driven and the undriven noise spectra at low frequencies are strongly dominated by TLSs (group I) with low energy splittings $E \leqslant kT$ and long relaxation times $T_1 = 1/\gamma \leqslant \omega^{-1}$.

However, by driving at a lower frequency $\hbar\Omega \lesssim kT$, the resonant group (group II) is shifted from fluctuators close to the qubit frequency to fluctuators at lower frequencies that contribute more strongly to the dephasing noise on the qubit. In this case we expect a strong reduction of the low frequency noise. From Eq. (20) (with $A = 0$) we see that every fluctuator with energy splitting less than temperature $\hbar E \leqslant kT$ gives a contribution of similar magnitude to the noise spectrum in the absence of driving. And from Eq. (21) we see that each fluctuator contributes equally to the noise spectrum in strong driving ($A > \gamma$). Therefore the frequency of driving is not important as long as the frequency is less than temperature $\hbar\Omega \lesssim kT$. Thus we find a transition from weak to strong suppression of the low-frequency noise at $\hbar\Omega \approx kT$; further reduction of $\Omega$ will not contribute significantly to further reduction of low-frequency noise, assuming a uniform distribution of fluctuator splittings $E$. It is also important to note that our treatment has limited applicability due to the rotating wave approximation. The RWA is a good approximation as long as $\Omega > A$, and outside

this domain of applicability we are not able to make strong predictions.

An important side effect of external driving of the TLSs that we can identify in Eq. (C1) is increased high-frequency noise around the renormalized Rabi frequency $A'$, the driving frequency $\Omega$, and at beatings between these two frequencies. In experiments where the relaxation time $T_1^Q$ is an important limiting factor in preserving the coherence of the qubit, and if the qubit fluctuator coupling is not assumed to be strictly diagonal, we expect that the increased high-frequency noise due to external driving will be counterproductive and one should take measures in order to make sure that the high-frequency peaks do not overlap with the qubit frequency.

## APPENDIX A: AVERAGING OVER THE PHASE OF THE DRIVING FIELD

The expression for the correlation function in the time domain, Eq. (10), can be written out explicitly by use of Eqs. (11) and (12). We obtain

$$\begin{aligned} G(t_1,t_2) &= \langle F(t_2)F(t_1)\rangle, \\ F(t) &\equiv \Delta\,\delta N(t) - \Delta_0\,[\delta R(t)\cos\Omega t - \delta I(t)\sin\Omega t]\,. \end{aligned} \tag{A1}$$

Here we have introduced the notations $\delta N(t) = N(t) - N_{\rm ss}$, $\delta R(t) = R(t) - R_{\rm ss}$, and $\delta I(t) = I(t) - I_{\rm ss}$. This expression depends explicitly on the exact phase of the driving field, $E_{ac}$, at times $t_2$ and $t_1$. In the following we assume that the phase of the field is random at the start of the pulse. This is typically the case if the rise time of the signal is long compared to the oscillation period $2\pi/\Omega$ of the signal. In order to average over repeated experiments with a random distribution of the phase of the field, we replace $\Omega t_1$ by $\Omega t_1 + \beta$, where we assume that $\beta$ is uniformly distributed on the interval $\beta \in [0,2\pi]$. With this assumption only products of sines and cosines contribute, while single terms vanish after averaging over the phase $\beta$. After this averaging procedure we find that the expression for the two-time correlation function Eq. (A2) is reduced to

$$\begin{aligned} &G(t,t+\tau) \\ &\quad = (4v^2/E^2)\big\langle \Delta^2 \delta N(t+\tau)\delta N(t) \\ &\qquad + \left(\Delta_0^2/2\right)\{\delta R(t+\tau)\,[\delta R(t)\cos\Omega\tau + \delta I(t)\sin\Omega\tau] \\ &\qquad + \delta I(t+\tau)\,[\delta R(t)\sin\Omega\tau - \delta I(t)\cos\Omega\tau]\}\big\rangle, \end{aligned} \tag{A2}$$

where the cross terms of Eq. (A2) proportional to $\Delta\Delta_0$ have canceled due to averaging over repeated experiments with random distribution of the initial phase of the driving field.

## APPENDIX B: COORDINATE TRANSFORMATION AND AVERAGING OVER INITIAL CONDITIONS

The Bloch-Redfield equations are equations of motion for the average of an ensemble of TLSs, where the individual members of the ensemble differ by details of the environment. By use of the Bloch-Redfield equations we avoid dealing with these details that we do not have control over. In place we get an equation of motion for the mean density matrix. While this method greatly simplifies the dynamics, since we are no longer required to keep track of fine details of the environment, the cost is loss of information about the time evolution of individual systems. Therefore the Bloch-Redfield equations cannot be used to calculate two-time correlation functions in a straightforward way.[30,31] The procedure we use in order to evaluate the two-time correlation function is the following. In general the two-time correlation function can be expressed as

$$\langle A(t_1)A(t_2)\rangle = \sum_{j,k} a_k(t_2)\zeta(a_k(t_2)|_{a_j(t_1)})a_j(t_1)\xi(a_j(t_1)).$$

Here $A(t)$ and $a(t)$ are an observable and a particular realization of this observable, respectively; $\zeta(a_k(t_2)|_{a_j(t_1)})$ is the conditional probability distribution for observing the value $a_k(t_2)$ at time $t_2$ conditioned upon that the value $a_j(t_1)$ was observed at $t_1$. And the $\xi(a_j(t_1))$ is simply the probability distribution for observing the value $a_j(t_1)$ at time $t_1$. We might then realize that $\sum_k a_k(t_2)\zeta(a_k(t_2)|_{a_j(t_1)}) = \langle A(t_2)\rangle|_{a_j(t_1)}$ is simply the solution of the Bloch-Redfield equation given the initial value $a_j(t_1)$. The two-time correlation function thus reduces to

$$\langle A(t_1)A(t_2)\rangle = \sum_j \langle A(t_2)\rangle|_{a_j(t_1)} a_j(t_1)\xi(a_j(t_1)). \tag{B1}$$

We note that this is a classical approximation, where we have not taken into account the fact that the commutator $[A(t), A(t')]$ might in general be finite. We are, however, interested in the pure dephasing rate, $1/T_2 - 2/T_1$, due to the so-called adiabatic noise, which does not produce real transitions; see, e.g., the discussion in Ref. 32. This noise is determined by the low-frequency tail of the noise spectrum, where $\hbar\omega$ is much less than both the temperature and the energy splittings of the qubit and fluctuator. Therefore, the adiabatic noise can be considered as classical and characterized by the symmetric part of the correlation function $\langle A(t_1)A(t_2)\rangle$.

If we now move to our specific problem of a driven TLS in a dissipative environment, the two-time correlation function we require, Eq. (10), does only contain terms with the deviation of the observable quantity from its steady-state value. From the explicit solutions of the Bloch-Redfield equations, Eqs. (8) and (9), we see that the time evolution of the deviation from the steady state is translation invariant, linear, and homogeneous. Therefore, we can write

$$\begin{aligned} &\langle q(t_2) - \bar{q}(t_2)\rangle|_{q_j(t_1)-\bar{q}(t_1)} \\ &\quad = (2d/E)\{[\Delta\lambda_{11}(\tau) - \Delta_0(\lambda_{21}(\tau)\cos\Omega\tau - \lambda_{31}(\tau)\sin\Omega\tau)][N_j(t_1) - N_{\rm ss}] + [\Delta\lambda_{12}(\tau) \\ &\qquad - \Delta_0(\lambda_{22}(\tau)\cos\Omega\tau - \lambda_{32}(\tau)\sin\Omega\tau)][R_j(t_1) - R_{\rm ss}] + [\Delta\lambda_{13}(\tau) - \Delta_0(\lambda_{23}(\tau)\cos\Omega\tau - \lambda_{33}(\tau)\sin\Omega\tau)][I_j(t_1) - I_{\rm ss}]\}. \end{aligned} \tag{B2}$$

Here $\tau = t_2 - t_1$ and $\lambda_{\alpha\beta}(\tau)$ are the elements of $\Lambda(\tau)$ given by Eq (8). This expression can be inserted directly into our general formula given by Eq. (B1). Unfortunately we still require the distribution function $\xi(N_j(t_1))$, and similarly, the distribution of $I$ and $R$. The distribution functions cannot be extracted from the Bloch-Redfield equations.[31] To make up for our lack of information, we make the following approximation. Assuming that a measurement of the TLS in the eigenbasis of $H_0$ will give either the outcome $N_{j=0} = 0$ or $N_{j=1} = 1$ with the mean value $N_{\rm ss}$, we find that

$$\sum_j N_j \xi(N_j) = N_0 \xi(N_0) + N_1 \xi(N_1) = N_{\rm ss},$$
$$\sum_j N_j^2 \xi(N_j) = N_0^2 \xi(N_0) + N_1^2 \xi(N_1) = N_{\rm ss}. \tag{B3}$$

In addition, with this choice of initial values, the initial values of the off-diagonal density matrix elements are always zero. We note that this choice of initial values only make sense if the steady-state density matrix lies on the axis between the points $N_{j=0} = 0$ or $N_{j=1} = 1$. In order to apply the method, we are therefore required to transform to the coordinate system where the steady-state value of $\rho$ lies on the $z$ axis of the Bloch sphere.

### 1. Coordinate transformation

The summation procedure derived above, Eq. (B3), works nicely as long as the assumptions behind the derivation of the Bloch-Redfield equations (the Born-Markov approximations) are fulfilled,[20,21] as well as the time translation invariance. However, the summation procedure can only be applied if the steady state of the density matrix lies along the $z$ axis of the relevant measurement operator. With driving, we see that the density matrix will in general be driven away from the $z$ axis, such that a summation over the eigenstates $|+\rangle$ and $|-\rangle$ of the $H_0$ operator given by Eq. (2) cannot possibly give the true average density matrix in steady state. However, we can do proper averaging by transforming to a new coordinate system where $N'_{++}$ denotes the occupation along the $z'$ axis in this new choice of coordinates. After this transformation the Bloch vector of the steady-state density matrix $N_{\rm ss}$ is a point on this axis. By this choice of axes the density matrix is diagonal. The coordinate transformation is given as

$$(N - 1/2) = (N' - 1/2)\cos\theta,$$
$$R = N' \sin\theta \sin\phi, \quad I = N' \sin\theta \cos\phi. \tag{B4}$$

We note that $R'_{\rm ss} = 0$ and $I'_{\rm ss} = 0$ since we have defined $N'_{\rm ss}$ to lie on the $z'$ axis in the new coordinate system. When we insert the explicit steady-state expressions into Eq. (13), the dependence on the equilibrium value $N_{\rm eq}$ vanishes, and the expressions reduce to

$$\tan\theta = \frac{a^2\gamma(z^2 + \gamma 2)}{4(\gamma^2 + z^2 + 2a^2\gamma)^2}, \quad \tan\phi = \frac{z}{\gamma}. \tag{B5}$$

Inserting into our expression for the correlation function Eq. (A2) we obtain the following formula:

$$G(t_1,t_2) = (2v^2/E^2)\big\langle 2\Delta^2 \delta N(t_1)[\lambda_{11}(\tau)\delta N(t_1) + \lambda_{12}(\tau)\delta R(t_1) + \lambda_{13}(\tau)\delta I(t_1)] + \Delta_0^2\{[\lambda_{21}(\tau)\delta N(t_1) + \lambda_{22}(\tau)\delta R(t_1) + \lambda_{23}(\tau)\delta I(t_1)][\delta R(t_1)\cos\Omega\tau + \delta I(t_1)\sin\Omega\tau] + [\lambda_{31}(\tau)\delta N(t_1) + \lambda_{32}(\tau)\delta R(t_1) + \lambda_{33}(\tau)\delta I(t_1)] \times [\delta R(t_1)\cos\Omega\tau + \delta I(t_1)\sin\Omega\tau]\}\big\rangle. \tag{B6}$$

We can now by use of Eq. (B4) move to the frame where the density matrix lies along the $z$ axis. By use of the summation formulas given by Eqs. (B1) and (B3), and inserting the explicit expressions for the elements of $\Lambda(\tau)$, given by Eq. (8), we obtain the following expression for the correlation function:

$$G(\tau,0) = (2v/EA')^2 N'_{\rm ss}(1 - N'_{\rm ss})\Big\{\Delta^2[(A^2\cos A'\tau + z^2)\cos^2\theta - zA(1 - \cos A'\tau)\cos\theta\sin\theta\sin\phi + AA'\sin A'\tau\cos\theta\sin\theta\cos\phi] + \frac{\Delta_0^2}{2}\Big[A'^2\sin^2\theta\cos\phi\cos A'\tau\cos\Omega\tau(\cos\phi - \sin\phi) + AA'\cos\theta\sin\theta\sin A'\tau \times (\sin\phi\sin\Omega\tau - \cos\phi\cos\Omega\tau) + \frac{z}{A'}\sin^2\theta\sin A'\tau\sin\Omega\tau + \frac{A^2}{A'^2}\sin^2\theta\sin\phi(\cos\phi\sin\Omega\tau - \sin\phi\cos\Omega\tau) + z^2\sin^2\theta\sin\phi\sin A'\tau(\cos\phi\sin\Omega\tau - \sin\phi\cos\Omega\tau) - zA\cos\theta\sin\theta(\cos\phi\sin\Omega\tau + \sin\phi\cos\Omega\tau) + zA\cos\theta\sin\theta\cos A'\tau(\cos\phi\sin\Omega\tau - \sin\phi\cos\Omega\tau)\Big]\Big\}. \tag{B7}$$

Here

$$N'_{\rm ss}(1 - N'_{\rm ss}) = N_{\rm ss}(1 - N_{\rm ss}) + \left(N_{\rm ss} - \frac{1}{2}\right)^2 \sin^2\theta - \frac{R_{\rm ss}^2}{4}\sin^2\theta\sin^2\phi - \frac{I_{\rm ss}^2}{4}\sin^2\theta\cos^2\phi - \left(N_{\rm ss} - \frac{1}{2}\right)R_{\rm ss}\cos\theta\sin\theta\sin\phi - \left(N_{\rm ss} - \frac{1}{2}\right)I_{\rm ss}\cos(\theta)\sin\theta\cos\phi - \frac{I_{\rm ss}R_{\rm ss}}{2}\sin^2\theta\cos\phi\sin\phi. \tag{B8}$$

Equation (B7) is our final expression for the two-time correlation function for a single fluctuator. We note that the correlation function has become fully translation invariant after the averaging procedure. The Fourier spectrum is computed in Appendix C.

## APPENDIX C: SPECTRAL DENSITY $S(\omega)$ AT ARBITRARY FREQUENCY

In this Appendix we give the full spectral density from a single TLS. The full spectrum is given by the Fourier transform with respect to $\tau = t_2 - t_1$ of Eq. (B7). Thus we calculate $S(\omega) = \sqrt{2/\pi}\int_{-\infty}^{\infty} e^{i\omega\tau} G(|\tau|,0)d\tau$. Carrying out the transform we obtain the result

$$\begin{aligned} S(\omega) = 8\sqrt{\frac{2}{\pi}}\left(\frac{v}{EA'}\right)^2 N'_{\rm ss}(1-N'_{\rm ss})\Bigg(\Delta^2\Bigg\{&(A^2\cos^2\theta + zA\sin\theta\cos\theta\sin\phi)[L(\omega+A')+L(\omega-A')] \\ &+ AA'\sin\theta\cos\theta\cos\phi\left[\frac{A'+\omega}{\gamma}L(\omega+A') + \frac{A'-\omega}{\gamma}L(\omega-A')\right] + (z^2\cos^2\theta - zA\sin\theta\cos\theta\sin\phi)L(\omega)\Bigg\} \\ &+ \frac{\Delta_0^2}{4}\sin\theta\Bigg\{b_{1-}[L(\omega+A'+\Omega)+L(\omega-A'-\Omega)] + b_{1+}[L(\omega+A'-\Omega)+L(\omega-A'+\Omega)] \\ &+ b_{2+}\left[\frac{A'+\Omega+\omega}{\gamma}L(\omega+A'+\Omega) + \frac{A'+\Omega-\omega}{\gamma}L(\omega-A'-\Omega)\right] \\ &+ b_{2-}\left[\frac{A'-\Omega+\omega}{\gamma}L(\omega+A'-\Omega) + \frac{-A'+\Omega+\omega}{\gamma}L(\omega-A'+\Omega)\right] \\ &+ 2b_3\Bigg\{\sin\phi[L(\omega+\Omega)+L(\omega-\Omega)] + \cos\phi\left[\frac{\Omega+\omega}{\gamma}L(\omega+\Omega) + \frac{\Omega-\omega}{\gamma}L(\omega-\Omega)\right]\Bigg\}\Bigg\}\Bigg), \end{aligned} \tag{C1}$$

$$\begin{aligned} b_{1\pm} &= [A'^2\sin\theta\cos\phi(\cos\phi-\sin\phi) \pm AA'\cos\theta(1+\cos\phi) + z\sin\theta + z^2\sin\theta\sin\phi + Az\cos\theta](\cos\phi+\sin\phi), \\ b_{2\pm} &= [-AA'\cos\theta\cos\phi \pm z^2\sin\theta\sin\phi \pm Az\cos\theta](\cos\phi+\sin\phi), \\ b_3 &= A^2\sin\theta\sin\phi - Az\cos\theta. \end{aligned} \tag{C2}$$

From Eq. (C1), we see that without driving (and the same for off-resonant driving), we have a single peak

$$S(\omega) \propto \frac{z^2\cos^2\theta - zA\sin\theta\cos\theta\cos\phi}{A^2+z^2}\frac{\gamma}{\gamma^2+\omega^2}$$

that is reduced as the driving increases (i.e., when the Rabi frequency $A$ approaches $z$). When the driving is strong, the intensity is shifted from the single peak at $\omega = 0$ to a large number of peaks. Most prominent are the peaks at the renormalized Rabi frequency, $\omega = A'$, but there are also peaks at the driving frequency and at sums and differences between $A'$ and $\Omega$. The noise at $\omega \approx \Omega$ has not been discussed in this paper but might be important for qubit operation if the driving field is the manipulating pulses used to control the qubit. This noise is then close to resonance with the qubit.

## APPENDIX D: DERIVATION OF THE ENSEMBLE-AVERAGED NOISE FOR STRONG DRIVING

In this section we will derive the ensemble-averaged spectrum of the low-frequency noise induced by strongly driven TLSs (i.e., $a^2 \gg \gamma_0$) for the distribution of TLS parameters given by Eq. (25). In order to evaluate the integral over the TLS parameters we make the following approximation. The full parameter domain $\gamma \otimes E \in [\gamma_{\rm min},\gamma_0]\otimes[0,\infty]$ is split in two sectors. In the first sector the TLSs are in resonance with the driving field defined by the criteria $a^2\gamma > z^2$ (group II). The second one contains the TLSs that are out of resonance (group I, defined by $a^2\gamma < z^2$). The domains of integration are specified in Fig. 5. For the fluctuators belonging to the resonant sector we use the expression for the noise spectrum in resonant strong driving given by Eq. (21), while in the off-resonant sector we use the expression for fluctuators out of resonance given by Eq. (20). Our strategy to evaluate the noise spectra is to first compute the ensemble-averaged noise spectrum in the absence of driving over the full domain, then subtract the contribution to the undriven spectrum from fluctuators that lie in the resonant sector, and finally add the contribution from the resonant fluctuators in group II. Therefore, the noise spectrum can be represented as

$$\bar{S}_{a^2>\gamma}(\omega) = \bar{S}_0(\omega) - \bar{S}_0^{(\rm res)}(\omega) + \bar{S}_{a^2>\gamma}^{(\rm res)}(\omega). \tag{D1}$$

Here the superscript denotes the resonant sector.

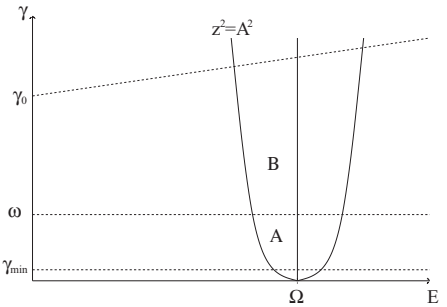


FIG. 5. The domains of integration.

We start by evaluating the spectrum in the absence of driving, by use of Eqs. (20) and (25). Similar calculation, without driving, is also done in Refs. 11 and 12. We get

$$\bar{S}_0(\omega)=\sqrt{\frac{8}{\pi}}\langle v^2\rangle\int_0^\infty\int_{\gamma_{\min}}^{\gamma_0}\frac{P_{\rm TLS}\sqrt{1-\frac{\gamma}{\gamma_0}}}{(\gamma^2+\omega^2)\cosh^2\frac{E}{2kT}}dEd\gamma. \tag{D2}$$

For $\gamma_{\min}\ll\omega\ll\gamma_0$ the integral over $\gamma$ can be estimated as

$$\int_{\gamma_{\min}}^{\omega}\frac{d\gamma}{\omega^2}+\int_{\omega}^{\gamma_0}\frac{1-\frac{\gamma}{2\gamma_0}}{\gamma^2}d\gamma\approx\frac{2}{\omega}-\frac{\gamma_{\min}}{\omega^2}-\frac{1}{\gamma_0}-\frac{1}{2\gamma_0}\ln\frac{\gamma_0}{\omega},$$

while the energy integral is $\int_0^\infty dE\,\cosh^{-2}(\frac{E}{2kT})=2kT$. Therefore

$$\bar{S}_0(\omega)=\mathcal{A}\left(\frac{2}{\omega}-\frac{\gamma_{\min}}{\omega^2}-\frac{1}{\gamma_0}-\frac{1}{2\gamma_0}\ln\frac{\gamma_0}{\omega}\right),$$

where $\mathcal{A}=\sqrt{8/\pi}\langle v^2\rangle P_{\rm TLS}kT$. For very low frequencies $\omega<\gamma_{\min}$ we get

$$\bar{S}_{a=0}(\omega)\approx\mathcal{A}\left(\frac{1}{\gamma_{\min}}-\frac{1}{\gamma_0}-\frac{1}{2\gamma_0}\ln\frac{\gamma_0}{\gamma_{\min}}\right). \tag{D3}$$

Next we proceed to calculate the contribution from the resonant sector in the absence of driving. The integral we need to evaluate is similar to that of Eq. (D2), but the integration should be performed over the TLSs from group II. The integration domain is restricted by the parabola $z^2\leqslant a^2\gamma$.

Assuming first that $\gamma_{\min}<\omega<\gamma_0$, we evaluate the integral by use of asymptotic expressions for the integrand in the different regions of Fig. 5. More precisely we use $\frac{1}{\gamma^2+\omega^2}\approx\frac{1}{\omega^2}$ in sector $A$ of Fig. 5, and $\frac{1}{\gamma^2+\omega^2}\approx\frac{1}{\gamma^2}$ in sector $B$. Furthermore we make the approximation $\cosh^2\frac{E}{2kT}\approx\cosh^2\frac{\hbar\Omega}{2k_BT}=$ const for all fluctuators inside the resonant sector. If we write $E=\hbar(\Omega-z)$, we find that since $z^2\leqslant a^2\gamma_0$ inside the resonant sector, the approximation is good as long as $\frac{\hbar z}{k_BT}\leqslant\frac{\hbar a\sqrt{\gamma_0}}{kT}\ll1$. However, the major contribution to the integral comes from $\gamma\lesssim\omega$, such that we can narrow our inequality to $\frac{\hbar z}{kT}\leqslant\frac{\hbar a\sqrt{\omega}}{kT}\ll1$. By use of the approximations described above, we find that the total contribution from the resonant sector in the absence of driving, in the frequency interval $\gamma_{\min}<\omega<\gamma_0$, is

$$\bar{S}_0^{(\rm res)}=\mathcal{A}\frac{2\hbar a}{kT\cosh^2\frac{\hbar\Omega}{2kT}}\left(\frac{8}{3\sqrt{\omega}}-\frac{3}{\sqrt{\gamma_0}}-\frac{2\gamma_{\min}^{3/2}}{3\omega^2}+\frac{\sqrt{\omega}}{\gamma_0}\right). \tag{D4}$$

For $\omega<\gamma_{\min}$, the calculations are similar, but somewhat simpler. The result is

$$\bar{S}_0^{(\rm res)}=\mathcal{A}\frac{2\hbar a}{kT\cosh^2\frac{\hbar\Omega}{2kT}}\left(\frac{2}{\sqrt{\gamma_{\min}}}-\frac{3}{\sqrt{\gamma_0}}+\frac{\sqrt{\gamma_{\min}}}{\gamma_0}\right). \tag{D5}$$

Finally, we proceed to the resonant sector in strong external driving, $a^2>\gamma$:

$$\bar{S}_{a^2>\gamma}^{(\rm res)}(\omega)=\frac{5\mathcal{A}}{2a^2kT}\iint_{\rm group\ II}\frac{\sqrt{1-\frac{\gamma}{\gamma_0}}}{\gamma}d\gamma dE, \tag{D6}$$

where we have used the expression for the resonant spectrum in strong driving given by Eq. (21). This integral is evaluated similarly to the corresponding integral for the same region in the absence of driving. After using asymptotic expressions in the different regions of Fig. 5, we find

$$\bar{S}_{a^2>\gamma}^{(\rm res)}(\omega)\approx\frac{25\mathcal{A}\hbar\sqrt{\gamma_0}}{16akT} \tag{D7}$$

for the total contribution from the resonant sector in the external field. This expression is valid for $\omega<\gamma_0$.

We have now computed the three contributions to the total ensemble-averaged noise spectrum given by Eq. (D1). For $\gamma_{\min}<\omega<\gamma_0$ the full spectrum is given by

$$\begin{aligned}\bar{S}_{a^2>\gamma}(\omega)\approx\mathcal{A}\Bigg[&\left(\frac{2}{\omega}-\frac{\gamma_{\min}}{\omega^2}-\frac{1}{\gamma_0}-\frac{1}{2\gamma_0}\ln\frac{\gamma_0}{\omega}\right)\\&+\frac{25\hbar\sqrt{\gamma_0}}{4akT}-\frac{2\hbar a}{kT\cosh^2\frac{\hbar\Omega}{2kT}}\left(\frac{8}{3\sqrt{\omega}}\right.\\&\left.-\frac{3}{\sqrt{\gamma_0}}-\frac{2\gamma_{\min}^{3/2}}{3\omega^2}+\frac{\sqrt{\omega}}{\gamma_0}\right)\Bigg].\end{aligned} \tag{D8}$$

Within the limits of the inequality used for the evaluation of the integrals, $\hbar a\sqrt{\omega}\ll k_BT$, and by using that $a>\sqrt{\omega}$, we see that the second term originating from the driven resonant sector is negligible compared to the undriven $1/\omega$ term. Thus we are left with

$$\begin{aligned}\bar{S}_{a^2>\gamma}(\omega)\approx\mathcal{A}\Bigg[&\left(\frac{2}{\omega}-\frac{\gamma_{\min}}{\omega^2}-\frac{1}{\gamma_0}\left(1+\ln\sqrt{\frac{\gamma_0}{\omega}}\right)\right)\\&-\frac{2\hbar a}{kT\cosh^2\frac{\hbar\Omega}{2kT}}\left(\frac{8}{3\sqrt{\omega}}-\frac{3}{\sqrt{\gamma_0}}-\frac{2\gamma_{\min}^{3/2}}{3\omega^2}+\frac{\sqrt{\omega}}{\gamma_0}\right)\Bigg].\end{aligned} \tag{D9}$$

For frequencies $\omega<\gamma_{\min}$ the contributions to the ensemble-averaged spectrum is given by Eqs. (D3), (D5), and (D7), giving

$$\begin{aligned}\bar{S}_{a^2>\gamma}(\omega)\approx\mathcal{A}\Bigg[&\left(\frac{1}{\gamma_{\min}}-\frac{1}{\gamma_0}-\frac{1}{2\gamma_0}\ln\frac{\gamma_0}{\gamma_{\min}}\right)\\&-\frac{2\hbar a}{kT\cosh^2\frac{\hbar\Omega}{2kT}}\left(\frac{2}{\sqrt{\gamma_{\min}}}-\frac{3}{\sqrt{\gamma_0}}+\frac{\sqrt{\gamma_{\min}}}{\gamma_0}\right)\Bigg].\end{aligned} \tag{D10}$$

[1]D. Vion, A. Aassime, A. Cottet, P. Joyez, H. Pothier, C. Urbina, D. Esteve, and M. H. Devoret, Science **96**, 886 (2002).
[2]P. Rebentrost, I. Serban, T. Schulte-Herbrüggen, and F. K. Wilhelm, Phys. Rev. Lett. **102**, 090401 (2009).
[3]Z. Kim, B. Suri, V. Zaretskey, S. Novikov, K. D. Osborn, A. Mizel, F. C. Wellstood, and B. S. Palmer, Phys. Rev. Lett. **106**, 120501 (2011).
[4]G. Ithier *et al.*, Phys. Rev. B **72**, 134519 (2005).
[5]R. W. Simmonds, K. M. Lang, D. A. Hite, S. Nam, D. P. Pappas, and J. M. Martinis, Phys. Rev. Lett. **93**, 077003 (2004).
[6]J. M. Martinis *et al.*, Phys. Rev. Lett. **95**, 210503 (2005).
[7]Y. Shalibo, Y. Rofe, D. Shwa, F. Zeides, M. Neeley, J. M. Martinis, and N. Katz, Phys. Rev. Lett. **105**, 177001 (2010).
[8]L. Tian and R. W. Simmonds, Phys. Rev. Lett. **99**, 137002 (2007).
[9]A. Shnirman, G. Schön, I. Martin, and Y. Makhlin, Phys. Rev. Lett. **94**, 127002 (2005).
[10]Y. M. Galperin, B. L. Altshuler, and D. V. Shantsev, in *Fundamental Problems of Mesoscopic Physics*, edited by I. V. Lerner, B. L. Altshuler, and Y. Gefen, NATO Science Series, Series II: Mathematics, Physics, and Chemistry (Springer, Dordrecht, 2004), Vol. 154, pp. 141–165.
[11]Y. M. Galperin, B. L. Altshuler, J. Bergli, and D. V. Shantsev, Phys. Rev. Lett. **96**, 097009 (2006).
[12]J. Bergli, Y. M. Galperin, and B. L. Altshuler, New J. Phys. **11**, 025002 (2009).
[13]M. Constantin, C. C. Yu, and J. M. Martinis, Phys. Rev. B **79**, 094520 (2009).
[14]E. Paladino, L. Faoro, and G. Falci, R. Fazio, Phys. Rev. Lett. **88**, 228304 (2002).
[15]S. Kogan, *Electronic Noise and Fluctuations in Solids* (Cambridge University Press, Cambridge, 1996).
[16]J. Lisenfeld, C. Müller, J. H. Cole, P. Bushev, A. Lukashenko, A. Shnirman, and A. V. Ustinov, Phys. Rev. B **81**, 100511 (2010).
[17]M. Neeley, M. Ansmann, R. Bialczak, M. Hofheinz, N. Katz, E. Lucero, A. O'Connell, H. Wang, A. N. Cleland, and J. M. Martinis, Nature Phys. **4**, 523 (2008).
[18]D. Vion, A. Aassime, A. Cottet, P. Joyez, H. Pothier, C. Urbina, D. Esteve, and M. H. Devoret, Europhys. Lett. **71**, 21 (2005).
[19]A. G. Phillips, *Amorphous Solids* (Springer-Verlag, Berlin, Germany, 1981).
[20]C. P. Schlichter, *Principles of Magnetic Resonance* (Springer-Verlag, Berlin, Germany, 1990).
[21]A. G. Redfield, IBM J. Res. Dev. **1** (1957).
[22]R. K. Wangsness and F. Bloch, Phys. Rev. **89**, 728 (1953).
[23]X. R. Wang, Y. S. Zheng, and S. Yin, Phys. Rev. B **72**, 121303 (2005).
[24]H. P. Breuer and F. Petruccione, *The Theory of Open Quantum Systems* (Oxford University Press, Oxford, 2002).
[25]A. A. Clerk, M. H. Devoret, S. M. Girvin, F. Marquardt, and R. J. Schoelkopf, Rev. Mod. Phys. **82**, 1155 (2010).
[26]W. A. Phillips, J. Low Temp. Phys. **7**, 351 (1972).
[27]P. W. Anderson, B. I. Halperin, and C. M. Varma, Philos. Mag. **25**, 1 (1972).
[28]J. Schriefl, Y. Makhlin, and A. Shnirman, New J. Phys. **8**, 1367 (2006).
[29]K. Rabenstein, V. A. Sverdlov, and D. V. Averin, JETP Lett. **79**, 646 (2004).
[30]M. Lax, Rev. Mod. Phys. **32**, 25 (1960).
[31]M. Lax, Phys. Rev. **129**, 2342 (1963).
[32]G. Falci, A. D'Arrigo, A. Mastellone, and E. Paladino, Phys. Rev. Lett. **94**, 167002 (2005); E. Paladino, A. D'Arrigo, A. Mastellone and G. Falci, New J. Phys. **13**, 093037 (2011).

2

# Importance of level statistics in the decoherence of a central spin due to a spin environment

Håkon Brox,[1] Joakim Bergli,[1] and Yuri M. Galperin[1,2,3]
[1]*Department of Physics, University of Oslo, PO Box 1048 Blindern, 0316 Oslo, Norway*
[2]*Centre for Advanced Study, Drammensveien 78, 0271, Oslo, Norway*
[3]*A. F. Ioffe Physico-Technical Institute of Russian Academy of Sciences, 194021 St. Petersburg, Russia*
(Received 3 February 2012; published 17 May 2012)

We study the decoherence of a central spin 1/2 due to a closed environment composed of spin-1/2 particles. It is known that a frustrated spin environment, such as a spin glass, is much more efficient for decoherence of the central spin than a similar-size environment without frustration. We construct a Hamiltonian where the degree of frustration is parametrized by a single parameter $\kappa$. By use of this model we find that the environment can be classified by two distinct regimes with respect to the strength of level repulsion. These regimes behave qualitatively different with respect to decoherence of the central spin and might explain the strong enhancement of decoherence observed for frustrated environments.

DOI: 10.1103/PhysRevA.85.052117 PACS number(s): 03.65.Yz, 75.10.Jm, 75.10.Nr, 03.67.−a

## I. INTRODUCTION

Quantum decoherence, where coherence in a quantum system is reduced due to interaction with its environment is a fundamental concept of physics. Testing of theories that go beyond unitary quantum mechanics [1–3] requires deep understanding and control of the decoherence process in order to distinguish the breakdown of unitarity predicted in these theories from decoherence. Decoherence is also a fundamental problem in the branch of nanoscience, where one seeks to use and manipulate quantum states for applications. Coherent manipulation and storage of quantum information are required in order to construct a working quantum computer and rely on reducing decohering interaction between its basic elements, the qubits, and their environment.

Recently, there has been increased experimental interest in electronic spin systems, where the most prominent source of decoherence is thought to be electronic or, in samples with high purity, nuclear spins. These systems are nitrogen-vacancy centers in diamond [4,5], semiconductor quantum dots [6–9], and large-spin magnetic molecules [10,11]. In addition, fluctuating two level defects are thought to be the major source of decoherence in solid state Josephson junction qubits (see Ref. [12] for a review). The coherence of a single spin interacting with a spin bath has been studied extensively in the limit of a noninteracting bath [13]. Decoherence due to interacting spins have also been studied recently in the weak-coupling limit [14] and it was found that the coherence of the central spin decays rapidly when the environment is close to a phase transition [15].

Decoherence, relaxation, and thermalization of a central system coupled to a closed, finite-size spin bath environment has been investigated in Refs. [16–21]. In Refs. [16,17], decoherence of a two-spin system was studied, and a large enhancement of decoherence was found for frustrated spin environments, the main conclusion being "For the models under consideration, the efficiency of the decoherence decreases drastically in the following order: spin glass, frustrated antiferromagnet, bipartite antiferromagnet, one-dimensional ring with nearest- neighbor antiferromagnetic interactions" [16]. A similar study found that the same was true also with regards to relaxation towards the ground state of the central system. Namely, frustrated environments are more efficient in relaxing the central system compared to an ordered environment [18]. Frustrated spin systems have been suggested to exist as localized electron states on the surface of superconducting quantum interference devices (SQUIDs) and flux qubits [22], where they are thought to be a major source of magnetic flux noise.

However, a detailed understanding of the physics behind the importance of a frustrated environment is still lacking. In this work we construct a model where we can continuously tune the degree of frustration in the environment by a single parameter $\kappa$, confirming that frustrated environments reduce the coherence of the central spin much more efficiently compared to an environment with a low degree of frustration, as previously found in Refs. [16,17]. Using this model we study the structure of the eigenvalues of the Hamiltonian of the environment, $H_{\mathrm{E}}$, in the presence of a central spin.

We find that we can explain the mechanism behind the efficiency of the frustrated environment by the structure of the eigenvalues of $H_{\mathrm{E}}$. The role of quantum chaos in the decoherence process has recently been subject to debate, where one line of reasoning claims that integrability enhances decoherence in the weak-coupling limit [23,24], while other works find the opposite behavior (see, e.g., Refs. [19,25]). Our results support the latter group: decoherence is enhanced by quantum chaos. The frustrated environment can be characterized by a Wigner-like distribution of eigenvalues and therefore has large repulsion between energy levels. The presence of an external object, like a central qubit, will therefore result in the mixing of a large fraction of the eigenvectors of the unperturbed system. In an ordered environment, however, the level repulsion is very weak, and coupling to the central spin will only alter the set of eigenvectors of the environment slightly, preserving the coherence of the central spin.

The link between the response of the eigenvectors of $H_{\mathrm{E}}$ to an external perturbation, and the decoherence of a central spin is found as follows: The initial state of the complete system is

$$|\Phi(t=0)\rangle = (1/\sqrt{2})(|\uparrow\rangle_S + |\downarrow\rangle_S) \otimes |\psi_0\rangle_{\mathrm{E}}, \qquad (1)$$

where the subscripts $S$ and $E$ denote the central system and the environment, respectively, and we have for simplicity assumed

 

the central system to be in an initial symmetric superposition. The state $|\uparrow\rangle$ means that the system is in the eigenstate of the operator $S^z$ with eigenvalue $+1/2$ and $|\psi_0\rangle_{\rm E}$ is the initial state of the environment. If the system and environment are coupled, the state of the system influences the dynamic evolution of the environment, and we can write the linear time evolution of the composite system as

$$(|\uparrow\rangle_S + |\downarrow\rangle_S)|\psi_0\rangle_{\rm E} \rightarrow |\uparrow\rangle_S|\psi(t)^{\uparrow}\rangle_{\rm E} + |\downarrow\rangle_S|\psi(t)^{\downarrow}\rangle_{\rm E}, \quad (2)$$

where $|\psi(t)^{\uparrow}\rangle_{\rm E}$ denotes the time evolution of the environment conditioned upon the initial state of the central system being $|\uparrow\rangle_S$. For now we assume that the system-environment coupling $H_{\rm SE}$ commutes with $S^z$, so that transitions between the levels of the central system is prohibited. We will characterize the decoherence by the off-diagonal matrix element of the density matrix,

$$\rho^S_{\uparrow\downarrow} = \langle\psi(t)^{\downarrow}|\psi(t)^{\uparrow}\rangle. \quad (3)$$

Let us expand the state of the environment in the set of eigenstates,

$$|\psi(t)^{\uparrow}\rangle = \sum_n \langle n^{\uparrow}|\psi_0\rangle|n^{\uparrow}\rangle e^{iE_n^{\uparrow}t}, \quad (4)$$

where $|n^{\uparrow}\rangle$ and $E_n^{\uparrow}$ denote the eigenstates and eigenvalues of the environment conditioned upon that the central spin points up, and similarly in the case where the central spin points down (throughout the paper we put $\hbar = 1$). Then the time evolution of the off-diagonal element of the density matrix is given by the expression

$$\rho^S_{\uparrow\downarrow}(t) = \sum_{n,m} \langle n^{\uparrow}|\psi_0\rangle\langle\psi_0|n^{\downarrow}\rangle\langle n^{\uparrow}|m^{\downarrow}\rangle \exp\left[i(E_n^{\uparrow} - E_m^{\downarrow})t\right]. \quad (5)$$

Thus $\rho^S_{\uparrow\downarrow}$ is determined by the magnitude of the overlap elements, unless the levels are degenerate. For degenerate states the corresponding phase factors of the overlap with each eigenstate of the degenerate level oscillate with the same phase.

The analysis is simplified if we assume that only the upper state of the central system couples to the environment, and that the environment is prepared in its ground state. In this case Eq. (5) simplifies to

$$\rho^S_{\uparrow\downarrow}(t) = \sum_n |\langle n^{\uparrow}|0\rangle|^2 \exp\left[i(E_n^{\uparrow} - E_m^{\downarrow})t\right], \quad (6)$$

and the picture is more transparent.

Evolution of $\rho^S_{\uparrow\downarrow}$ is then determined by quantum beatings between the overlap contributions oscillating at frequencies $(E_n^{\uparrow} - E_0)$; that is, by the differences between eigenvalues of $H_{\rm E}$ and the eigenvalues of the environment in the presence of the central spin. In the following we will investigate this further by numerical study of an explicit model.

The paper is organized as follows: In Sec. II we describe our model of a central spin 1/2 interacting with a spin environment with a tuneable degree of frustration. In Sec. III A we study the different regimes of decoherence of our model, while in Sec. III B we explain the physical mechanism behind the enhancement of decoherence by frustration in detail. Furthermore, in Sec. III C we describe the sensitivity to the initial state and in Sec. III D we suggest a method to reduce the negative impact from frustrated environments on coherence. Finally, the results will be discussed in Sec. IV and we conclude in Sec. V.

## II. MODEL

We model a central spin 1/2 interacting with a spin environment by the Hamiltonian

$$\begin{aligned} H &= H_S + H_{\rm SE} + H_{\rm E}, \\ H_{\rm SE} &= \frac{1}{2}\sum_i \Delta_i \left(S^z - \frac{1}{2}\right) s_i^z, \\ H_E &= \sum_{i,j,\alpha} \Omega_{ij}^{'\alpha} s_i^{\alpha} s_j^{\alpha}, \end{aligned} \quad (7)$$

where $H_S$, $H_{\rm SE}$, and $H_{\rm E}$ are the Hamiltonians for the central spin, the spin-environment coupling, and the environment, respectively, $S$ is the operator of the central spin, while $s_i$ are the operators of the environmental spins. We set both the energy splitting and the tunneling element of the central system to zero. The parameters $\Delta_i$ and $\Omega_{ij}^{'\alpha}$ specify the coupling strength along the $\alpha$ axis between the central spin and the environment and the intra-environment coupling, respectively. The parameters $\Delta_i$ are chosen randomly in the interval $[-\Delta, \Delta]$.

In order to study the importance of frustration we specify $H_{\rm E}$ as

$$H_E = -\Gamma \sum_{i,j,\alpha} \left[(1-\kappa) s_i^z s_j^z + \kappa \Omega_{ij} s_i^{\alpha} s_j^{\alpha}\right], \quad (8)$$

where $\Omega_{ij}$ is a random number in the interval $[-\Omega, \Omega]$. The degree of disorder is then parametrized by $\kappa \in [0,1]$. In this model we can continuously tune our environment by the parameter $\kappa$ from a perfect ferromagnet ($\kappa = 0$) to a highly frustrated spin glass ($\kappa = 1$). In the following, all the energies will be measured in the units of $\Gamma$; therefore $\Gamma = 1$. Correspondingly, time is measured in units of $\Gamma^{-1}$.

The simulation procedure is the following: We select a set of model parameters. Then we compute the eigenstates and eigenvalues of $H$ by numerical diagonalization. The composite system is prepared in the state (1) where $|\psi_0\rangle$ is the initial state of the environment and the central spin is prepared in a superposition of eigenstates of $S^z$. Unless otherwise stated, the initial state of the environment is always the ground state in the absence of coupling, $|\psi_0\rangle_{\rm E} = |0\rangle_{\rm E}$. In general, the initial state is therefore a complicated superposition of eigenstates of the composite system $H$.

Decoherence in this model is solely due to entanglement between the central system and the environment. In general, the state evolves according to the Schrödinger equation into an entangled state as in Eq. (2). The reduced density matrix of the system is obtained by tracing over the degrees of freedom of the environment: $\rho^S(t) = {\rm Tr}_{\rm E}\{\Phi(t)\}$.

## III. RESULTS

Using the simulation procedure described above we can study the dynamics of the reduced density matrix of the central system. The time evolution of the off-diagonal element of the density matrix for different values of the environment

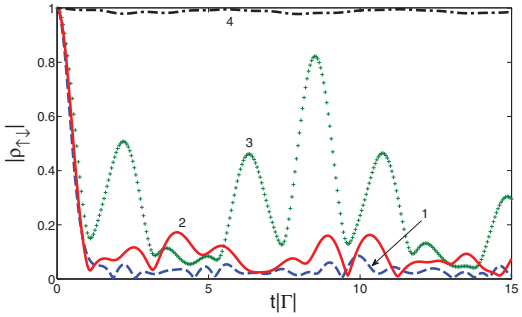


FIG. 1. (Color online) Time evolution of off-diagonal density matrix element $|\rho^S_{\uparrow\downarrow}(t)|$ for $N = 9$ spins in the environment and different values for the disorder parameter $\kappa$, ranging from 1 for the spin-glass phase ($\kappa = 1.0$, blue dashed line) to 4 for the ferromagnetic phase ($\kappa = 0.1$, dashed-dotted black line). Other arrangements are frustrated ferromagnet $\kappa = 0.5$ (2, solid red line) and, for comparison, we plot the time evolution for the completely disconnected bath with Heisenberg-like $H_{\rm SE}$ and $\kappa = 1$, $\Omega = 0.0$ (3, green crosses). In this configuration there are no correlations between the different systems in the environment. The strength of the system-environment coupling is $\Delta = 3.0$.

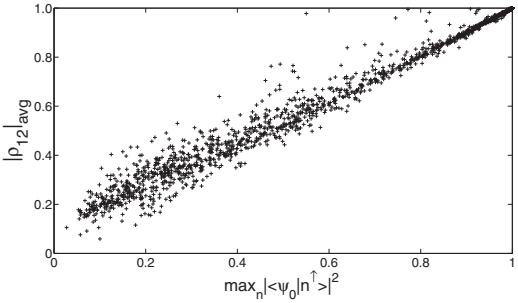


FIG. 2. Correlation between $|\rho^S_{\uparrow\downarrow}(t)|_{\rm avg}$ and the largest overlap element between the ground state of $H_{\rm E}$ and the set of eigenstates $\{|n^\uparrow\rangle\}$ of the environment in the presence of $H_{\rm SE}$. We see that the size of the largest overlap element is strongly correlated with the decoherence $|\rho^S_{\uparrow\downarrow}(t)|_{\rm avg}$, which is defined by the average of $\rho_{12}(t)$ over the interval $t \in [200,300]$ (i.e., after the initial rapid decoherence has taken place). We call this the efficiency of decoherence [18]. The details of averaging do not matter as long as $t$ is much larger than the initial decay time, and the averaging interval is much larger than the correlation length of the oscillations. The statistics are obtained by sampling over the parameter range $\Omega \in [0,1]$, $\Delta \in [0,3]$. The number of spins in the environment is 7.

parameters is shown in Fig. 1. We find that, in general, a higher degree of frustration, controlled by the parameter $\kappa$, results in a stronger and more robust decay of $\rho^S_{\uparrow\downarrow}$. The initial evolution is similar and Gaussian in time for all values of $\kappa$; however, for smaller $\kappa$ we find rapid revivals of coherence in the central system.

From Fig. 1 we see that it is useful to distinguish between the initial decoherence and the efficiency of decoherence. We define the *initial decoherence* as the evolution of coherence in the central system in the characteristic time during which $\rho^S_{\uparrow\downarrow}$ decays by a factor $e$ and the *efficiency of decoherence* as the mean value of the off-diagonal elements of the density matrix over a period that is large compared with the dynamics of the environment.

From Fig. 1 we thus find that initially $|\rho^S_{\uparrow\downarrow}|$ decays following the Gaussian law, $\rho^S_{\uparrow\downarrow} \propto e^{-(t/t^*)^2}$, with practically $\kappa$-independent decay time $t^*$. The efficiency of the decoherence is, however, much higher for the frustrated environment $\kappa = 1.0$. If the efficiency of decoherence is low, as for the ferromagnetic environment, the error might be corrected by use of quantum error correction [26]. In fact, we show in Fig. 1 that a completely disconnected bath, $\Gamma = 0$, gives stronger decoherence than the ferromagnetic bath.

The picture we obtain is the following: The decoherence of the central spin is dependent on the sensitivity of the environment to the state of the central system. The response of the environment to an external system is closely related to the sensitivity of the Hamiltonian of the environment to a small perturbation. The latter can, in turn, be related to the so-called Loschmidt echo defined as the overlap between the two states evolving from the same initial wave function under the influence of two distinct Hamiltonians, the unperturbed $H_0$, and a perturbed $H_\Lambda = H_0 + \Lambda$ (see Ref. [27] for details). Therefore, in most cases, the Loschmidt echo of the environment and the efficiency of the decay of the off-diagonal elements of $\rho_S$ will be strongly correlated, even though there are exceptions [28]. Thus our analysis applies to the purity of the central system as well as to the sensitivity to perturbations of the environment.

The sensitivity of the state of the environment to a perturbation (in our case, to a flip of the central spin) and, therefore, the efficiency of decoherence can be characterized by overlaps between the initial state of the environment, $|0\rangle_{\rm E}$, and the set of eigenstates of the environment in the presence of the perturbation, $\{|n^\uparrow\rangle\}$. We find that the largest of the overlap elements serves as a very good indicator for the decoherence of the central spin. We measure the efficiency of the environment by the modulus of the off-diagonal element of the reduced density matrix $|\rho_{12}|_{\rm avg}$, averaged over the interval $t \in [200,300]$, which is long compared to the typical oscillation periods in $|\rho^S_{\uparrow\downarrow}(t)|$ (cf. Fig. 1). The relationship between $|\rho_{12}|_{\rm avg}$ and the largest overlap element is plotted in Fig. 2. The fact that the largest overlap element correlates so well with the decoherence suggests that the probability of finding degenerate eigenstates among the states with the largest overlap element is relatively small and that the detailed distribution of overlapping vectors $\{|n^\uparrow\rangle\}$ is less important.

In the rest of the article we will use numerical simulations to clarify the difference with respect to decoherence of a central system interacting with a ferromagnetic or a frustrated environment. In view of the strong correlation demonstrated in Fig. 2 we will use $\max_n |\langle n^\uparrow|0\rangle_{\rm E}|^2$ as a measure of the efficiency of the decoherence.

### A. Decoherence in terms of overlap with initial state

We decompose the initial state of the environment in the eigenstates of $H_{\rm E}$ and use the ground state $|\psi_0\rangle_{\rm E} = |0\rangle_{\rm E}$ as the

initial state. In Ref. [17], decoherence was studied both using the ground state as initial state and a random superposition of eigenstates corresponding to "infinite temperature." We will focus first on the ground state and address a more complicated initial state in Sec. III C. In the absence of disorder, $\kappa = 0$, the ground state of $H_{\mathrm{E}}$ will be the ferromagnetic state where all spins point in the same direction $|\uparrow\uparrow\ldots\uparrow\rangle_{\mathrm{E}}$, or in general a linear combination of the two degenerate ground states. In order to avoid the exact degeneracy, we use a small static symmetry breaking field acting on a single spin in the environment.

In the ferromagnetic phase, if the strength of the system-environment coupling is weaker than the intra-environment coupling, $\Delta \ll N\Omega$, the presence of the central spin will not alter the ground state significantly. Therefore, the overlap between the ground state of the isolated environment with the ground state of the perturbed environment, $\langle 0|0^{\uparrow}\rangle_{\mathrm{E}}$, will be very close to one [i.e., the magnitude of all the terms of Eq. (6) will be close to zero except for the term $\langle 0|0^{\uparrow}\rangle_{\mathrm{E}}$, where $|0^{\uparrow}\rangle_{\mathrm{E}}$ is the ground state of the environment given the perturbation]. Thus, the ground state will still be ferromagnetic in the presence of the central spin, which will therefore not entangle sufficiently with its environment, preserving the coherence. In Fig. 3 we show numerical simulations for different values of frustration in the environment. As long as the disorder parameter $\kappa$ is small, the largest overlap element between the unperturbed ground state of the environment $|0\rangle_{\mathrm{E}}$ and the set of eigenstates $\{|n^{\uparrow}\rangle\}$ when the system-environment coupling $H_{\mathrm{SE}}$ is turned on, is very close to one. The ground state is ferromagnetic and the interaction with the central spin is insufficient to break the ferromagnetic order.

If we now increase the disorder parameter $\kappa$, the ground state of the environment will be only slightly altered, until the frustration in $H_{\mathrm{E}}$ given by $\kappa$, together with the frustrated

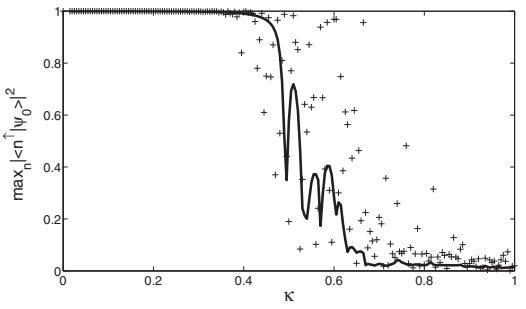


FIG. 3. Largest overlap element plotted versus disorder strength $\kappa$. For small values of $\kappa$ the ferromagnetic ground state is strongly favored energetically and the perturbation represented by the central spin is not able to significantly alter the ground state. Close to $\kappa = 0.5$ we find a "phase transition" to a more disordered state. In this regime the coupling to the central spin is sufficient to alter the ground state of the environment. For $\kappa \approx 1.0$ the set of eigenstates are completely altered in the presence of the central spin, and the overlap with the original set is typically very small. The number of environmental spins is $N = 9$, $\Delta = 3.0$ and the same seed is used in generating the distributions of $\Omega_{ij}$ and $\Delta_i$ for each value of $\kappa$ (solid line), while the crosses correspond to a random seed for each value of $\kappa$.

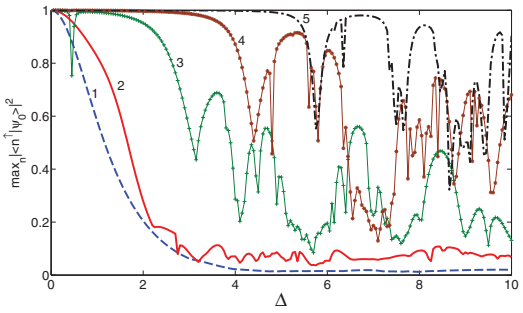


FIG. 4. (Color online) Largest overlap element computed according to Eq. (6), plotted versus the perturbation strength $\Delta$, for different values of the disorder parameter $\kappa$. The numbered curves correspond to the following values of $\kappa$: 1 is for spin glass $\kappa = 1.0$ (dashed blue line), 2 is for $\kappa = 0.8$ (solid red line), 3 is for $\kappa = 0.6$ (green crosses), 4 is for $\kappa = 0.4$ (brown stars), 5 is for $\kappa = 0.2$ (dash-dotted black line). The environment is prepared in the ground state of $H_{\mathrm{E}}$. The number of environmental spins is $N = 9$, and the same seed is used for each value of $\Delta$.

Ising-type system-environment coupling $H_{\mathrm{SE}}$, becomes large enough to break the ferromagnetic order. This "phase transition" is evident from Fig. 3, where in these particular simulations it takes place at about $\kappa \approx 0.5$, but the value is in general dependent on the size of the system, and the strength and nature of $H_{\mathrm{SE}}$. The physics during and after the phase transition will be addressed in more detail in Sec. III B. We can make a rough estimate as follows: A single spin is in general subject to two competing interaction effects, the ferromagnetic interaction $(1-\kappa)\Omega N$ and the spin-glass interaction $\propto\kappa$. Assuming that the latter is random it should be of magnitude $\kappa\Omega\sqrt{N} + \Delta$. The transition between the ferromagnetic and the spin-glass phase should therefore take place at

$$\kappa\Omega\sqrt{N} + \Delta \approx (1-\kappa)\Omega N. \tag{9}$$

If we insert the parameters from Fig. 3 we find the critical value $\kappa = 0.5$. Summarized, if the total frustration induced together by $\kappa$ and $H_{\mathrm{SE}}$ is insufficient to break the ordered ground state, both $|0\rangle_{\mathrm{E}}$ and $|0^{\uparrow}\rangle_{\mathrm{E}}$ will have a large overlap with one of the states $|\uparrow\uparrow\ldots\uparrow\rangle_{\mathrm{E}}$ or $|\downarrow\downarrow\ldots\downarrow\rangle_{\mathrm{E}}$, according to Eq. (6) and, in this regime, the coherence of the central system will be preserved.

In Fig. 4 we follow the largest overlap element $\max_n |\langle n^{\uparrow}|0\rangle_{\mathrm{E}}|^2$ as a function of the strength of the system-environment coupling $\Delta$, keeping $\kappa$ constant. In each of the simulations $H_{\mathrm{SE}}$ is random and Ising like. We find that, for small values of $\kappa$, the strength of the random, frustrated system-environment coupling $H_{\mathrm{SE}}$ needs to be sufficiently large in order to break the ferromagnetic interaction, in accordance with Eq. (9). Indeed, using Eq. (9) we predict the following values for the critical $\Delta$:

| $\kappa$ | 0.2 | 0.4 | 0.6 | 0.8 | 1 |
|---|---|---|---|---|---|
| $\Delta$ | 6.6 | 4.2 | 1.8 | −0.6 | −3.0 |

which agrees surprisingly well with Fig. 4. Until ferromagnetic order is destroyed by $H_{\mathrm{SE}}$ the ground state of the perturbed system is very close to parallel with the unperturbed ground state, $\langle 0^{\uparrow}|0\rangle_{\mathrm{E}} \approx 1$. For larger values of $\Delta$, we find strong oscillations in the size of the overlap element as a function of $\Delta$. This effect does not take place for $\kappa \geqslant 0.8$. In this regime the oscillations are less pronounced and the decay of the overlap element takes place for smaller values of $\Delta$. This regime is characterized by a highly frustrated ground state in the absence of $H_{\mathrm{SE}}$. The presence of the central spin only alters microscopic details of the ground state, not its qualitative features.

In summary, an environment with frustrated interactions induces more effective decoherence than an unfrustrated environment. This effect can be quantified by the strength of a perturbation (here $H_{\mathrm{SE}}$) which alters the set of eigenstates $\{|n\rangle_{\mathrm{E}}\}$. If the environment is dominated by frustrated interactions, the set of eigenstates $\{|n^{\uparrow}\rangle_{\mathrm{E}}\}$ in the presence of the perturbation $H_{\mathrm{SE}}$ will, in general, be very different from $\{|n\rangle_{\mathrm{E}}\}$. We can think of this process as follows: In an environment with a large number of opposing interactions and a large set of almost-degenerate low-energy states, the presence of a central spin will in general cause a rotation of a subset of the eigenvectors $\{|n\rangle_{\mathrm{E}}\}$. If there is a rotation and given that the subset contains the ground state $|0\rangle_{\mathrm{E}}$, the maximal overlap element $\max_n |\langle n^{\uparrow}|0\rangle_{\mathrm{E}}|^2$ and therefore the coherence of the central spin will decay. We will discuss the detailed physics behind this process in more detail in Sec. III B.

### B. Decoherence in terms of avoided level crossings

In order to gain a deeper understanding of the differences between the ordered and the frustrated environment with respect to dephasing of the central spin, we study in detail the behavior of the eigenvalues. We use the same model as defined previously by Eq. (8) and an Ising-like random $H_{\mathrm{SE}}$. Then we perform simulations where we gradually increase the coupling parameter $\Delta$ for different values of the disorder parameter $\kappa$.

In Fig. 5 (top), we plot the 20 lowest eigenvalues against the coupling strength $\Delta$. The disorder parameter is set to $\kappa = 0.1$ and the environment is therefore dominated by the ferromagnetic interaction. In the absence of perturbation we have two almost-degenerate eigenvalues, the gap to the third-lowest state is large. For small values of $\Delta$ the overlap between the ground state $|0\rangle_{\mathrm{E}}$ of $H_{\mathrm{E}}$ and the ground state of the perturbed environment $|0^{\uparrow}\rangle_{\mathrm{E}}$ is very close to one: $\langle 0^{\uparrow}|0\rangle_{\mathrm{E}} \approx 1$. At $\Delta \approx 0.2$ there is an avoided level crossing between the two lowest levels. Close to the avoided level crossing, the eigenvectors of the two states evolve rapidly in Hilbert space and end up switching directions [29]. Thus, after the level crossing the first-excited state overlaps completely with what was the the ground state before the level crossing took place $\langle 1^{\uparrow}|0\rangle \approx 1$. The overlap with the the ground state of $H_{\mathrm{E}}$ is, however, still very close to one as long as only two states take part in the crossing. The eigenvector corresponding to a large overlap with the original ground state has simply been swapped with its neighbor and the coherence of the central system is conserved according to Eq. (6).

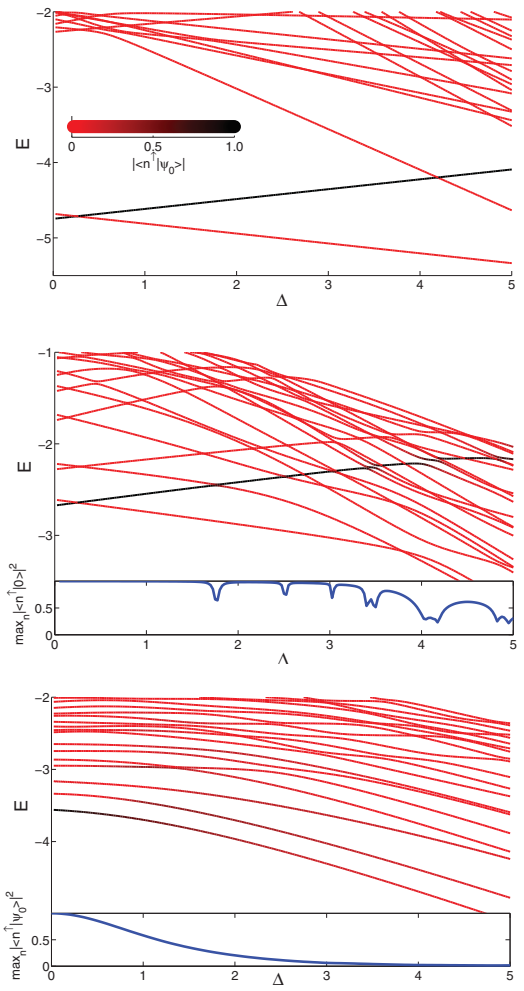


FIG. 5. (Color online) The 20 lowest eigenvalues plotted against the perturbation strength $\Delta$ for different values of frustration in the environment. $\kappa = 0.1$ (top), 0.5 (middle), 1.0 (bottom). The overlap with the ground state of the unperturbed Hamiltonian $H_{\mathrm{E}}$ is indicated by the color tone. A large overlap element increase the darkness of the corresponding eigenvalue (color bar is shown in upper figure). The bottom plot shows the largest overlap element between the ground state of $H_{\mathrm{E}}$ and the eigenstates of $H_{\mathrm{E}}$ in the presence of the interaction $H_{\mathrm{SE}}$, $\max_n |\langle n'|0\rangle|^2$. The number of spins in the environment is $N = 8$.

When the disorder of $H_{\mathrm{E}}$ increases, the picture becomes more complex. In Fig. 5 (middle) we plot the 20 lowest eigenvalues against $\Delta$, but we use a higher degree of disorder in the environment ($\kappa = 0.5$). Since the environment has a larger contribution from frustrated couplings in $H_{\mathrm{E}}$, the spacing between the energy levels is more uniform due to the level-repulsion effect [30]. In this particular case, the energy of the original ground state $|0\rangle_{\mathrm{E}}$ is shifted upward by the perturbation.

The energy of this state can be tracked by the dark line, highlighting the eigenvalues corresponding to eigenvectors with large overlap element with the original ground state. In Fig. 5 (middle) we can compare the eigenvalues with the maximal overlap element. We find that the reduction in the maximal overlap element correspond to values of $\Delta$ where avoided level crossings take place. For large values of $\Delta$ the levels are closer, and we find avoided crossings where three or more levels are involved. Thus the overlap element is split between several states. The maximal overlap element is therefore reduced at these values of $\Delta$.

Having developed the sufficient understanding, we are now also able to explain the oscillatory behavior during the "phase transition" in Fig. 3. In the region of the transition ($\kappa \approx 0.5$), more levels are present close to the ground state, and the repulsion width increases with $\kappa$. When the ground state gets close enough to the first-excited state to feel repulsion, the corresponding eigenvectors begin rotating in the subspace they span. The overlap element is initially reduced and transferred to the first-excited state. Eventually, the first-excited state will be the closest in Hilbert space to the original ground state $|0\rangle$, explaining the sharp cusps of Fig. 3. When $\kappa$ is increased even more, the picture grows more complex as several levels are involved.

In Fig. 5 (bottom) we have reduced the ferromagnetic part of $H_{\mathrm{E}}$ to zero ($\kappa = 1.0$). In this spin-glass phase the effect of level repulsion is strongly pronounced. The space between levels at which the eigenvectors start to repel each other is related to the size of the off-diagonal elements of the Hamiltonian in the basis of the perturbation (in this particular case—the coupling to the central spin in the $S_i^z$ eigenbasis) [31]. When $\kappa$ is large, the off-diagonal elements in the Hamiltonian (7) are larger than the average level spacing. This means that avoided crossings take place continuously as the parameter $\Delta$ is increased. In the parameter range where the distance between levels is smaller than the width of repulsion, the eigenvectors will, in general, evolve with $\Delta$ in the Hilbert space spanned by the eigenvectors of the repelling levels.

Thus, we find a crossover between two regimes. In the weak-repulsion regime, the repulsion width is smaller than the typical distance between levels. In this regime we will have few and pronounced avoided crossings; the crossings will typically involve only two levels and the probability of multilevel crossings is strongly suppressed. Each two level avoided crossing will result in a swap between the eigenvectors involved, but does not reduce the largest overlap element after the crossing has taken place. The overlap element is reduced only during the crossing, still the coherence of the central system is only slightly altered, due to the levels approaching degeneracy. In the second regime, we have strong level repulsion. In this regime, the repulsion width is of the same order or larger than the typical distance between levels such that each level is, for a large range of $\Delta$, repelled by more than one level at the same time. When the repulsion width is much larger than the average level splitting, a large fraction of the levels become connected in the sense that the effect of an interaction between two levels will again influence the next levels by a domino-like effect, until eventually the spacing between to adjacent levels are larger than the repulsion width. The corresponding eigenvectors will then evolve continuously in the Hilbert space spanned by this cluster of levels.

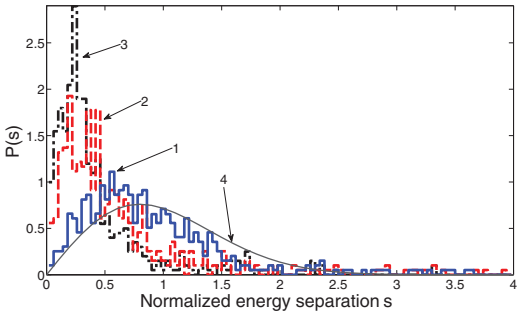


FIG. 6. (Color online) Level-spacing distribution different degrees of disorder. The curve labeled 1 (solid blue line) is for spin glass, $\kappa = 1$, 2 is for intermediate frustration (red dashed line), $\kappa = 0.5$, 3 is for the ferromagnetic phase (black dashed-dotted line), $\kappa = 0.25$. For comparison we also plot the Wigner-Dyson distribution $P(s) = (s\pi/2)e^{-s^2\pi/4}$ (curve 4, thin solid gray line). The number of spins in the environment is $N = 10$.

The energy levels of a system where the repulsion width is larger than the level splitting is expected to be characterized by a distribution of energy levels following Wigner-Dyson statistics [31]. In Fig. 6 we plot the level-spacing distribution of $H_{\mathrm{E}}$ for different values of the disorder parameter $\kappa$. For large values of $\kappa$ we find that the distribution is consistent with the Wigner-Dyson distribution, implying that the repulsion width is larger than the average splitting. At the same time, for small values of $\kappa$, where we have a ferromagnet, we find a special distribution of eigenvalues with two (almost) degenerate ground states (i.e., $|\uparrow\uparrow\ldots\uparrow\rangle_{\mathrm{E}}$ and $|\downarrow\downarrow\ldots\downarrow\rangle_{\mathrm{E}}$) and the next levels having a high degree of degeneracy. Each of the two ground states correspond to the bottom of a potential well, excited states belonging to different wells cannot be connected by flipping of two spins. The statistics obtained in Fig. 6 is therefore sorted by magnetization; the level statistics for each potential well of $H_{\mathrm{E}}$ is treated separately.

In summary, we find a weak-repulsion regime, when $H_{\mathrm{E}}$ has a low degree of disorder. In this regime the overlap element, $\langle n^{\uparrow}|0\rangle_{\mathrm{E}}$, between the original ground state and the set of eigenstates of the Hamiltonian in the presence of the central spin is conserved even if we make the coupling to the central spin strong. In the second regime, when $H_{\mathrm{E}}$ has high degree of disorder, we have strong repulsion between large clusters of states. In this regime, the set of eigenvectors of $H_{\mathrm{E}}$ is very sensitive to the presence of the central spin. The largest overlap element $\langle n^{\uparrow}|0\rangle_{\mathrm{E}}$ is therefore rapidly reduced as the coupling to the central spin is increased.

### C. Initial state of environment

In Ref. [17], the importance of the initial state of the environment was studied. More efficient and stable decoherence was found for an initial state corresponding to infinite temperature; however, no detailed explanation of this observation was given. If the initial state of the environment is no longer the ground state, but a linear combination of

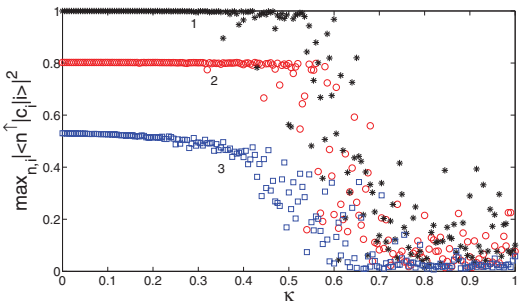


FIG. 7. (Color online) Largest overlap element plotted versus the disorder strength $\kappa$: The curve labeled 1 is for low temperature $T = 0.01$ (black stars), 2 is for intermediate temperature $T = 0.10$ (red circles), and 3 is for high temperature $T = 1.00$ (blue squares). The coupling to the central spin is $\Delta = 2.0$ and the number of spins in the environment is $N = 9$.

eigenstates from the set $\{|n\rangle_{\rm E}\}$ such that $|\psi_0\rangle_{\rm E} = \sum_i c_i|i\rangle_{\rm E}$, where $|i\rangle_{\rm E} \in \{|n\rangle_{\rm E}\}$, Eq. (6) has to be replaced by

$$\rho^S_{\uparrow\downarrow} = \sum_{n,i} |c_i \langle n^\uparrow|i\rangle_{\rm E}|^2 e^{i(E'_n - E_i)t}. \qquad (10)$$

For finite temperature the overlaps are distributed over a number of eigenstates according to their Boltzmann weight, $e^{-E/(kT)}$. The coherence of the central spin, however, is conserved ($|\rho^S_{\uparrow\downarrow}| = 1$) as long as the perturbation introduced by the central spin does not alter the eigenvalues of the environment. If there is a significant perturbation, the coherence is reduced by an additional factor given by the square of the largest amplitude of the expansion $|\psi_0\rangle_{\rm E} = \sum_i c_i|i\rangle$. The effect is shown in Fig. 7.

### D. Enhancement of coherence by external magnetic field

As a consequence of the preceding analysis we find that the presence of an external magnetic field, $H_{\rm ext}$, might enhance the coherence of the central system (see Fig. 8). The magnetic field will polarize the spins in the environment, resulting in a larger overlap element between the ground state $|\psi_0\rangle_{\rm E}$ of the unperturbed environment $H_{\rm E}$ and the set of eigenstates $\{|n^\uparrow\rangle_{\rm E}\}$ in the presence of the central spin. When the magnetic field is sufficiently strong to break the frustration in the ground state $|0\rangle_{\rm E}$ (i.e., when the magnitude of the external field is of the same order as the coupling between the spins in the environment), $H_{\rm ext} \gg \sqrt{N}\Omega$, the presence of the central spin will not significantly alter the magnetized ground state of the environment unless the coupling to the environment is strong compared to the external field. Thus, if the spin environment of the central system is disordered, magnetization is beneficial to the coherence of the central system. This procedure has already been applied experimentally (see Refs. [5,10]).

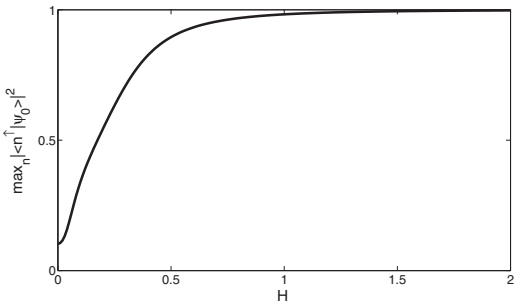


FIG. 8. Largest overlap element $|\langle n^\uparrow|\psi_0\rangle_{\rm E}|^2$ plotted versus external magnetic field $H$. The disorder parameter is $\kappa = 1.0$, the coupling to the central spin is $\Delta = \sqrt{N}$ and the number of spins in the environment is $N = 9$.

## IV. DISCUSSION

In this article, we have considered the special case where the central spin is coupled diagonally to its environment. Then no transitions can take place between the eigenstates of the central system and the decoherence is entirely due to renormalization of its energy splitting (pure dephasing). This choice of coupling simplifies the treatment since the effect of the central spin upon the environment can be treated as a static perturbation. If we loosen this restriction and also include real transitions between the eigenstates ($T_1$ processes) the central system will participate in the complex many-body dynamics of the total system. However, if the number of spins in the environment is large, the fine details of the coupling, $H_{\rm SE}$, should not result in qualitatively different behavior of the environment with respect to level repulsion. The microscopic details of the dynamics will, of course, strongly depend on the exact nature of the coupling. Therefore, we believe that the central spin will preserve its coherence much longer in the ordered environment, compared to a frustrated environment also in the presence of nondiagonal system-environment coupling $H_{\rm SE}$. The numerical analysis in Refs. [17,18] supports this hypothesis.

We considered an arrangement where the central system coupled to each spin in the environment. In the presence of a very large environment, where the connectivity between the subsystems is limited, this approximation might fail. As an example, the central spin might couple to only a few spins of the environment. However, even if the central spin couples only to few spins, in the presence of a ferromagnetic environment this might be sufficient for coupling to collective modes of excitation (i.e., spin waves).

Since we treat a closed quantum system, we do not expect details of our analysis to carry on to realistic open systems. In the thermodynamic limit we expect that the environment will be damped, forgetting interactions with the central spin at times earlier than the correlation time. However, the analysis should be relevant to systems where the effective temperature is much less than the typical splitting between states in the environment.

We found it useful, in light of the correlations shown in Fig. 2, to discuss the decoherence of the central spin in terms of the overlap elements between the ground state of $H_{\rm E}$ and the eigenstates $\{|n^\uparrow\rangle\}$ of the environment in the presence of the central spin. However, the largest overlap element of Eq. (6) does not necessarily give the whole picture. The coherence of the central spin may differ from what was predicted by the

overlap element due to the phase factor $\exp[i(E_n^{\uparrow} - E_m^{\downarrow})t]$. If the ground state of $H_{\mathrm{E}}$ is degenerate due to symmetry, and the central system is unable to break this symmetry, then coherence will persist in the central system even if the overlap with the ground state of $H_{\mathrm{E}}$ is split between several degenerate states. If the degeneracy is not exact, coherence might still decay extremely slowly if the difference $|E_n^{\uparrow} - E_m^{\downarrow}|$ of the states overlapping with $|\psi_0\rangle_{\mathrm{E}}$ is small.

## V. CONCLUSION

In conclusion, we have analyzed the efficiency of decoherence using the overlap elements, $\langle n^{\uparrow}|0\rangle_{\mathrm{E}}$, between the ground state of the isolated environment and the set of eigenstates of the environment in the presence of the central spin. It was shown that the square of the largest overlap element, $\max_n |\langle n^{\uparrow}|\psi_0\rangle|^2$, is a very good indicator for the efficiency of decoherence. The size of the largest overlap element tends to be much larger for an environment with no competing interactions than for an environment with many frustrated couplings. The underlying mechanism behind this effect can be explained by the statistics of the eigenvalues of $H_{\mathrm{E}}$. Coupling to an external object (e.g., a central spin) results in avoided level crossings between the levels of the environment. In the absence of frustration, the level repulsion is weak and the avoided crossings will take place in a short interval in the coupling parameter to the external object, $\Delta$. The eigenvectors corresponding to the involved levels will simply switch, and the overlap element remains unaltered. In this weak repulsion regime, multilevel crossings are strongly suppressed. In the opposite regime, characterized by strong level repulsion, eigenvalues within large fractions of Hilbert space are subject to mutual level repulsion. In this strong-repulsion regime the corresponding eigenvectors will rapidly mix when increasing $\Delta$, resulting in very efficient decoherence of the central object.

We have shown that a external magnetic field can transfer the environment from the strong- to the weak-repulsion regime provided it is stronger than the frustrated couplings present, thereby enhancing the coherence of the central spin. Thus, it should be possible to enhance the coherence time of a central spin in the presence of a spin-glass–like environment by applying an external magnetizing field that is of the same magnitude or larger than the internal coupling in the environment.


[1] A. J. Leggett, Phys. Condens. Matter **14**, R415 (2002).
[2] A. Bassi and G. Ghirardi, Phys. Condens. Matter **379**, 257 (2003).
[3] J. van Wezel, J. van den Brink, and J. Zaanen, Phys. Rev. Lett. **94**, 230401 (2005).
[4] T. Gaebel *et al.*, Nature Phys. **2**, 408 (2006).
[5] R. Hanson, V. V. Dobrovitski, A. E. Feiguin, O. Gywat, and D. D. Awschalom, Science **320**, 352 (2008).
[6] T. D. Ladd, D. Press, K. De Greve, P. L. McMahon, B. Friess, C. Schneider, M. Kamp, S. Höfling, A. Forchel, and Y. Yamamoto, Phys. Rev. Lett. **105**, 107401 (2010).
[7] R. Hanson, L. P. Kouwenhoven, J. R. Petta, S. Tarucha, and L. M. K. Vandersypen, Rev. Mod. Phys. **79**, 1217 (2007).
[8] W. A. Coish and D. Loss, Phys. Rev. B **70**, 195340 (2004).
[9] O. Tsyplyatyev and D. Loss, Phys. Rev. Lett. **106**, 106803 (2011).
[10] S. Takahashi, R. Hanson, J. van Tol, M. S. Sherwin, and D. D. Awschalom, Phys. Rev. Lett. **101**, 047601 (2008).
[11] S. Takahashi, I. S. Tupitsyn, J. van Tol, C. C. Beedle, D. N. Hendrickson, and P. C. E. Stamp, Nature (London) **476**, 76 (2011).
[12] J. Bergli, Y. M. Galperin, and B. L. Altshuler, New J. Phys. **11**, 025002 (2009).
[13] N. V. Prokof'ev and P. C. E. Stamp, Rep. Prog. Phys. **63**, 669 (2000).
[14] S. Camalet and R. Chitra, Phys. Rev. B **75**, 094434 (2007).
[15] S. Camalet and R. Chitra, Phys. Rev. Lett. **99**, 267202 (2007).
[16] S. Yuan, M. Katsnelson, and H. De Raedt, JETP Lett. **84**, 99 (2006).
[17] S. Yuan, M. I. Katsnelson, and H. De Raedt, Phys. Rev. B **77**, 184301 (2008).
[18] S. Yuan, M. I. Katsnelson, and H. De Raedt, Phys. Rev. A **75**, 052109 (2007).
[19] J. Lages, V. V. Dobrovitski, M. I. Katsnelson, H. A. De Raedt, and B. N. Harmon, Phys. Rev. E **72**, 026225 (2005).
[20] A. Melikidze, V. V. Dobrovitski, H. A. De Raedt, M. I. Katsnelson, and B. N. Harmon, Phys. Rev. B **70**, 014435 (2004).
[21] S. Yuan, M. I. Katsnelson, and H. D. Raedt, J. Phys. Soc. Jpn. **78**, 094003 (2009).
[22] S. K. Choi, D.-H. Lee, S. G. Louie, and J. Clarke, Phys. Rev. Lett. **103**, 197001 (2009).
[23] R. Alicki, e-print arXiv:quant-ph/0205173v1.
[24] T. Prosen and M. Znidaric, J. Phys. A **35**, 1455 (2002).
[25] W. Zurek, Nature (London) **412**, 712 (2001).
[26] M. A. Nielsen and I. L. U. P. Chuang, *Quantum Computation and Quantum Information* (Cambridge University Press, Cambridge, 2000).
[27] F. M. Cucchietti, D. A. R. Dalvit, J. P. Paz, and W. H. Zurek, Phys. Rev. Lett. **91**, 210403 (2003).
[28] B. Casabone, I. García-Mata, and D. A. Wisniacki, Europhys. Lett. **89**, 50009 (2010).
[29] J. R. Rubbmark, M. M. Kash, M. G. Littman, and D. Kleppner, Phys. Rev. A **23**, 3107 (1981).
[30] M. L. Mehta, *Random Matrices* (Academic, New York, 1991).
[31] T. C. Hsu and J. C. Angle's d'Auriac, Phys. Rev. B **47**, 14291 (1993).

3

# Decoherence of a qubit due to either a quantum fluctuator, or classical telegraph noise

Henry J. Wold,[1] Håkon Brox,[1] Yuri M. Galperin,[1,2,3] and Joakim Bergli[1]
[1]*Department of Physics, University of Oslo, P.O. Box 1048 Blindern, 0316 Oslo, Norway*
[2]*Centre for Advanced Study, Drammensveien 78, Oslo, Norway 0271, Oslo, Norway*
[3]*A. F. Ioffe Physico-Technical Institute of Russian Academy of Sciences, 194021 St. Petersburg, Russia*
(Received 11 June 2012; published 5 November 2012)

We study the domain of applicability of the classical telegraph noise model in the study of decoherence in qubits. We investigate the decoherence of a qubit coupled to either a quantum fluctuator, a quantum two-level system (TLS) again coupled to an environment, or to a classical fluctuator modeled by random telegraph noise. In order to do this, we construct a model for the quantum fluctuator where we can adjust the temperature of its environment, and the decoherence rate independently. The model has a well-defined classical limit at any temperature and this corresponds to the appropriate random telegraph process, which is symmetric at high temperatures and becomes asymmetric at low temperatures. We find that the difference in the qubit decoherence rates predicted by the two models depends on the ratio between the qubit-fluctuator coupling and the decoherence rate in the pointer basis of the fluctuator. This is then the relevant parameter, which determines whether the fluctuator, has to be treated quantum mechanically or can be replaced by a classical telegraph process. We also compare the mutual information between the qubit and the fluctuator in the classical and the quantum model.

DOI: 10.1103/PhysRevB.86.205404 PACS number(s): 03.65.Yz, 03.67.Lx, 03.67.Bg, 74.78.Na

## I. INTRODUCTION

The interaction between a quantum system and its environments leads to loss of quantum coherence, or decoherence, in the system. Understanding decoherence is crucial for grasping the boundary between quantum and classical physics.[1–4] It is also essential for testing theories describing quantum measurements.[5–8]

From an engineering point of view, the decay of coherence in quantum bit devices (qubits) is the most important obstacle for constructing a working quantum computer. Solid state qubits are leading candidates in the projects of designing quantum circuits, where the coherence times of the qubits are required to be sufficiently long to allow for manipulations and transfer of information by logical gates. The most important source of decoherence in many realizations of solid state qubits are believed to be bistable fluctuators— two-level systems (TLSs), present as tunneling states in the amorphous substrate[9,10] used to fabricate the qubit, or in the tunneling junction in superconductor-based devices.[11–18]

These fluctuators are quantum-mechanical systems that are, in turn, coupled to their own environments, which are conventionally considered as uncorrelated thermal baths. Usually, one does not worry about the fine details of the environment of the fluctuators, but rather uses simplified models. The most popular is the Bloch-Redfield approach,[19] where the environment is taken into account by introduction of the relaxation and decoherence rates of the fluctuators. If the fluctuators couple more strongly to their own environment than to the qubit, they are usually treated classically. This means that the dynamical description of the quantum fluctuator is replaced by a classical dynamics of a fluctuating system, which switches randomly between its two metastable states according to a random telegraph process (RTP).[20,21] This approach is often referred to as the spin-fluctuator model.[11,18,22] In many cases, however, the decoherence of the qubit is determined by only a few fluctuators that are more strongly coupled to the qubit than others.[23–27] In such cases, one might question the validity of the classical model. From a practical point of view, it is therefore important to know when such a simplified classical description can replace the full quantum mechanical one. It is also of more fundamental interest in view of the decoherence approach to the quantum-classical transition.[1–4]

In this paper, we will develop a simple model allowing to show when a quantum system can in practice be replaced by a classical one, in the sense that interference effects can no longer be observed due to the entanglement with the environment. However, we believe that this is only a question of a system becoming *in practice* classical, i.e., when we can use a classical model to calculate a physical property of a quantum system. It does not directly shed any light on the fundamental limitations of quantum mechanics, in particular, the measurement problem, where one can discuss deviations from linear quantum mechanics, see Ref. 5 for a discussion.

Previously, the boundary between quantum and classical regime for the fluctuator has been explored in a model where the qubit is coupled to an impurity state, and an electron can tunnel between this state and an electron reservoir (metal).[28,29] The same model has also been used in order to study the effect of Coulomb interaction between the charged impurities and the reservoir electrons.[30]

The qubit dephasing rate calculated in the quantum model was found to converge to the classical result in the high-temperature limit. In the study by Abel and Marquardt,[29] a threshold for strong coupling between the qubit and the fluctuator was defined by the onset of visibility oscillations in the qubit as a function of the ratio between the coupling to the qubit and the reservoir. The threshold for visibility oscillations was found for higher values of the qubit coupling in the quantum model compared to the classical model, the thresholds finally converge at high $T/\gamma$, where $\gamma$ is the fluctuator-reservoir coupling. Thus both in the decoherence rate and in the visibility oscillations the classical limit is recovered at high temperature. In this model, the temperature plays a dual role: it affects both the energy relaxation rate

 

of the fluctuator, which maps to the switching rate of the RTP, and it affects the dephasing rate of the fluctuator. The usefulness of separation of the two effects is seen by the fact that it is perfectly possible to consider finite-temperature classical fluctuators by using an asymetric RTP.[31,32] This is never obtained in any limit of the model discussed in Refs. 28 and 29.

The subsequent considerations are based on the following qualitative picture: the dephasing of the qubit is caused by the generation of entanglement between the qubit and the environment. If the qubit and the fluctuator are strongly coupled, then they behave as a combined four-level quantum system and the quantum nature of the fluctuator will be important. In such a situation, one cannot replace it by a classical RTP. On the other hand, if the fluctuator is sufficiently strongly coupled to the environment, it means that the information about its state is continuously transferred to the environment and this prevents any quantum interference to take place. From this, we can guess that the relevant quantity determining whether the fluctuator can be considered either classical or quantum is the ratio of the qubit-fluctuator coupling (which determines the rate of entanglement generation between the qubit and the fluctuator) and the fluctuator dephasing rate.

The goal of this paper is to study the applicability of the classical model for qubit decoherence due to a quantum fluctuator. In order to achieve this, we study a model where the dephasing rate of the fluctuator can be varied independently of the temperature, so that the classical limit can be taken at any temperature and correspond to the proper assymetric RTP. By use of a model borrowed from the study of fluctuators in glasses, but where we allow for more freedom in the choise of parameters than we find in typical glasses, we compare the pure decoherence rate of the qubit subject to either a quantum fluctuator, in turn coupled to its environment, or a classical fluctuatur, modeled by random telegraph noise. Our model allows us to separate the effects of temperature, coupling to the bath, and decoherence rate of the fluctuator. We find that the difference in the qubit decoherence rate predicted by the quantum model and the classical one depends on the ratio, $\xi/\bar{\gamma}_2$, where $\xi$ is the qubit-fluctuator coupling strength and $\bar{\gamma}_2$ is the decoherence rate of the fluctuator in the pointer basis.

## II. MODEL

### A. Quantum model for the fluctuator

We start by describing the quantum-mechanical model for the fluctuator. The model we use for the fluctuator originates in the study of tunneling states in glasses, i.e., a particle, or a group of particles that can be approximated by a single configurational coordinate in a double-well potential.[33] It gives rise to a potential on the qubit that depends on its position in the double well.

Following Refs. 9, 10, and 33, the Hamiltonian for the coupled qubit fluctuator is split into the Hamiltonians $H_q$ for the qubit, $H_f$ for the fluctuator, $H_i$ for the qubit-fluctuator interaction, $H_e$ for the environment and $H_{fe}$ for the fluctuator-environment interaction:

$$\begin{aligned} H &= H_q + H_f + H_i + H_e + H_{fe}, \quad H_q = E_q\tau_z, \\ H_f &= (1/2)(\Delta\sigma_z + \Delta_0\sigma_x), \quad H_i = (1/2)\,\xi\,\tau_z\sigma_z, \end{aligned} \tag{1}$$

where the Pauli matrices $\tau_\alpha$ and $\sigma_\alpha$ are operators in the Hilbert spaces of the qubit and the quantum fluctuator, respectively.

The energy splitting $\Delta$ and the tunnel amplitude $\Delta_0$ can be calculated from the shape of the double-well potential.[33] The energy of the qubit depends on the position of the particle in the double well (we will in the following refer to the eigenstates of $\sigma_z$ as the position basis) and the coupling strength is given by $\xi$. In this work, we will assume the simplified case where the qubit does not directly interact with the environment and therefore has no intrinsic dynamics in the absence of the fluctuator. Furthermore, we consider a model where the qubit is subject to pure dephasing, $[H_q, H_i] = 0$, there is no energy relaxation of the qubit in this model and the decoherence of the qubit is therefore insensitive to the qubit energy splitting $E_q$. When energy relaxation is present, coherent beatings between the qubit and resonant fluctuators are observed.[23,34] In this strong coupling regime, the fluctuator has to be treated as a quantum system. Our present work concentrates solely on nonresonant fluctuators, which are typically modeled classically.

The double-well potential is, in general, perturbed by electromagnetic and strain fields modifying the asymmetry energy $\Delta$, while perturbations of the barrier height can usually be ignored.[35–37] In our model, we therefore assume that the environment couples to the fluctuator in the position basis, i.e., the eigenbasis of $\sigma_z$. Rather than formally specifying $H_e$ and $H_{fe}$ we take the freedom to consider two kinds of interaction between the fluctuator and the external environment, resonant and nonresonant. We will later in addition also use parameters for the fluctuator-environment coupling that are outside what we typically encounter in glasses. This is done in order to have more freedom to tune the parameters that are relevant to study the domain of applicability of the RTP model.

The resonant phonons creates a strain field $u_{ik}$ that modifies the double-well potential of the TLS as follows:

$$\Delta = \Delta^{(0)} + \lambda_{ik}u_{ik}, \quad \Delta_0 = \text{const},$$

where $\Delta^{(0)}$ is the energy splitting in the absence of the strain field and $\lambda_{ik}$ is the deformation potential of the fluctuator. In the energy basis of the fluctuator, this interaction creates two terms:

$$\left(\frac{\Delta}{\sqrt{\Delta^2+\Delta_0^2}}\tilde{\sigma}_z + \frac{\Delta_0}{\sqrt{\Delta^2+\Delta_0^2}}\tilde{\sigma}_x\right)\lambda_{ik}u_{ik},$$

where $\tilde{\sigma}_z$ and $\tilde{\sigma}_x$ act in the energy eigenbasis of the fluctuator.

The first term will give rise to pure dephasing of the fluctuator, while the second gives rise to relaxation. We will in the following assume that the rate of resonant phonons is small compared to the nonresonant ones, and that the contribution to pure dephasing given by the first term can be neglected. Resonant interaction, e.g., phonons with frequency close to the eigenfrequency of the fluctuator, are therefore responsible for direct transitions between the eigenstates of the fluctuator, $|\psi_g\rangle$ and $|\psi_e\rangle$.

We model this interaction by use of the generalized measurement operators defined for a small time step $\Delta t$ as[38]

$$M_1(\Delta t) = \sqrt{\gamma_{\rm ab}(T)\Delta t}\, I \otimes \sigma_x |\psi_g\rangle\langle\psi_g|,$$
$$M_2(\Delta t) = \sqrt{\gamma_{\rm em}(T)\Delta t}\, I \otimes \sigma_x |\psi_e\rangle\langle\psi_e|, \qquad (2)$$
$$M_3(\Delta t) = \sqrt{1 - M_1^\dagger M_1 - M_2^\dagger M_2}\,.$$

Here, $I$ is the identity matrix in the Hilbert space of the qubit and the matrices $\sigma_x|\psi_{g(e)}\rangle\langle\psi_{g(e)}|$ "measures" whether the fluctuator is in the ground (excited) state, projects the fluctuator onto this state and flips it. The rates for absorbtion and emission are

$$\gamma_{\rm ab}(T) = \gamma_1 N(E) = \frac{\gamma_1}{e^{E/T} - 1},$$
$$\gamma_{\rm em}(T) = \gamma_1[N(E) + 1] = \frac{\gamma_1}{1 - e^{-E/T}}. \qquad (3)$$

Here, $T$ is the temperature, $N(E) = (e^{E/T} - 1)^{-1}$ is the Planck distribution, and $E = \sqrt{\Delta^2 + \Delta_0^2}$ is the energy splitting of the fluctuator. The nonresonant interaction does not cause transitions between the eigenstates of the fluctuator. However, we might assume that, in general, the state of a phonon interacting with the fluctuator is perturbed by the interaction, and that the perturbation depends on the position of the system in the double well. These are assumed to be low-frequency phonons $\hbar\omega \ll E$, which does not significantly alter the level splitting of the fluctuator. Schematically, we can write

$$|\psi_i\rangle|\phi_0^{\rm ph}\rangle \xrightarrow{t} |\psi_i\rangle|\phi_i^{\rm ph}\rangle, \qquad (4)$$

where $i \in \{0,1\}$ index the state of the fluctuator in the position basis, $|\phi_0^{\rm ph}\rangle$ is the initial state of the phonon and $|\phi_i^{\rm ph}\rangle$ is the state of the phonon after the interaction, conditioned upon that the fluctuator was initially in the state indexed by $i$. The interaction (4) results in entanglement between the phonon and the fluctuator, reducing the coherence of the latter. The rate of decoherence due to nonresonant phonons depends on the overlap element $\alpha = \langle\phi_0^{\rm ph}|\phi_1^{\rm ph}\rangle$ and on the rate of phonons interacting with the system. We model this interaction by the single parameter $\gamma_2$, which is responsible for the decay rate of the off-diagonal density matrix elements of the fluctuator in the position basis.

In this model, we effectively adjust the nature of $H_{fe}$ by the ratio $\Delta_0/\Delta$. Therefore the equilibrium density matrix of the fluctuator will not necessarily lie along the $z$ axis of the Bloch sphere. The equilibrium density matrix is determined by the rate $\gamma_2$ due to nonresonant phonons responsible for decay perpendicular to the $z$ axis on the Bloch sphere and by relaxation to the thermal level along the $z'$ axis in the eigenbasis of the fluctuator induced at the rate $\gamma_1$ by resonant phonons.

Note also that differences in the qubit decoherence between the quantum and the classical model is not observed when the $z'$ axis is parallel with the $z$ axis. The situation is illustrated in Fig. 1. We define the decoherence rate of the fluctuator, $\bar{\gamma}_2$, by the rate at which the off-diagonal density matrix elements decay in the basis where the density matrix is diagonal in equilibrium.

The time evolution in the quantum model is obtained by numerical integration of the von Neumann equation for the Hamiltonian given by Eq. (1), with two modifications. We add

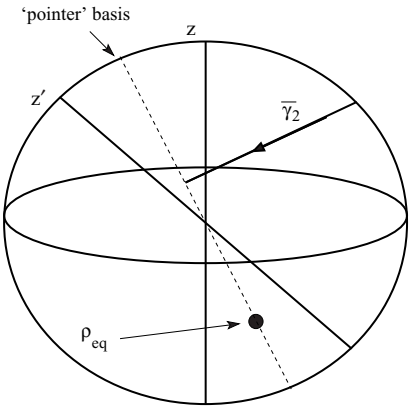


FIG. 1. The Bloch sphere for the fluctuator coupled to both nonresonant and resonant phonons. The nonresonant phonons are responsible for decay perpendicular to the $z$ axis, the eigenbasis of $\sigma_z$, while the resonant phonons are responsible for relaxation parallell to the $z'$ axis, which is the eigenbasis of the fluctuator. We define the pointer basis by the basis in which the equilibrium density matrix $\rho_{\rm eq}$ is diagonal. The rate of decay perpendicular to this axis is denoted by $\bar{\gamma}_2$.

a damping term $\gamma_2$ to our differential equation:

$$\dot{\rho}_{\alpha\alpha'} = i\langle\alpha|[\rho, H]|\alpha'\rangle - \Lambda_{\alpha\alpha'}\rho_{\alpha\alpha'}, \qquad (5)$$

where $\rho$ is the density matrix of the system composed of the qubit and the fluctuator and $\Lambda = \gamma_2 I \otimes \sigma_x$, which determines the decay of the off-diagonal density matrix elements of the fluctuator in the eigenbasis of $\sigma_z$. In addition, the fluctuator absorbs and emits phonons at the rates $\gamma_{\rm ab}(T)$ and $\gamma_{\rm em}(T)$. The absorption and emission of phonons is implemented as follows: for each time step $\Delta t$, we make a transformation to the eigenbasis of the fluctuator,

$$\bar{\rho} = R(\theta)\rho R^\dagger(\theta), \qquad (6)$$

using the rotation matrix

$$R(\theta) = I \otimes \begin{pmatrix} \cos\frac{\theta}{2} & \sin\frac{\theta}{2} \\ -\sin\frac{\theta}{2} & \cos\frac{\theta}{2} \end{pmatrix}, \quad \theta \equiv \arctan\left(\frac{\Delta_0}{\Delta}\right).$$

The density matrix is then updated according to the rates of absorption and emission as

$$\bar{\rho}' = M_1\bar{\rho}M_1^\dagger + M_2\bar{\rho}M_2^\dagger + M_3\bar{\rho}M_3^\dagger, \qquad (7)$$

before we make the inverse transform $\rho' = R^\dagger(\theta)\bar{\rho}'R(\theta)$, back to the position basis. Here, $\rho'$ is the density matrix after the (potential) interaction with the resonant phonons.

### B. Classical telegraph noise

Pure dephasing of the qubit by a classical telegraph noise can be described by the interaction Hamiltonian

$$H_i = (1/2)\xi(t)\tau_z, \qquad (8)$$

where $\xi(t) = \pm\xi$ is the position of the fluctuator at time $t$. For details on this model see, e.g., Ref. 39 and references therein.

The probability for the fluctuator to switch from the state $\xi_-$ to $\xi_+$, and from $\xi_+$ to $\xi_-$ in the interval $dt$ is given by $\Gamma_{-+}dt$ and $\Gamma_{+-}dt$, respectively. To describe finite temperature, we will consider the situation where the flipping rates $\Gamma_{-+}$ and $\Gamma_{+-}$ of the fluctuator are, in general, not identical, but the states are symmetric $\xi_- = -\xi_+$. The situation with asymmetric switching rates was previously studied in Refs. 31 and 32. The equilibrium average is given by

$$\langle \xi \rangle = \xi(p_+^{\rm eq} - p_-^{\rm eq}) = \xi(\Gamma_{-+} - \Gamma_{+-})/\Gamma, \tag{9}$$

where

$$\Gamma = \Gamma_{-+} + \Gamma_{+-}, \tag{10}$$

and $p_\pm(t)$ is the probability for the fluctuator to be found in the state $\xi_\pm$. The relaxation towards equilibrium is exponential with rate $\Gamma$.

The decoherence of the qubit is obtained by averaging over the realizations and initial conditions of the noise process $\xi(t)$. For a given realization of $\xi(t)$, the Schrödinger equation yields a superposition of the eigenstates of the qubit with a contribution to the relative phase $\phi(t) = \int_0^t \xi(t')dt'$. Averaged over the realizations of the stochastic process $\xi(t)$, we obtain the qubit coherence $D(t) = \langle e^{i\phi(t)} \rangle$. Here, we will use the transfer matrix method developed by Joynt *et al.*,[40] where we obtain directly the ensemble averaged Bloch vector of the qubit.

The state of the qubit-fluctuator system can be stored in the six-dimensional vector

$$\vec{q}(t) = \vec{m}_+(t) \otimes \begin{pmatrix} 1 \\ 0 \end{pmatrix} p_+(t) + \vec{m}_-(t) \otimes \begin{pmatrix} 0 \\ 1 \end{pmatrix} p_-(t), \tag{11}$$

where $\vec{m}_\pm$ is the Bloch vector of the qubit conditioned upon the state $\xi_\pm$ of the fluctuator. The propagator for $\vec{q}$ averaged over the individual realizations of the RTP can be expressed as $A(t) = e^{-Bt}$, where

$$B = I_3 \otimes V - i\frac{\xi}{2} L_z \otimes \upsilon_z, \quad V = \begin{pmatrix} \Gamma_{+-} & -\Gamma_{-+} \\ -\Gamma_{+-} & \Gamma_{-+} \end{pmatrix},$$

while $I_3$ and $L_z$ are generators of the $SO_3$ group and $\upsilon_Z$ is the Pauli matrix. A direct advantage of this approach is that the qubit state conditioned upon whether the fluctuator is in the state $\xi_\pm$, $\rho_q^\pm$ follows directly from $\vec{q}$.

## III. RESULTS

In order to compare the decoherence of the qubit subject to either the quantum fluctuator, or the classical telegraph noise, we calculate similar relaxation rates towards the equilibrium level in the two models. First, we choose a set of parameters, $\Delta$, $\Delta_0$, $\gamma_1$, $\gamma_2$, and $T$ for the quantum model and prepare the fluctuator in the initial state $|\psi_1\rangle$. At this preliminary stage, we are not interested in the qubit and consider the fluctuator and its environment decoupled from the qubit. We compute numerically the equilibrium occupation probabilities $p_0^{\rm eq}$ and $p_1^{\rm eq}$ of the quantum fluctuator in the position basis as well as the relaxation rate $\Gamma$. Note that both the equilibrium occupations and the relaxation rate are, in general, complicated functions of all the parameters in our model. In this work, we always restrict ourselves to the regime where the fluctuator is overdamped $\Delta, \Delta_0 \ll \gamma_2$, i.e., the decoherence rate is sufficiently large such that coherent oscillations are not observed in the fluctuator. In this regime, the decay of the fluctuator towards its equilibrium value can be fitted to a simple exponential. Beyond this regime, the fluctuator behave as a quantum system, and can therefore not be modeled by the classical telegraph process. Note also that since the states $|\psi_i\rangle$ are not eigenstates of the Hamiltonian, the occupation numbers $p_i^{\rm eq}$ are not given by the Boltzmann weights at the bath temperature.

The decoherence rate is expressed through the rates $\Gamma_{\pm\mp}$ and the equilibrium occupancy $\langle \xi \rangle$ with the help of Eqs. (9) and (10). The qubit decoherence rate is, in general, a sum over multiple rates. For symmetric telegraph noise and pure dephasing, the decay of coherence in the qubit $D(t)$ is given by[39]

$$D(t) = \frac{e^{-\Gamma t/2}}{2\mu}[(\mu+1)e^{\Gamma\mu t/2} + (\mu-1)e^{-\Gamma\mu t/2}], \tag{12}$$

where $\mu \equiv \sqrt{1 - (2\xi/\Gamma)^2}$. However, in the regime where the coupling to the qubit is weak compared to the damping of the fluctuator, $\Gamma > \xi$, the long-time behavior of the decoherence is strongly dominated by a single rate,

$$\Gamma_q^c = \Gamma(1-\mu)/2.$$

We finally compute the decoherence rate $\Gamma_q^q$ of the qubit when it is coupled to the same quantum fluctuator from which we calculated the relaxation rate and equilibrium occupations previously, but this time the initial state of the fluctuator is the thermal equilibrium state. The decoherence rate of the qubit is calculated by numerical simulation of the coupled qubit-fluctuator density matrix $\rho(t)$ from which we can find the qubit density matrix by tracing out the degrees of freedom of the quantum fluctuator. From the qubit density matrix, $\rho^q(t) = {\rm Tr}_f[\rho(t)]$, we find the coherence $|\rho^q_{\uparrow\downarrow}(t)|$, where $\uparrow$ and $\downarrow$ denote the eigenstates of the qubit. Finally, the long-time behavior of $|\rho^q_{\uparrow\downarrow}(t)|$ is fitted to the exponential function $e^{-\Gamma_q^q t}$. Note that the initially $|\rho^q_{\uparrow\downarrow}(t)|$ might have contributions from several rates, like in the classical model (12). Note also that in the regime where the fluctuator is near resonant with the qubit, these two systems need to be treated as a four-level system, and the dynamics is characterized by four distinct rates. This regime was studied in Ref. 41 in order to characterize the effect of coherent impurities on the qubit.

The relative difference in the decoherence rate of the qubit due to classical telegraph noise and the quantum fluctuator is defined as

$$\delta\Gamma_q = \left(\Gamma_q^q - \Gamma_q^c\right)/\Gamma_q^c, \tag{13}$$

where $\Gamma_q^q$ and $\Gamma_q^c$ are the decoherence rate of the qubit subject to the quantum fluctuator and to the classical telegraph noise, respectively. This quantity is presented in Fig. 2 as a function of the dephasing rate of the fluctuator $\gamma_2$ and temperature $T$. We have restricted ourselves to a parameter range where the fluctuator does not undergo coherent oscillations. It is evident that the relative difference in the qubit decoherence rate is small for strong decoherence of the fluctuator, and for high temperatures. In this case, we can safely use the simple RTP model rather than the much more complicated quantum model. Superimposed on the contours for $\delta\Gamma_q$, we have plotted curves where the ratio $\xi/\bar{\gamma}_2$ is constant. We find that the

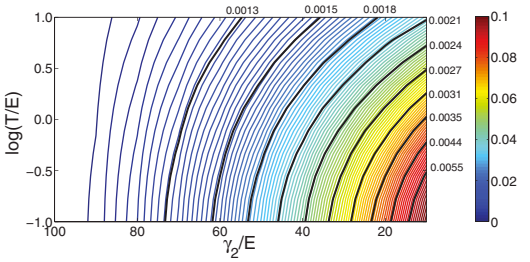


FIG. 2. (Color online) Contour plot of the relative difference $\delta\Gamma_q$ in the decoherence rate of the qubit subject to either classical telegraph noise, or a quantum fluctuator. In units of the fluctuator energy splitting $E$, the parameters of the quantum fluctuator are $\Delta = \Delta_0 = 1/\sqrt{2}$ and $\gamma_1 = 1.0$, the coupling to the qubit is $\xi = 0.1$. Color coding for $\delta\Gamma_q$ is shown on the right. The relaxation rate to equilibrium along the $\sigma_z$ axis is the same for both the quantum and the classical fluctuator. Contours where the ratio $\xi/\bar{\gamma}_2$ is constant are plotted for comparison (black lines).

difference between the quantum and the classical fluctuator depends to a very good accuracy on the ratio $\xi/\bar{\gamma}_2$. Note that we have numerically checked that the dependence of the qubit decoherence on the parameter $\xi/\bar{\gamma}_2$ holds also in the regime where $\xi > \Gamma$ confirming that the RTP model can be applied in the strong-coupling regime also in the case when the qubit couples strongly to the fluctuator, as long as $\xi \ll \bar{\gamma}_2$. The requirement $\Gamma > \xi$ is only needed to ensure that the qubit decoherence follows a simple exponential law.

When the qubit is put in contact with the quantum fluctuator, the qubit and the fluctuator will in general entangle due to their coupling. The mutual information, the information about the state of one of the systems that can be inferred by measuring the other, will for the quantum fluctuator have an entanglement contribution in addition to the classical correlation.

The mutual information for the qubit-quantum fluctuator is defined straightforwardly by the von Neumann entropy[38]

$$S(q:f) = S(\rho_q) + S(\rho_f) - S(\rho_{qf}), \tag{14}$$

where $\rho_q$, $\rho_q$, and $\rho_{qf}$ are the density matrices of the qubit, the fluctuator, and the composite system, respectively. When we treat the qubit subject to a classical telegraph noise, we introduce quantum states $|\pm\rangle$ corresponding to the states $\xi_\pm$ of the RTP and use the formula

$$\rho_{qf} = p_+\rho_q^+\rho_{f+} + p_-\rho_q^-\rho_{f-}. \tag{15}$$

Here, $p_\pm$ is the probability for the telegraph process to be found in the state $\xi_\pm$, $\rho_q^\pm$ is the density matrix of the qubit conditioned upon that the telegraph process is in the state $\xi_\pm$ and $\rho_{f\pm} = |\pm\rangle\langle\pm|$.

The time evolution of the mutual information for a qubit coupled either to the quantum or the classical fluctuators is shown in Fig. 3. The entanglement between the two systems builds up at a rate given by the coupling $\xi$ but is lost to the environment at a rate given by the decoherence rate of the quantum fluctuator, $\bar{\gamma}_2$. The increased information about the qubit encoded in the quantum fluctuator, compared to the classical fluctuator, increases the transfer of entropy to

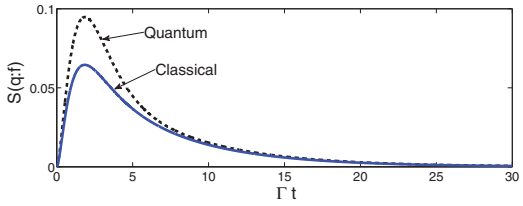


FIG. 3. (Color online) Mutual information $S(q:f)$ for the qubit coupled to the quantum fluctuator (black, dashed) and the qubit subject to the classical spin fluctuator (blue, solid). The mutual information is larger when both systems are treated as quantum objects, due to quantum entanglement between the two systems. In this simulation the parameters, in units of $E$, are $\xi = 0.1$, $\Delta = \Delta_0 = 1/\sqrt{2}$, $\gamma_1 = 1.0$, $\gamma_2 = 20$, and $E/T = 1.0$.

the environment, thus increasing the decoherence rate of the qubit. This effect might explain the positive $\delta\Gamma_q$ found for low values of $T$ and $\gamma_2$. It has been stated, see, e.g., Refs. 42 and 43, that there exist situations where increased information transfer decreases the decoherence rate of the qubit. However, we are not sure that the information transfer is reduced in the particular system discussed in Refs. 42 and 43.

Experimentally, since the composite density matrix $\rho_{qf}$ is required, the mutual information can only be extracted in the case where one has access to measurement on both the qubit and the fluctuator simultaneously. Since the fluctuator by definition is a system of the environment outside our control, this cannot be achieved. However, the mutual information could potentially be studied in two coupled qubits, where one of the qubits are subject to controlled noise and takes the role of the fluctuator. Qubits subject to engineered noise under the control of the experimentalist has been realized in optically trapped $^9Be^+$ ions,[44] where also the required quantum gates has already been implemented in a similar systems.[45]

## IV. DISCUSSION

In general, the dynamics of the quantum fluctuator in an environment depends on three parameters; the relaxation rate $\gamma_1$, the dephasing rate $\gamma_2$ and the temperature $T$ determining the equilibrium occupations. In this paper, we use a model where the processes responsible for pure dephasing couple to the position basis, while the relaxation processes take place in the eigenbasis of the fluctuator. This model was used in order to study the relevance of the classical RTP model for description of decoherence of a qubit. If the interaction responsible for pure dephasing processes in the fluctuator (characterized by $\gamma_2$) commutes with the qubit-fluctuator Hamiltonian, i.e., $\Delta_0 = 0$ in our model, then the pure dephasing rate $\gamma_2$ will not have any effect on the decoherence rate of the qubit as long as the fluctuator is prepared in the thermal equilibrium state. The quantum fluctuator will in this case *always behave as a classical fluctuator* and can therefore straightforwardly be modeled by the classical telegraph noise.

In general, the difference in decoherence rate $\delta\Gamma$ depends on the ratio $\Delta_0/\Delta$ in addition to the ratio $\xi/\bar{\gamma}_2$. We find that $\delta\Gamma$

increases monotonously as a function of the ratio $\Delta_0/\Delta$ for $\Delta_0/\Delta \in [0,\pi/4]$ and that $\delta\Gamma = 0$ for $\Delta_0/\Delta = 0$. However, the contours of constant $\xi/\bar{\gamma}_2$ in the $\ln T$ versus $\gamma_2$ plot, match those of constant $\delta\Gamma$ for all values of $\Delta_0/\Delta$.

Furthermore, we note that our results do not tell us that it is, in principle, not possible in ad hoc fashion to construct a classical telegraph model, e.g., a classical model with feedback, providing the same decoherence rate for the qubit as the quantum fluctuator, even in the regime where the deviation $\delta\Gamma_q$ between the two models are large according to Fig. 2. We show that the decoherence rate of the qubit differs in the two models in the case where the relaxation rates of the classical and quantum fluctuator are identical. To the best of our knowledge, there exist no general relationship between the quantum fluctuator model and the classical spin-fluctuator model. Therefore one should be careful in applying the classical telegraph model unless one expects the decoherence rates of the fluctuators to be much larger than the qubit-fluctuator coupling. $\xi/\bar{\gamma}_2 \ll 1$. However, in systems such as glasses this inequality is usually expected to hold, and the quantum fluctuator can be treated effectively by random telegraph noise,[33] with an exception if the system is subject to an external ac field.[46]

The pointer states of a quantum system are defined as the pure states that are the least affected by environmental decoherence.[1,3] It is generally believed that when the dynamics of the system is dominated by the interaction with the environment, the pointer states are the eigenstates of the interaction Hamiltonaian.[1] On the other hand, when the system is weakly coupled to the environment, the pointer states are assumed to be the eigenstates of the isolated system.[2] Our model can be considered to interpolate between the two extremes. If we define the pointer basis as the basis where the Bloch vector of the system lies along the $z$ axis in equilibrium, the decoherence rate $\bar{\gamma}_2$ of the system is the rate of decay of the off-diagonal elements of the density matrix in this basis.

As a final note we mention that our main result, that the difference in decoherence rate of the qubit between the quantum fluctuator model and the telegraph noise model, might be model specific. Further work is needed in order to settle whether or not this result is universal.

In conclusion, we have constructed a model for the quantum fluctuator where we can study its effect on the qubit as a function of both the temperature and its decoherence due to its interaction with the environment. We have compared the decoherence rate of the qubit found in this model, and in the widely used classical telegraph noise model. We find that the difference in the qubit decoherence rates depends on the ratio $\xi/\bar{\gamma}_2$ between the strength of the qubit-fluctuator coupling and decoherence rate of the fluctuator in the pointer basis. In the limit $\xi/\bar{\gamma}_2 \ll 1$, the fluctuator behaves essentially classically and the qubit decoherence rate can accurately be predicted by the telegraph noise model. Our results validate the application of the RTP model for the study of decoherence in qubits also when the coupling between the qubit and the fluctuator is strong as long as the fluctuator couples even more strongly to its own environment.

This work is part of the master project of one of the authors (H.J.W.) and more details can be found in his thesis.[47]

## ACKNOWLEDGMENTS

We acknowledge useful comments by S. Gurvitz, A. Aharony, O. Entin-Wohlman, and E. Paladino.

[1] W. H. Zurek, Phys. Rev. D **24**, 1516 (1981).
[2] J. P. Paz and W. H. Zurek, Phys. Rev. Lett. **82**, 5181 (1999).
[3] W. H. Zurek, Rev. Mod. Phys. **75**, 715 (2003).
[4] M. Schlosshauer, Rev. Mod. Phys. **76**, 1267 (2005).
[5] A. J. Leggett, J. Phys.: Condens. Matter **14**, R415 (2002).
[6] J. van Wezel and T. H. Oosterkamp, Proc. R. Soc. A **468**, 35 (2012).
[7] A. Bassi and G. Ghirardi, Phys. Rep. **379**, 257 (2003).
[8] S. L. Adler and A. Bassi, Science **325**, 275 (2009).
[9] P. W. Anderson, B. I. Halperin, and C. M. Varma, Philos. Mag. **25**, 1 (1972).
[10] W. A. Phillips, J. Low Temp. Phys. **7**, 351 (1972).
[11] E. Paladino, L. Faoro, G. Falci, and R. Fazio, Phys. Rev. Lett. **88**, 228304 (2002).
[12] R. W. Simmonds, K. M. Lang, D. A. Hite, S. Nam, D. P. Pappas, and J. M. Martinis, Phys. Rev. Lett. **93**, 077003 (2004).
[13] J. M. Martinis, K. B. Cooper, R. McDermott, M. Steffen, M. Ansmann, K. D. Osborn, K. Cicak, S. Oh, D. P. Pappas, R. W. Simmonds *et al.*, Phys. Rev. Lett. **95**, 210503 (2005).
[14] Y. Shalibo, Y. Rofe, D. Shwa, F. Zeides, M. Neeley, J. M. Martinis, and N. Katz, Phys. Rev. Lett. **105**, 177001 (2010).
[15] L. Tian and R. W. Simmonds, Phys. Rev. Lett. **99**, 137002 (2007).
[16] A. Shnirman, G. Schön, I. Martin, and Y. Makhlin, Phys. Rev. Lett. **94**, 127002 (2005).
[17] Y. M. Galperin, B. L. Altshuler, and D. V. Shantsev, in *Fundamental Problems of Mesoscopic Physics*, NATO Science Series, Vol. 154 (Springer Netherlands, 2004), pp. 141–165.
[18] Y. M. Galperin, B. L. Altshuler, J. Bergli, and D. V. Shantsev, Phys. Rev. Lett. **96**, 097009 (2006).
[19] C. P. Schlichter, *Principles of Magnetic Resonance* (Springer-Verlag, Berlin, 1990).
[20] S. Kogan, *Electronic Noise and Fluctuations in Solids* (Cambridge Univ. Press, Cambridge, 1996).
[21] M. Kirton and M. Uren, Adv. Phys. **38**, 367 (1989).
[22] J. Bergli, Y. M. Galperin, and B. L. Altshuler, Phys. Rev. B **74**, 024509 (2006).
[23] R. W. Simmonds, K. M. Lang, D. A. Hite, S. Nam, D. P. Pappas, and J. M. Martinis, Phys. Rev. Lett. **93**, 077003 (2004).
[24] O. Astafiev, Y. A. Pashkin, Y. Nakamura, T. Yamamoto, and J. S. Tsai, Phys. Rev. Lett. **93**, 267007 (2004).
[25] R. H. Koch, D. P. DiVincenzo, and J. Clarke, Phys. Rev. Lett. **98**, 267003 (2007).
[26] Y. M. Galperin, D. V. Shantsev, J. Bergli, and B. L. Altshuler, Europhys. Lett. **71**, 21 (2005).

[27]C. Müller, A. Shnirman, and Y. Makhlin, Phys. Rev. B **80**, 134517 (2009).
[28]A. Grishin, I. V. Yurkevich, and I. V. Lerner, Phys. Rev. B **72**, 060509 (2005).
[29]B. Abel and F. Marquardt, Phys. Rev. B **78**, 201302 (2008).
[30]I. V. Yurkevich, J. Baldwin, I. V. Lerner, and B. L. Altshuler, Phys. Rev. B **81**, 121305 (2010).
[31]G. Falci, E. Paladino, and R. Fazio, in *Quantum Phenomena in Mesoscopic Systems*, Proceedings of the International School of Physics "Enrico Fermi", Vol. 151 (IOS Press Amsterdam, 2003), pp. 173–198.
[32]Y. Jung, E. Barkai, and R. J. Silbey, Chem. Phys. **284**, 181 (2002).
[33]W. A. Phillips, Rep. Prog. Phys. **50**, 1657 (1987).
[34]J. Lisenfeld, C. Müller, J. H. Cole, P. Bushev, A. Lukashenko, A. Shnirman, and A. V. Ustinov, Phys. Rev. Lett. **105**, 230504 (2010).
[35]A. C. Anderson, Phys. Rev. B **34**, 1317 (1986).
[36]W. A. Phillips, *Amorphous Solids: Low-Temperature Properties*, Vol. 24 (Springer, Berlin, 1981).
[37]Y. M. Galperin, V. G. Karpov, and V. I. Kozub, Adv. Phys. **38**, 669 (1989).
[38]M. A. Nielsen and I. L. Chuang, *Quantum Computation and Quantum Information* (Cambridge University Press, Cambridge, 2000).
[39]J. Bergli, Y. M. Galperin, and B. L. Altshuler, New J. Phys. **11**, 025002 (2009).
[40]B. Cheng, Q.-H. Wang, and R. Joynt, Phys. Rev. A **78**, 022313 (2008).
[41]E. Paladino, M. Sassetti, G. Falci, and U. Weiss, Phys. Rev. B **77**, 041303 (2008).
[42]A. Aharony, S. Gurvitz, O. Entin-Wohlman, and S. Dattagupta, Phys. Rev. B **82**, 245417 (2010).
[43]Y. Ye, Y. Cao, X.-Q. Li, and S. Gurvitz, Phys. Rev. B **84**, 245311 (2011).
[44]M. J. Biercuk, H. Uys, A. P. VanDevender, N. Shiga, W. M. Itano, and J. J. Bollinger, Phys. Rev. A **79**, 062324 (2009).
[45]D. Leibfried, B. DeMarco, V. Meyer, D. Lucas, M. Barrett, J. Britton, W. M. Itano, B. Jelenkovic, C. Langer, T. Rosenband *et al.*, Nature (London) **422**, 412 (2003).
[46]H. Brox, J. Bergli, and Y. M. Galperin, Phys. Rev. B **84**, 245416 (2011).
[47]H. J. Wold, Master's thesis, University of Oslo, Norway, 2011, http://urn.nb.no/URN:NBN:no-28902.